Epigenetic and Phenotypic Plasticity as Mediators of Resistance to Oncogenic Pathway Targeting

Inaugural-Dissertation

zur

Erlangung des Doktorgrades

Dr. rer. nat.

der Fakultät für

Biologie

an der

Universität Duisburg-Essen

vorgelegt von

Laura Kristina Godfrey

geb. Dierichs

aus Haan

Juni 2020

DOI: 10.17185/duepublico/73164
URN: urn:nbn:de:hbz:465-20220906-115704-0

Die der vorliegenden Arbeit zugrunde liegenden Experimente wurden am Brückeninstitut für Experimentelle Tumortherapie in der Abteilung für Translationale Onkologie Solider Tumore (DKFZ/DKTK Partnerstandort Essen) des Universitätsklinikums Essen durchgeführt.

1. Gutachter: Prof. Dr. Jens T. Siveke
2. Gutachter: Prof. Dr. Bernhard Horsthemke
3. Gutachter: Prof. Dr. Christoph Plass

Vorsitzender des Prüfungsausschusses: Prof. Dr. Ralf Küppers

Tag der mündlichen Prüfung: 08. Oktober 2020

Parts of this thesis were submitted for publication

Godfrey L.K., Forster J., Liffers S.T., Schröder C., Köster J., Henschel L., Ludwig K.U., Behrens D., Scarpa A., Lawlor R.T., Trajkovic-Arsic M., Witzke K.E., Sitek B., Rahmann S., Horsthemke B., Zeschnigk M., Siveke J.T.
Pancreatic cancer acquires MEK_i resistance by clonal expansion and adaptive DNA hypermethylation. Submitted.

Meiner Familie gewidmet

INDEX

LIST OF ABBREVIATIONS

Å	angstrom
°C	degree Celsius
2D	two-dimensional
3D	three-dimensional
5-FU	5-fluorouracil
5mC	5-methylcytosine
µl	microliter
A	adenine
Alt	alternative allele
ANOVA	analysis of variance
AP-1	activator protein 1
asinh	inverse hyperbolic sine
ATAC-seq	assay for transposase-accessible chromatin and sequencing
ATF	activating transcription factor
ATP	adenosine triphosphate
BCA	bicinchoninic acid
BET	bromodomain and extra-terminal motif
BET_i	bromodomain and extra-terminal motif inhibitor
bp	base pairs
BSA	bovine serum albumin
C	cytosine
CA 19-9	carbohydrate antigen 19-9
CDH1	E-Cadherin
CDH2	N-Cadherin
cDNA	complementary DNA
ChIP-seq	chromatin immunoprecipitation and sequencing
cm	centimeter
cm^3	cubic centimeter
CpG	cytosine-guanine dinucleotide
Cre	causes recombination

CRE	cyclic adenosine monophosphate response elements
Da	Dalton
DAPI	4′,6-diamidino-2-phenylindole
DMEM	Dulbecco's Modified Eagle medium
DMR	differentially methylated region
DMSO	dimethyl sulfoxide
DNA	deoxyribonucleic acid
DNMT	DNA methyltransferase
$DNMT_i$	DNA methyltransferase inhibitor
DPBS	Dulbecco’s phosphate-buffered saline
ECOG	Eastern Cooperative Oncology Group
EDTA	ethylenediaminetetraacetic acid
e.g.	*exempli gratia* (for example)
EMT	epithelial-to-mesenchymal transition
ERK1/2	extracellular signal-regulated kinases 1 and 2
FACS	fluorescence activated cell sorting
FBS	fetal bovine serum
FDA	U.S. Food and Drug Administration
FDR	false discovery rate
FITC	fluorescein isothiocyanate
FLP	flippase
FOLFIRINOX	folinic acid, fluorouracil, irinotecan and oxaliplatin
FRT	flippase recombinase target
G	guanine
g	gravitational constant
G−C	gemcitabine−capecitabine
GEMM	genetically engineered mouse model
GRCm38	Genome Reference Consortium Mouse Build 38
GSEA	Gene Set Enrichment Analysis
GUSB	beta-glucuronidase
h	hour
HAT	histone acetyltransferase

HDAC	histone deacetylase
$HDAC_i$	histone deacetylase inhibitor
HMT	histone methyltransferase
HSD	honest significant difference
HSP	heat shock protein
IC50	half maximal inhibitory concentration
IGF1R	insulin-like growth factor 1 receptor
IgG	immunoglobulin G
InDels	insertions and deletions
kb	kilobase
kde	kernel density estimation
kDa	kilodalton
KDM	histone lysine demethylase
kg	kilogram
KRAS	kirsten rat sarcoma viral oncogene homolog
LC	liquid chromatography
LoxP	locus of crossing-over, bacteriophage P1
mAb	monoclonal antibody
MEK	mitogen-activated protein kinase
MEK_i	mitogen-activated protein kinase kinase inhibitor
min	minute
miRNA	micro RNA
mm^2	square millimeter
mm^3	cubic millimeter
mRNA	messenger RNA
ms	millisecond
MS	mass spectrometry
mTRE	methylated TRE-like sequence
m/z	mass-to-charge ratio
n	number
na	not available
nab	nanoparticle albumin-bound

NaDOC	sodium deoxycholate
nal	nanoliposomal
NCBI	National Center for Biotechnology Information
ng	nanogram
nl	nanoliter
nM	nanomolar
NMRI	Naval Marine Research Institute
NOD/SCID	non-obese diabetic/severe combined immunodeficiency
Norm.	normalized
NSCLC	non-small-cell lung cancer
NSG	NOD/SCID gamma
pAb	poly-clonal antibody
PCR	polymerase chain reaction
PDAC	pancreatic ductal adenocarcinoma
PDX	patient-derived xenografts
PDX1	pancreatic and duodenal homeobox 1
PI	propidium iodide
PI3K	phosphatidylinositol 3-kinase
ppm	parts per million
PTF1A	pancreas transcription factor 1 subunit alpha
P5	passage 5 after drug withdrawal
P12	passage 12 after drug withdrawal
P40	passage 40 after drug withdrawal
RECIST	response evaluation criteria in solid tumors
Ref	reference allele
Rel.	relative
RFU	relative fluorescence units
RIPA	radio-immunoprecipitation assay
RNA	ribonucleic acid
RNA-seq	RNA-sequencing
RT-PCR	real-time PCR
s	second

SAHA	suberoylanilide hydroxamic acid
SD	standard deviation
SEM	standard error of the mean
SIFT	sorting intolerant from tolerant
SNV	single nucleotide variant
SV	structural variant
T	thymine
TAE	tris-acetate-EDTA
TES	transcription end site
TET	ten eleven translocation
TFA	trifluoroacetic acid
TFBS	transcription factor binding sites
TK_i	tyrosine kinase inhibitor
TRE	12-O-tetradecanoylphorbol-12-acetate response elements
Trp53	transformation related protein 53
TSS	transcription start site
U	unit
UCSC	University of California, Santa Cruz
UKCCCR	United Kingdom Coordinating Committee of Cancer Research
VAF	variant allelic fraction
VCL	vinculin
VpP	variant present in parental
VpPR	variant present in parental and resistant
VpR	variant present in resistant
WGBS	whole genome bisulfite sequencing
WGS	whole genome sequencing
w/v	weight by volume

ZUSAMMENFASSUNG

Das duktale Adenokarzinom der Bauchspeicheldrüse (PDAC) ist durch eine enorme Resistenz gegen alle bisher getesteten Therapien gekennzeichnet, deren Ursache weitgehend unverstanden und vermutlich multifaktoriell ist. Um verschiedene Regulationsebenen in MEK-Inhibitor (MEK_i) resistentem PDAC zu untersuchen, wurden (Epi-)Genom-, Transkriptom- und Proteomanalysen integriert und durch funktionelle Analysen ergänzt. Dazu wurde ein auf primären, von einem genetisch modifizierten Maus-Modell abgeleiteten, PDAC Zelllinien basierendes *in vitro* Modell generiert.

Trotz fehlendem Tumorstroma entwickelten alle zehn initial MEK_i sensitiven Zelllinien eine MEK_i Resistenz, sodass ein zell-intrinsischer Mechanismus angenommen werden konnte. Die resistente Zellpopulation entstand durch Expansion eines einzelnen Zellklons ohne Hinweise auf direkt resistenzverleihende Mutationen. Der resistente Phänotyp war durch Plastizität gekennzeichnet, die mit epithelialer-mesenchymaler Transition und einem PDAC Subtypen-Wechsel hin zum aggressiveren mesenchymalen Subtyp einherging. Des Weiteren führte die Abwesenheit von MEK_i im Kulturmedium zu einem sukzessiven Resistenzverlust. Unter Einbeziehung dieses dritten Zellstadiums war es mittels einer genomweiten DNA Methylierungsanalyse möglich, Regionen zu definieren, deren differentielle Methylierung mit dem Grad der MEK_i Resistenz korrelierte. Dabei wurde in den resistenten Zellen eine adaptive DNA Hypermethylierung von regulatorischen Elementen wie Enhancern und Transkriptionsfaktorbindestellen nachgewiesen. Zusätzlich konnte durch Integration der Methylierungsdaten mit Expressionsanalysen die MEK_i-abhängige Modulation von CASP3 identifiziert werden. Die daraus resultierende Attenuation von MEK_i-induzierter Apoptose wurde durch Inhibition von DNA Methyltransferasen (DNMTs) aufgehoben, wobei nur die resistenten Zellen eine DNMT-Inhibitor Sensitivität aufwiesen.

Zusammenfassend konnten im Rahmen dieser Arbeit bekannte Resistenzphänomene wie ein Subtypenwechsel und die Vermeidung von Therapie-induzierter Apoptose in den Kontext umfassender (Epi-)Genomanalysen gesetzt werden. Insgesamt kann aus den Daten ein Konzept von MEK_i Resistenz im PDAC als klonale Selektion von Zellen mit epigenetischer Plastizität, die eine Adaption an die Therapie unter anderem durch Attenuation von MEK_i-induzierter Apoptose ermöglicht, abgeleitet werden. Zusammen mit den dynamischen DNA Methylierungsänderungen bei An- und Abwesenheit von MEK_i birgt die alleinige DNMT-Inhibitor Sensitivität der resistenten Zellen das Potential, MEK_i-basierte Therapien von PDAC Patienten zu verbessern.

SUMMARY

Therapy resistance represents a hallmark of pancreatic ductal adenocarcinoma (PDAC) and is understood as a multifactorial process. The present work integrated comprehensive (epi-)genomics, transcriptome and proteome analyses complemented by functional assays to study MEK inhibitor (MEK_i) resistance in PDAC at different levels of regulation. This multi-omics approach was applied to an *in vitro* model based on primary cell lines derived from a genetically modified mouse model that develops spontaneous PDAC. Thereby, influencing factors such as interindividual differences and stromal cell contamination were minimized in order to prevent distortion of global analyses. All ten initially MEK_i sensitive cell lines analyzed were able to develop resistance independently of a tumor microenvironment, indicating that in this model system, resistance relied on cell-intrinsic mechanisms.

The resistant cells emerged based on the expansion of a single cell clone, but whole genome sequencing revealed no evidence for resistance as a direct consequence of pre-existing or acquired mutations. The underlying mechanism was associated with phenotypic plasticity involving epithelial-to-mesenchymal transition in accordance with a PDAC subtype switch to the more aggressive mesenchymal-like subtype. In addition, reversibility of the resistant phenotype was observed in the absence of MEK_i. The inclusion of this third state in an unbiased genome-wide DNA methylation analysis enabled the identification of differentially methylated regions that correlated with the degree of MEK_i resistance. An adaptive DNA hypermethylation pattern was linked to regulatory elements such as active enhancers and transcription factor binding sites. By integrating methylome with expression data a methylation associated modulation of CASP3 expression and activity was identified. The resulting attenuation of treatment-induced apoptosis could be reversed by DNA methyltransferase inhibition, for which a remarkable sensitivity was detected exclusively in the resistant cells.

Overall, it was possible to embed known resistance phenomena as tumor subtype switching and cell death evasion into the context of comprehensive (epi-)genomics. This study proposes a concept of MEK_i resistance in PDAC based on the selection of a cell clone with epigenetic plasticity that enables treatment adaption. The identified dynamic DNA methylation changes in the presence and absence of MEK_i and the distinct vulnerability of the resistant cells to DNA methyltransferase inhibitors hold the potential to improve MEK_i-based therapy of PDAC patients.

1 INTRODUCTION

1.1 The human pancreas

The human pancreas is an elongated glandular organ located behind the stomach in the upper abdomen (Shih *et al.*, 2013) (Figure 1-1A). Macroscopically, it can be divided into head, neck, body and tail. Its two main functions are mediated by distinct compartments and include the production of pancreatic juice for digestion as well as control of the blood sugar levels (Edlund, 2002). The larger exocrine pancreas is mainly formed by acinar cells secreting a variety of digestive enzymes and by bicarbonate ion-producing ductal cells, which form a complex tubular system that delivers the molecules into the duodenum (Edlund, 2002; Grapin-Botton, 2005) (Figure 1-1B). The endocrine tissue makes up less than 5 % of the adult pancreas. It is organized in the so-called islets of Langerhans which consist of five different types of hormone producing cells (Figure 1-1B).

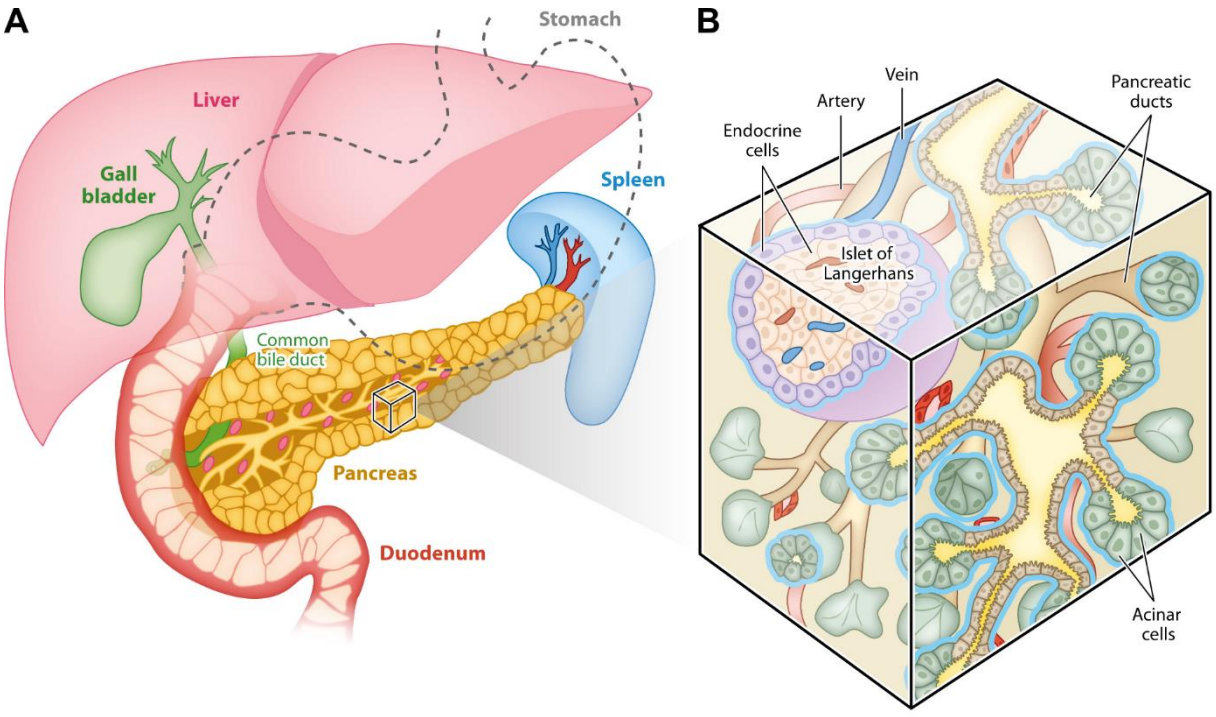

Figure 1-1: Anatomy (A) and cellular composition (B) of the human pancreas

(From: Shih *et al.*, 2013; Reproduced with permission from the Annual Review of Cell and Developmental Biology, Volume 29 © 2013 by Annual Reviews, http://www.annualreviews.org).

Insulin-producing beta cells account for the largest proportion (50-75 %) and together with glucagon-secreting alpha cells that make up around 25-35 % of the islets they are crucial for blood sugar homeostasis (Noguchi and Huising, 2019). Upon food intake,

insulin is released, stimulating glucose uptake in liver, muscles and fat tissue while simultaneously inhibiting glycogenolysis and gluconeogenesis in the liver, which together lead to a decrease of the blood sugar level (Edlund, 2002; Noguchi and Huising, 2019). In contrast, glucagon secretion is triggered at low blood glucose levels and enhances glycogenolysis and gluconeogenesis to restore normoglycemia in the blood (Noguchi and Huising, 2019). Delta cells account for about 5-10 % of the islets of Langerhans and due to their secretion of somatostatin they have amongst others an inhibitory and thereby regulatory function on the hormone release of alpha and beta cells (Edlund, 2002). Additionally, pancreatic-polypeptide-producing cells and epsilon cells that release ghrelin can be found at low frequencies (Noguchi and Huising, 2019).

1.2 Pancreatic ductal adenocarcinoma

Different types of pancreatic cancer can arise from both the exo- and the endocrine compartment. However, pancreatic ductal adenocarcinomas (PDACs) represent the largest group, accounting for more than 90 % of all reported cases (Hidalgo *et al.*, 2015). The following work focused exclusively on this tumor type.

1.2.1 Epidemiology and clinicopathology of human PDAC

With a 5-year survival rate < 8 % PDAC belongs to the deadliest tumor entities (Kleeff *et al.*, 2016). The median survival for patients suffering from a resectable tumor is 17-23 months and only 4-6 months for metastatic patients (Vincent *et al.*, 2011).

In 2018, nearly 460,000 new pancreatic cancer cases worldwide were registered ranking it on the 11th position of new tumor cases. However, it was the 7th most common cause of cancer deaths. The incidence is predicted to rise over the next decade, possibly due to the higher life expectancy of the population, as age has a major impact on the development of pancreatic cancer (Kleeff *et al.*, 2016; Rahib *et al.*, 2014). In median, the diagnosis is made at the age of 72 (Raimondi *et al.*, 2009). Further risk factors are environmental factors, mainly smoking, alcohol consumption and obesity. Additionally, diabetes and chronic pancreatitis lead to an increased risk for developing pancreatic cancer, although the sudden onset of diabetes can also be one of the symptoms (Raimondi *et al.*, 2009). A minority of 5-10 % of pancreatic cancers are due to hereditary germline mutations of *BRCA2*, *PALB2*, *CDKN2A*, *STK11* and *PRSS1* (Raimondi *et al.*, 2009; Vincent *et al.*, 2011). In total, only 25-30 % of the cases can be associated with known risk factors (Kleeff *et al.*, 2016).

The symptoms of early-stage PDACs are usually rare or non-specific, which explains why most diagnoses are made in advanced stages. Typically patients suffer from pain in the abdomen or mid-back, observe jaundice and weight loss (Vincent *et al.*, 2011). Biomarker for early detection are lacking, but tumor recurrence, progression and therapy response can be monitored by the carbohydrate antigen 19-9 (CA 19-9) serum level. However, elevated CA 19-9 is not specific for PDAC and about 5-10 % of the Caucasian population are Lewis antigen negative and therefore do not express any CA 19-9 (Hidalgo, 2010). If a PDAC is suspected, imaging techniques such as multidetector CT and ultrasound should be used to confirm the diagnosis, predict the resectability of the tumor and define the metastatic status (Hidalgo, 2010; Kleeff *et al.*, 2016; Leitlinienprogramm Onkologie (Deutsche Krebsgesellschaft. Deutsche Krebshilfe. AWMF), 2013).

1.2.2 Biology and molecular characteristics of human PDAC

Three major types of PDAC precursor lesions have been described: microscopically small pancreatic intraepithelial neoplasia, larger intraductal papillary mucinous neoplasia and mucinous cystic neoplasms (Riva *et al.*, 2018). However, their relationship and potential differences in the evolving PDACs remain poorly understood (Hezel *et al.*, 2006).

PDACs are characterized by desmoplasia, a dense stroma, creating a hypoxic, nutrient-deprived and immunosuppressive tumor microenvironment (Kleeff *et al.*, 2016). Furthermore, tumor-stromal crosstalk influences tumor growth and can contribute to intratumoral heterogeneity (Erkan *et al.*, 2012; Ligorio *et al.*, 2019; Nicolle *et al.*, 2017). In contrast, other studies suggest a protective function of tumor stroma and its depletion would lead to more aggressive PDACs (Neesse *et al.*, 2015; Rhim *et al.*, 2014).

The molecular landscape of PDACs is complex and heterogeneous (Figure 1-2). Genetically, only four commonly mutated genes (*KRAS*, *TP53*, *CDKN2A*, *SMAD4*) have been detected, while a plethora of rare alterations in various genes can be found (Cancer Genome Atlas Research Network, 2017; Chan-Seng-Yue *et al.*, 2020; Waddell *et al.*, 2015).

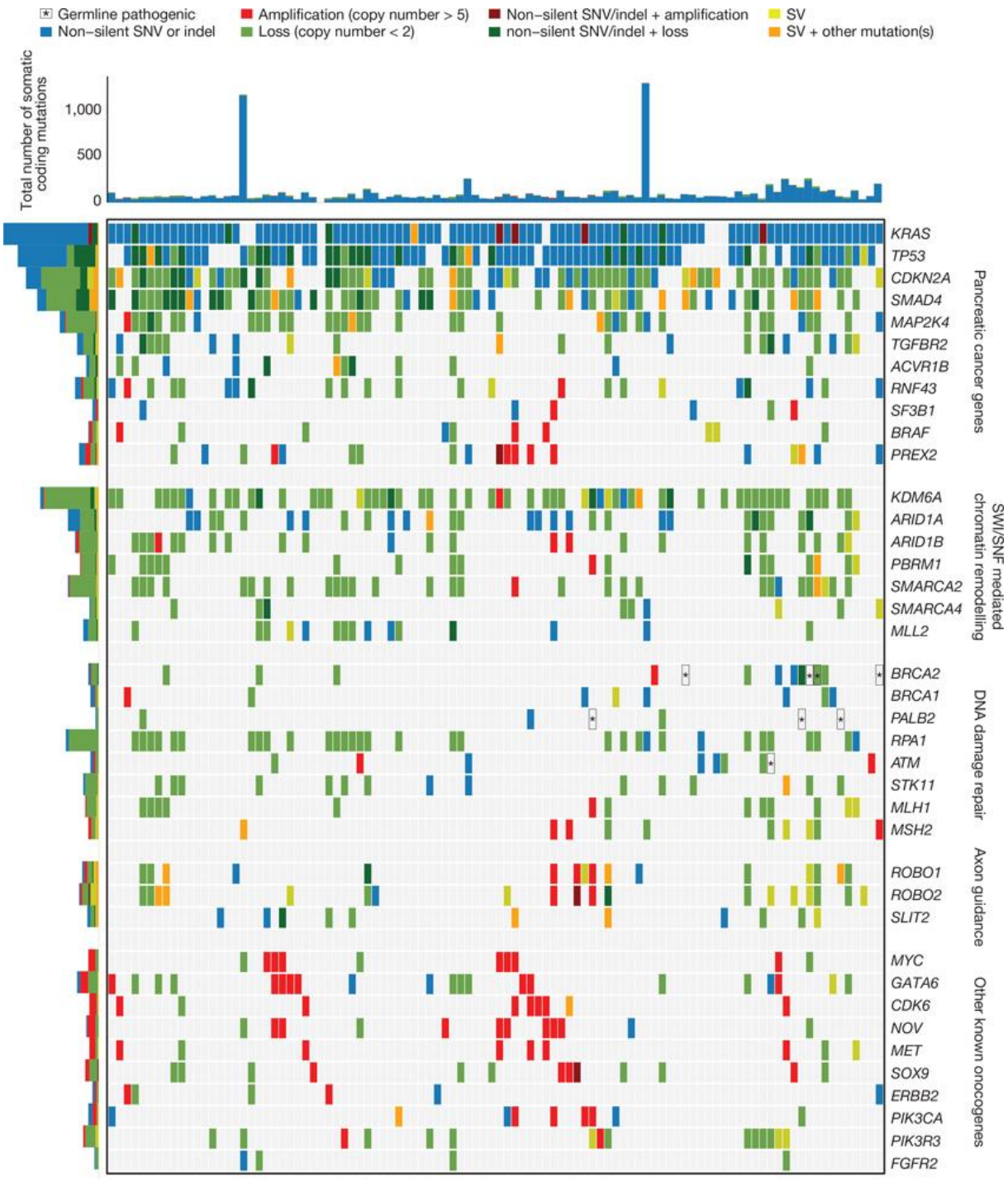

Figure 1-2: Mutational landscape of PDAC analyzed by whole genome sequencing

The oncomap displays single nucleotide variants (SNVs), copy number alterations, insertions and deletions (indel) and structural variants (SVs) of selected genes in 100 primary PDACs and corresponding germline samples derived from circulating lymphocytes. (From: Waddell et al., 2015; Reproduced with permission from Springer Nature Customer Service Centre GmbH).

Activating *KRAS* mutations, which are known to be essential for PDAC tumorigenesis and progression are found in more than 90 % of the tumors and are already present in many non-invasive precursor lesions (Collins *et al.*, 2012; Ying *et al.*, 2016).

Since subtyping of PDACs based on their genetic alterations failed, it is most likely, that the remarkable heterogeneity observed not only in PDAC, but in many tumor entities, is mediated beyond the genetic level (Assenov *et al.*, 2018; Lomberk *et al.*, 2019). There is growing evidence that epigenetic modulation (1.3) contributes to the diversity of tumor cells and their ability to react upon environmental stimuli (Assenov *et al.*, 2018). So far, the only reproducible PDAC subtypes on the molecular level could be identified based on transcriptome data (Bailey *et al.*, 2016; Cancer Genome Atlas Research Network, 2017; Collisson *et al.*, 2011; Moffitt *et al.*, 2015). Notably, epigenetic profiling of DNA methylation, regulatory RNA expression and chromatin states could reproduce the transcriptome-defined subtypes (Bailey *et al.*, 2016; Lomberk *et al.*, 2018; Nicolle *et al.*, 2017). Common to all studies is the description of a more epithelial-like subtype (described as classical or pancreatic progenitor subtype) and a mesenchymal-like subtype (termed quasi-mesenchymal, squamous or basal-like subtype throughout the different studies), which is associated with a worse prognosis. Their clinical relevance for therapeutic options is currently under evaluation. Moffitt and colleges (Moffitt *et al.*, 2015) showed a larger benefit of adjuvant therapy in the mesenchymal subtype.

1.2.3 Therapy of human PDAC

In general, PDACs are characterized by a tremendous intrinsic or acquired resistance against conventional chemotherapy and radiation but also all targeted approaches that have been applied so far (Ciliberto *et al.*, 2016; Long *et al.*, 2011) (1.4). Furthermore, the only four commonly mutated genes in PDAC are not yet druggable. The choice of therapy depends on the tumor stage and the physical condition of the patient usually measured by Eastern Cooperative Oncology Group (ECOG) score (Figure 1-3). Standard of care for patients with resectable disease remains surgery followed by adjuvant chemotherapy with the nucleoside analogue gemcitabine or the nucleobase analogue 5-fluoruracil (Hidalgo, 2010; Kleeff *et al.*, 2016). To date, tumor resection is the only potentially curative therapy for PDAC but only available for less than 20 % of the patients (Garrido-Laguna and Hidalgo, 2015). However, despite adjuvant chemotherapy, around 80 % of resected patients will relapse and die from their disease (Kleeff *et al.*, 2016; Leitlinienprogramm Onkologie (Deutsche Krebsgesellschaft. Deutsche Krebshilfe. AWMF), 2013). The prognosis for a non-resectable, locally advanced disease is even worse meaning a median survival of 12-14 months which in case of metastasis further decreases to 4-6 months. (Hidalgo, 2010; Vincent *et al.*,

2011). Currently, gemcitabine monotherapy or combination chemotherapy are recommended for palliative therapy. Radiotherapy is only indicated for symptomatic metastases (Kleeff *et al.*, 2016; Leitlinienprogramm Onkologie (Deutsche Krebsgesellschaft. Deutsche Krebshilfe. AWMF), 2013).

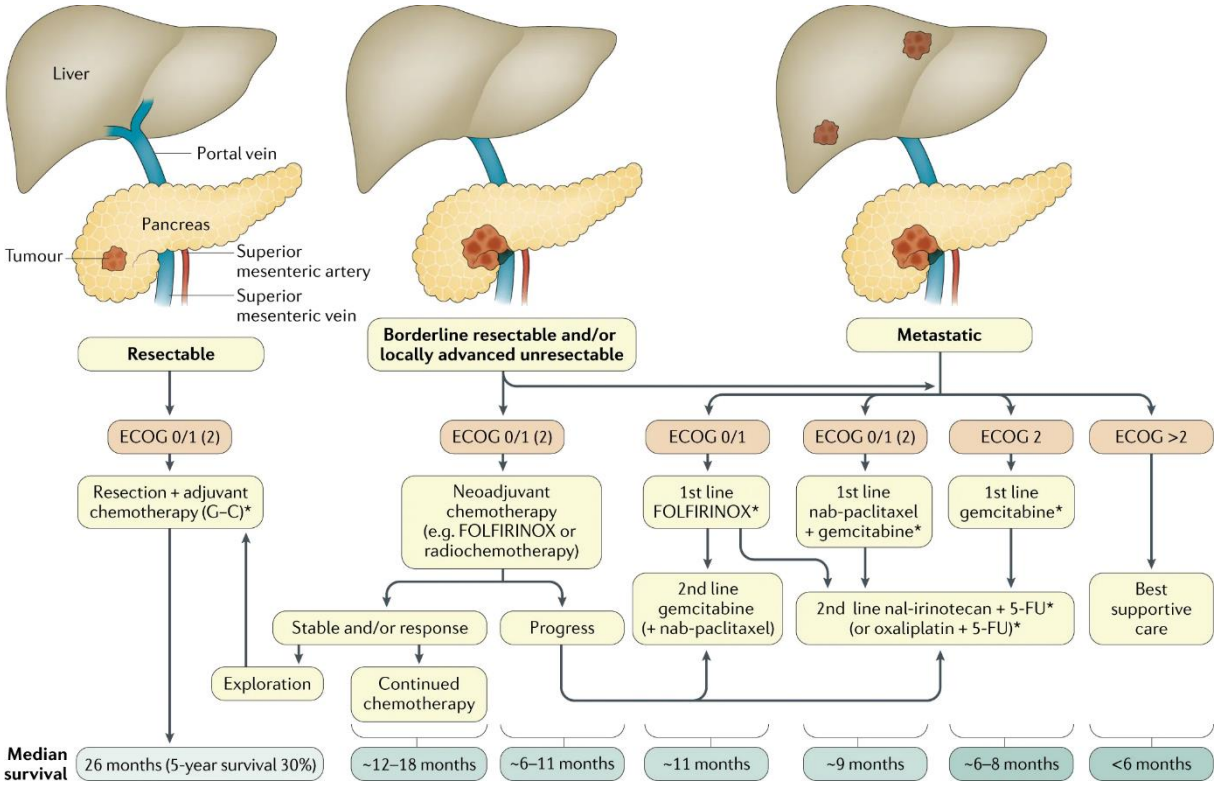

Figure 1-3: Current recommended treatment schema for PDAC according to the tumor stages and the physical condition of the patients

Physical conditions were categorized according to the Eastern Cooperative Oncology Group (ECOG) score.
(5-FU, 5-fluorouracil; FOLFIRINOX, folinic acid, fluorouracil, irinotecan and oxaliplatin; G−C, gemcitabine−capecitabine; nab, nanoparticle albumin-bound; nal, nanoliposomal. From: Neoptolemos *et al.*, 2018; Reproduced with permission from Springer Nature Customer Service Centre GmbH).

With increasing knowledge of the molecular mechanisms underlying pancreatic cancer, numerous clinical studies have evaluated the efficacy of targeted therapies (reviewed in (Neoptolemos *et al.*, 2018; Ottaiano *et al.*, 2017)). The only significant benefit has so far been achieved with the EGFR inhibitor erlotinib in combination with gemcitabine (Moore *et al.*, 2007). However, the effect was marginal and markers to identify patients that could likely benefit stronger than others are still missing (Garrido-Laguna and Hidalgo, 2015; Neoptolemos *et al.*, 2018). Current pre-clinical and clinical studies are focusing on different fields: targeting of tumor microenvironment either to enhance immune reaction or to improve drug delivery across the dense tumor stroma;

or inhibition of essential pathways in the tumor cells. As activation *KRAS* mutations are found in more than 90 % of PDACs, it is regarded as a promising therapeutic target. Inhibitors for targeting of the *KRAS* p.G12C variant are available, but it only accounts for about 1 % of the *KRAS* mutations found in PDAC (Lim *et al.*, 2014; Ostrem *et al.*, 2013; Waters and Der, 2018). Direct inhibitors for the most frequent p.G12D and p.G12V variants are still missing. Indirect KRAS targeting e.g. by inhibition of post-translational modifications or membrane-accessibility of the protein were ineffective for the treatment of PDACs (Collins and Pasca di Magliano, 2013; Macdonald *et al.*, 2005; Waters and Der, 2018). In contrast, potent and specific inhibitors for downstream KRAS effectors e.g. mitogen-activated protein kinase kinases 1 and 2 (MEK1/2) exist. Although promising pre-clinical results have been obtained with cell lines, genetically-engineered mouse models (GEMMs) and patient-derived xenografts (PDX) (Collisson *et al.*, 2012; Vena *et al.*, 2015; Walters *et al.*, 2013), several clinical trials testing various MEK inhibitors (MEK_is) failed (Chung *et al.*, 2017; Infante *et al.*, 2014; Van Cutsem *et al.*, 2018; Van Laethem *et al.*, 2017). Several other trials targeting e.g. the phosphatidylinositol 3-kinase (PI3K) or (insulin-like growth factor 1 receptor) IGF1R pathways in combination with gemcitabine also revealed no benefit for PDAC patients (Ottaiano *et al.*, 2017). Due to rising evidence of epigenetic alterations (1.3.4) that contribute to PDAC development, heterogeneity and its remarkable therapy resistance (1.4.2), targeting of epigenetic modifications is under evaluation (Hessmann *et al.*, 2017). Several clinical trials are currently focusing on chromatin organization either by modulation of histone acetylation or the inhibition of bromodomain and extra-terminal motif (BET) proteins partly with combinatory chemotherapy (Hessmann *et al.*, 2017). In pre-clinical studies, a synergistic effect of the histone deacetylase inhibitor ($HDAC_i$) suberoylanilide hydroxamic acid (SAHA) with the BET inhibitor (BET_i) JQ1 could be demonstrated (Mazur *et al.*, 2015a). Low-dose treatment with the DNA methyltransferase inhibitor ($DNMT_i$) decitabine showed promising results in a genetic mouse model of PDAC (Shakya *et al.*, 2013).

Overall, regardless of improved early detection methods, there is an urgent need for new therapeutic strategies to treat PDAC. Not only the development of new drugs and the evaluation of promising drug combinations play an important role. In addition, an appropriate patient stratification is necessary to improve the efficacy especially of targeted therapies (Kleeff *et al.*, 2016; Neoptolemos *et al.*, 2018). Furthermore, a better understanding of potential intrinsic and acquired resistance mechanisms (1.4) will provide new therapeutic options for PDAC patients.

1.2.4 Pre-clinical models of PDAC

For a better understanding of PDAC's molecular characteristics and their translation into clinical advance, suitable pre-clinical model systems are needed. Several *in vitro* and *in vivo* models with different advantages and disadvantages have already been established. Two-dimensional (2D) cultivation of murine and human cell lines enables a time- and cost-efficient approach to study PDAC (Deer *et al.*, 2010). However, growing in monolayers on tissue culture plastic provides a highly artificial environment. Therefore, it is likely that aggressive, fast growing cell clones will be selected. Especially established cell lines, which are usually propagated over many years, harbor an additional risk of genetic drifts (Hwang *et al.*, 2016). In contrast, newly generated cell lines still seem to represent the genetic characteristics of their primary tumor (Knudsen *et al.*, 2017). Thus, shortly passaged cell lines should be preferred to the established ones. In 2015, the first three-dimensional (3D) organoid models of murine and human PDAC were described (Boj *et al.*, 2015). 3D cultivation increases cell-cell interactions and thus resembles the cellular organization observed *in vivo*. In contrast to the classical 2D approach, also normal and pre-neoplastic pancreas cells can be grown as organoids (Boj *et al.*, 2015). However, both 2D and 3D cell culture models lack the tumor stroma characteristic for PDAC (Hwang *et al.*, 2016). Nevertheless, it can be advantageous to exclude the heterogeneous influence of non-tumor cells on especially complex genome, methylome, transcriptome or proteome analyses (Moffitt *et al.*, 2015; Nicolle *et al.*, 2017; Schubeler, 2015).

The subcutaneous or orthotopic transplantation of cell lines into immunodeficient mice provides a way to compensate for some of their *in vitro* limitations. Further advantages are achieved by PDX generated from freshly resected pieces of primary tumor tissue (Mazur *et al.*, 2015b). PDX retain the genetic features of their primary tumor stably over several passages and can be used to predict clinical outcome (Hidalgo *et al.*, 2014; Knudsen *et al.*, 2017; Rubio-Viqueira *et al.*, 2006). However, successful engraftment is challenging and requires a certain amount of tumor tissue that is usually only available in the minority of PDAC patients whose tumor is resected (Hwang *et al.*, 2016).

The only way to model PDAC surrounded by an intact immune system are engineered mice exhibiting distinct tissue-specific mutations in onco- and/or tumor suppressor genes. For PDAC, a plethora of these models exists that recapitulate different stages of the human carcinogenesis (reviewed in (Gopinathan *et al.*, 2015; Mazur *et al.*, 2015b)). Pancreas-specific mutations are introduced by expressing e.g. the Cre

recombinase or flippase (FLP) under promotor control of the pancreas-specific transcription factors PDX1 or PTF1A that are both active during pancreatic organogenesis (Gopinathan *et al.*, 2015; Hingorani *et al.*, 2003). Sometimes off-target effects can be observed as PDX1 is also active in the epidermis and the developing foregut, while PTF1A is also expressed in the brain (Mazur *et al.*, 2015b).

These recombinase expressing mice are crossed with strains containing the desired transgene. Thereby, either the expression of a mutated target gene is activated when a stop cassette flanked by recombinase recognition sites (LoxP for Cre recombinase; flippase recombinase target (FRT) for FLP) is excised or an allele is silenced when recognition sites flank parts of its coding region (Gopinathan *et al.*, 2015).

The most common model for PDAC is based on a heterozygous activating *Kras* p.G12D mutation together with a heterozygous *Trp53* p.R172H mutation or its homozygous deletion (Bardeesy *et al.*, 2006; Hingorani *et al.*, 2005). These models recapitulate the human disease, thus proving a powerful tool to study tumorigenesis (Hingorani *et al.*, 2005). PDACs develop with nearly 100 % penetrance after a short latency of around 6 to 12 weeks (Gopinathan *et al.*, 2015). Despite all advantages, GEMMs remain limited mainly by the interspecies differences between mouse and human. Furthermore, their generation is complex, which makes them comparatively expensive and time-consuming (Mazur *et al.*, 2015b).

1.3 Epigenetics

1.3.1 Fundamental principles

The term epigenetics goes back to Conrad Waddington, who defined it in the early 1940s as ‘the branch of biology which studies the causal interactions between genes and their products, which bring the phenotype into being’ (Waddington, 1942, 1968). Today, epigenetics is understood as the study of all changes that modify gene expression and the cellular phenotype without modification of the underlying DNA sequence (Goldberg *et al.*, 2007). It comprises changes on the chromatin level such as DNA methylation and various histone modifications as well as post-transcriptional regulation by RNA interference (Esteller, 2008) (Figure 1-4). Interaction between the different mechanisms is possible and modifications can influence each other.

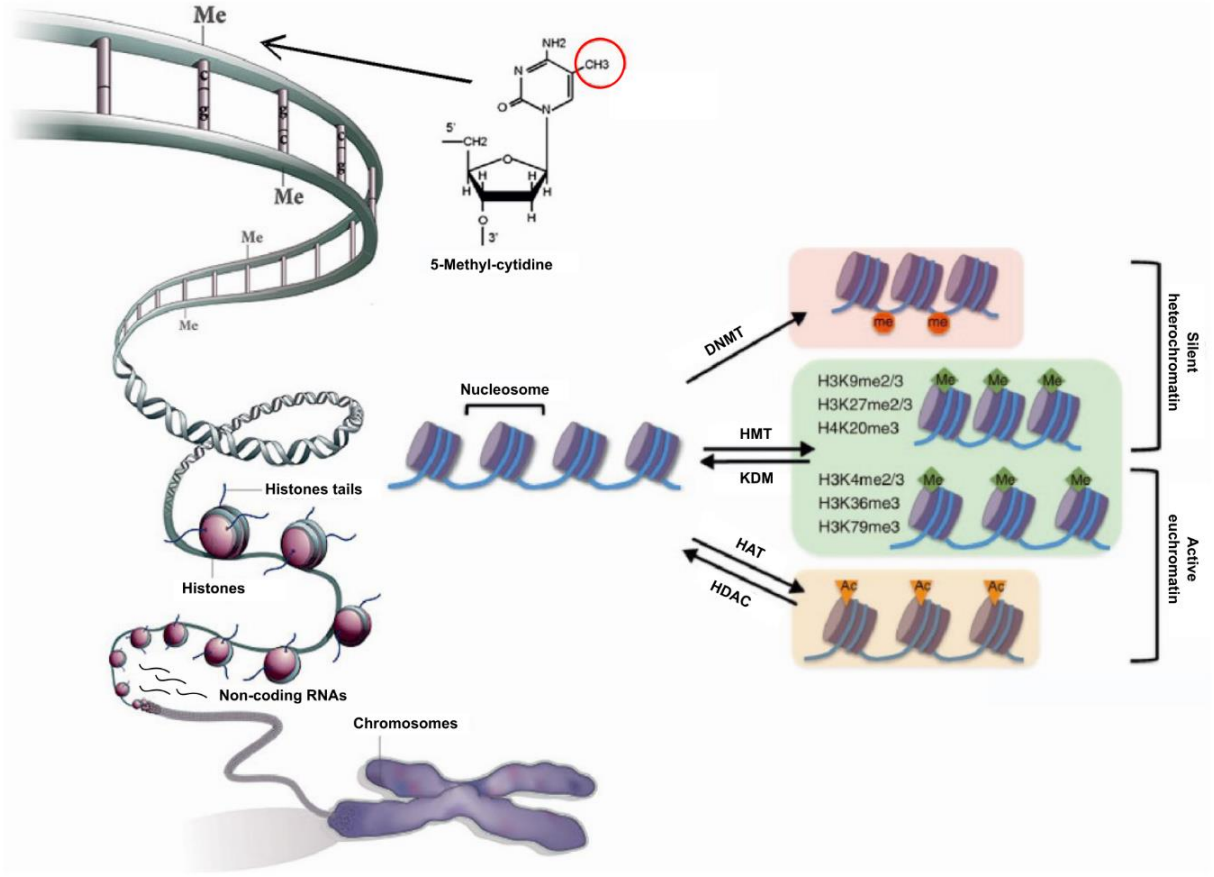

Figure 1-4: Schema of epigenetic chromatin regulation mediated by epigenetic readers that e.g. catalyze DNA methylation or histone modification as methylation and acetylation

(DNMT, DNA methyltransferase; HMT, histone methyltransferase; KDM, histone lysine demethylase; HAT, histone acetyltransferase; HDAC, histone deacetylase. Adapted from: Maleszewska and Kaminska, 2013. Distributed under the Creative Commons Attribution License CC BY 3.0).

Chromatin is the complex organizational structure of an eukaryotic genome to condense around 2 m of DNA per cell. It is composed of repeating nucleosomes consisting of 146 bp DNA wrapped 1.65 times around an octamer of histone proteins (Luger *et al.*, 1997). Four different core histones exist, of which H2A and H2B as well as H3 and H4 build up a heterodimer. Afterwards, two dimers each assemble to the histone octamer. In addition, the linker DNA between the nucleosomes is occupied and further condensed by histone H1. Nucleosome positioning is dynamically mediated by adenosine triphosphate (ATP)-dependent nucleosome remodeling complexes in response to various in- and extrinsic stimuli (Klemm *et al.*, 2019).

The N-terminal histone tails that protrude from the nucleosome core but also the core itself can be modified by a plethora of post-translational modifications providing a dynamic level of transcriptional regulation by altering chromatin structure and function (Zhao and Shilatifard, 2019). In addition, DNA can be modified by methylation where

a methyl group is covalently bound to the carbon at position 5 in the pyrimidine ring of cytosines (5mC). There is a complex enzymatic network of epigenetic writers that add chromatin modifications, erasers that remove them, and readers that interact with them through specific domains, thereby recruiting transcription factors to the DNA (Kouzarides, 2007).

Epigenetic modulation of gene expression is involved in various fundamental cellular processes e.g. the global reprogramming during gametogenesis and embryogenesis, the regulation of imprinted genes or the X-chromosome inactivation in females, maintenance of genome integrity through silencing of transposable elements and cell differentiation (Li, 2002). Epigenetic alterations are potentially found in all cancers and include e.g. aberrant DNA methylation patterns, changes in histone modifications and mutations in epigenetic modulator enzymes (Baylin and Jones, 2016; Plass *et al.*, 2013; Shen and Laird, 2013).

1.3.2 Histone modifications

Histone modifications regulate chromatin and gene expression either by changing the physical contact between nucleosomes and DNA or the recruitment of epigenetic readers (Kouzarides, 2007). The effect depends on the modification itself and its position on the histone octamer. Several modification types have been described, including acetylation, methylation, phosphorylation, ubiquitination and various less frequently occurring or newly identified modifications. (Tan *et al.*, 2011; Zhao and Shilatifard, 2019). In general, histone modifications are enzymatically reversible. Both adding and removal, occur rapidly, thereby enabling a dynamic regulation of chromatin and transcription (Barth and Imhof, 2010; Katan-Khaykovich and Struhl, 2002).

The acetylation of lysines neutralizes their positive charge, thereby weakening their affinity for the negatively charged DNA backbone. Thus, the chromatin structure is less condensed and enables gene transcription (Lee *et al.*, 1993; Tse *et al.*, 1998). Furthermore, acetylated lysines are recognized by bromodomain-containing proteins that serve as a platform for chromatin remodeling complexes and transcriptional regulators (Fujisawa and Filippakopoulos, 2017). For example, the acetylation of H3 at lysine 27 (H3K27ac) is considered as a marker for active enhancers (Creyghton *et al.*, 2010). Lysine acetylation is catalyzed by histone acetyltransferases (HATs), whereas the removal is mediated by histone deacetylases (HDACs). Both processes can occur rapidly within minutes (Katan-Khaykovich and Struhl, 2002).

Histone methylation of nitrogen atoms on lysine and arginine residues has a dual role depending on its location and the number of added methyl groups. While H3K4 mono-methylation (H3K4me1) and tri-methylation (H3K4me3) are amongst others associated with active transcription and found in enhancer as well as promotor regions, H3K27 methylation is an example characteristic for repressed chromatin (Cao *et al.*, 2002; Greer and Shi, 2012; Heintzman *et al.*, 2007). Activating H3K4me3 and repressive H3K27me3 marks can be found together in so called bivalent domains mainly in promotors of developmental genes in pluripotent stem cells keeping the gene in poised state that can be rapidly activated upon differentiation (Bernstein *et al.*, 2006; Mikkelsen *et al.*, 2007). Bivalent chromatin domains have also been described in cancer and their disturbance might contribute to an aberrant expression of developmental genes (Bernhart *et al.*, 2016).

Histone methyltransferases (HMTs) add methyl groups using S-adenosyl methionine as a donor and histone lysine demethylases (KDMs) remove them (Rea *et al.*, 2000; Shi *et al.*, 2004). Compared to acetylation, methylation is suggested to be more stable (Zee *et al.*, 2010). Several proteins that harbor a methyl binding domain are known to interact with methylated histones (Greer and Shi, 2012).

Phosphorylation of histones mediated by kinases and removed by phosphatases is mainly associated with DNA repair and chromatin condensation during mitosis and meiosis (Celeste *et al.*, 2003; Wei *et al.*, 1999; Zhao and Shilatifard, 2019). In addition, phosphorylation is linked to open chromatin and actively transcribed genes (Dawson *et al.*, 2009; Dawson *et al.*, 2012).

In contrast to the other three small molecule modifications, ubiquitination is the adding of one or more 8.5 kDa ubiquitin proteins mainly to H2A and H2B (Cao and Yan, 2012). Ubiquitinated H2A is associated with gene silencing while ubiquitination of H2B mostly correlates with active gene transcription (Zhao and Shilatifard, 2019). Both mono- and polyubiquitination of H2A and H2B are found at DNA damage sites and are essential for the recruitment of the repair machinery (Cao and Yan, 2012).

1.3.3 DNA methylation

DNA methylation in mammals occurs almost exclusively at cytosines of a cytosine-guanine dinucleotide (CpG) sequence in which a cytosine is followed by a guanine (Sharma *et al.*, 2010a). In a healthy somatic cell, most of the CpGs in the genome are methylated while CpG islands, genomic regions with a high CpG density are mainly unmethylated (Jones, 2012). DNA methylation does not affect C to G base pairing,

however, 5mCs are susceptible for deamination resulting in a C to T transition mutation (Schubeler, 2015). Therefore, CpGs are underrepresented in the genome but locally enriched in CpG islands that are usually unmethylated and thereby protected for C to T transitions (Jones, 2012). Around 70 % of all gene promotors harbor a CpG island in their vicinity (Saxonov *et al.*, 2006). In general, CpG island methylation of promotors is associated with gene silencing. It is still being discussed, whether DNA methylation is causal for transcriptional silencing or the consequence of transcriptional inactivation to maintain the inactive state (Bestor *et al.*, 2015; Jones, 2012; Schubeler, 2015). In contrast to CpG island methylation, gene body methylation has been shown to be associated with actively transcribed genes. Thereby, DNA methylation is potentially involved in the regulation of splicing and the maintenance of genome integrity due to silencing of transposable elements (Chodavarapu *et al.*, 2010; Jones, 2012; Maunakea *et al.*, 2013). DNA methylation of regulatory elements can either enable the binding of methylation-specific transcription factors or prevent the binding of others (Xuan Lin *et al.*, 2019; Yin *et al.*, 2017). Overall, the function of DNA methylation seems context-specific and depends on its localization in the genome. The DNA methylation pattern of a cell is highly tissue-specific and also relies on its differentiation status (Roadmap Epigenomics Consortium, 2015; Wallner *et al.*, 2016). In mammals three DNA methyltransferases (DNMTs) are known that catalyze the transfer of a methyl group donated by S-adenosyl methionine to the fifths carbon atom of cytosines (Goll and Bestor, 2005). While DNMT3A and DNMT3B *de novo* methylate DNA, DNMT1 maintains DNA methylation during cell division thereby enabling the propagation of DNA methylation patterns to the daughter cell (Greenberg and Bourc'his, 2019). Hemi-methylated DNA as a result of DNA replication is bound by the E3 ubiquitin-protein ligase UHRF1 that recruits DNMT1 (Nishiyama *et al.*, 2013). For *de novo* methylation, chromatin binding of DNMT3A and DNMT3B is prevented or promoted by distinct histone modifications (Greenberg and Bourc'his, 2019).

DNA demethylation can either occur passively when 5mC is not restored on the daughter strand after DNA replication or actively catalyzed by ten eleven translocation (TET) enzymes (Schubeler, 2015). Three TET enzymes with partially redundant function have been identified that oxidase 5mC to 5-hydroxymethylcytosine and further via 5-formylcytosine to 5-carboxylcytosine (Li and Zhang, 2014). The unmethylated cytosine is either restored by passive demethylation as these oxidized 5mC variants cannot be recognized as hemi-methylated during cell division or an active, glycosylase-dependent DNA repair mechanism (Li and Zhang, 2014).

1.3.4 Epigenetic dysregulation in PDAC

In addition to the genetic alterations (1.2.2), which alone cannot explain the remarkable tumor heterogeneity, PDACs exhibit a broad spectrum of epigenetic modifications (Lomberk *et al.*, 2019). Several studies found mutations in epigenetic modifiers, which are mainly involved in chromatin remodeling and dysregulation of regulatory RNAs (Peng *et al.*, 2016; Waddell *et al.*, 2015; Witkiewicz *et al.*, 2015). Aberrant DNA methylation of various genes can already be detected in pre-neoplastic lesions of the pancreas (Sato *et al.*, 2008; Sato *et al.*, 2002). Comparable to other cancers, in PDAC several genes are silenced by promotor hypermethylation including *CDKN2A* one of the four commonly mutated genes (Kleeff *et al.*, 2016; Nones *et al.*, 2014; Sato and Goggins, 2006; Schutte *et al.*, 1997). A loss of the protein kinase LKB-1 resulted in metabolic changes including increased serine biosynthesis and DNMT upregulation thereby leading to DNA hypermethylation and increased $DNMT_i$ sensitivity (Kottakis *et al.*, 2016). It has also been reported that the downregulation of miRNA-192, which promotes PDAC progression, is mediated by promoter hypermethylation (Botla *et al.*, 2016). The use of DNA methylation based biomarkers in cell-free DNA of patient plasma or serum as a prognostic factor or for early detection has been discussed but did not find clinical application (Henriksen *et al.*, 2017; Yi *et al.*, 2013). Hypomethylation of gene promotors as of *VAV1*, *MET* and *ITGA2* has also been reported in PDAC, which is correlating with their activation (Fernandez-Zapico *et al.*, 2005; Nones *et al.*, 2014; Sato and Goggins, 2006).

A global reprogramming of DNA methylation and histone modifications was recently shown to be involved in the evolution of PDAC distant metastasis (McDonald *et al.*, 2017). Consistently, Roe and colleges (Roe *et al.*, 2017) described various changes of enhancer activity based on histone modification changes in organoids derived from murine PDAC tumors and metastasis. In several studies epigenetic alterations reflected PDAC tumor subtypes classified based on expression profiles which suggests a potential epigenetic control of transcriptional activity (Bailey *et al.*, 2016; Lomberk *et al.*, 2018; Nicolle *et al.*, 2017). In addition, DNA hydroxymethylation levels at regulatory regions differed between PDAC and non-neoplastic pancreatic epithelial cells (Bhattacharyya *et al.*, 2017).

1.4 Therapy resistance of cancer

1.4.1 Fundamental principles

Therapy resistance is one of the major challenges in cancer treatment. Tumors can already be resistant at treatment initiation (intrinsic resistance) or the resistance may develop as a consequences of therapy (acquired resistance) (Wang *et al.*, 2011b). In many cases both factors together contribute to therapy failure (Vasan *et al.*, 2019). In general, resistance can be understood as a multifactorial process, which depends on the type of therapy, the tumor type and its individual characteristics (Konieczkowski *et al.*, 2018) (Figure 1-5).

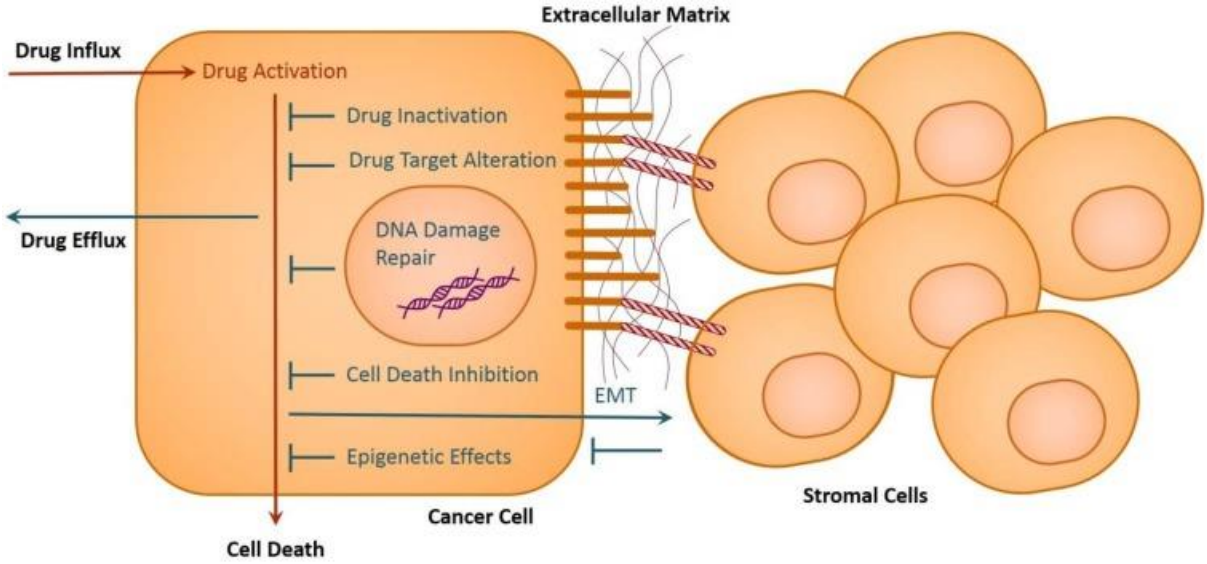

Figure 1-5: Potential resistance mechanisms of a tumor cell mediated intrinsically or by the tumor microenvironment

(EMT, epithelial-to-mesenchymal transition. From: Housman *et al.*, 2014. Distributed under the Creative Commons Attribution License CC BY 3.0).

In addition to intrinsic mechanisms of the tumor cells, host factors of the patient can cause a lack of response either by poor absorption, rapid clearance or poor tolerance which forces a reduction of the applied dose (Gottesman, 2002). Furthermore, insufficient drug delivery through stroma-rich or poorly perfused tumors and high molecular weight agents can prevent their anti-cancer effect on the tumor (Gottesman, 2002). Besides the barrier effect, interaction via soluble factors with cells of the tumor microenvironment or extracellular matrix proteins can lead to a protection of the tumor cells against chemo- and targeted therapy but also radiation or immunotherapy (Konieczkowski *et al.*, 2018; Sethi *et al.*, 1999; Straussman *et al.*, 2012; Sun *et al.*, 2012). Resistance mediated by the tumor cell itself often involves unspecific

mechanisms as increased drug efflux by active transport, drug detoxification or decreased uptake which cause multi-drug resistance against several agents with unrelated structure and mechanism of action (Gottesman, 2002). Enhanced DNA damage response and evasion of cell death can also confer resistance mainly against cytotoxic drugs (Housman *et al.*, 2014). Furthermore, drug resistance is often accompanied by epithelial-to-mesenchymal transition (EMT) that is known to be linked to stem-cell properties enabling tumor cells to adapt to the treatment (Shibue and Weinberg, 2017). For targeted therapies, three superordinate mechanisms are known with pathway re-activation being the most frequent. Thereby, re-activation occurs either by alterations of the drug target, which impair the inhibitor binding, or by overexpressing the target, e.g. by gene amplification, or by altering upstream, downstream or parallel mediators in the same signaling pathway (Konieczkowski *et al.*, 2018). In addition, bypassing of the targeted pathway through the activation of an alternative pathway can also be observed during treatment (Konieczkowski *et al.*, 2018). In contrast to re-activation or bypassing, tumor cells can also lose their dependency for the targeted pathway by transition of their cell state e.g. through EMT (Konieczkowski *et al.*, 2018).

The chance that a tumor cell population contains a resistant clone that is able to grow out under the selective pressure of a treatment and leads to resistance is the higher, the larger the tumor size and the higher its mutation rate and heterogeneity (Vasan *et al.*, 2019). Therefore, early detection and start of therapy reduces the probability of resistance development (Vasan *et al.*, 2019). Monitoring the response under therapy and the resulting possibility to adjust the schema in a timely manner can help to detect and prevent resistances early on (Vasan *et al.*, 2019). In order to avoid resistance, combinatory therapy using agents with different modes of action seems promising. However, due to multi-drug resistance mechanisms the concept of combined chemotherapy is only successful in some forms of lymphoma, breast cancer or germ-cell cancer (Vasan *et al.*, 2019). It is therefore necessary to identify individual tumor vulnerabilities that can be targeted efficiently and simultaneously based on a rationale to enable deeper responses (Konieczkowski *et al.*, 2018; Vasan *et al.*, 2019). However, many known tumor drivers are still considered undruggable and several drug combinations result in severe toxicity (Konieczkowski *et al.*, 2018). Due to their higher flexibility and error rate compared to genetic mutations, there is rising evidence, that also epigenetic modifications confer resistance to tumor cells (Assenov *et al.*, 2018;

Jones *et al.*, 2016). Considering their reversibility, they represent a rewarding target for the treatment of resistant tumors.

1.4.2 Therapy resistance of PDAC

Resistance not only against conventional chemotherapy and radiation but also all targeted approaches tried so far is a hallmark of PDAC (Ciliberto *et al.*, 2016; Long *et al.*, 2011). As pointed out in 1.2.1, the fact that PDACs are usually diagnosed in advanced stages increases the risk for the occurrence of resistance (Vasan *et al.*, 2019). However, the underlying molecular mechanisms are still poorly understood. The dense stroma, which accounts for up to 80 % of the PDAC tumor mass, can act as a physical barrier that prevents drug delivery to the tumor cells (Erkan *et al.*, 2012; Provenzano *et al.*, 2012). In addition, inflammation of the surrounding tissue involving NF-κB and different proinflammatory cytokines is associated with resistance (Delitto *et al.*, 2015; Müerköster *et al.*, 2004). Several studies indicate that factors secreted by pancreatic stellate cells contribute to chemo- and radiotherapy resistance (Dauer *et al.*, 2017).

Also the tremendous intratumoral heterogeneity of PDAC contributes remarkably to its resistance (Wang *et al.*, 2011b). Furthermore, a metabolic reprogramming involving various glycolysis enzymes has been linked to chemoresistance (Grasso *et al.*, 2017). In accordance with the worse prognosis of mesenchymal PDAC subtypes (Bailey *et al.*, 2016; Collisson *et al.*, 2011), EMT characteristics correlate with treatment failure (Arumugam *et al.*, 2009; Wang *et al.*, 2011b). Expression changes of distinct miRNAs in resistant PDAC cells suggest mechanisms beyond gene alterations as underlying cause for drug insensitivity (Hessmann *et al.*, 2017; Swayden *et al.*, 2018; Wang *et al.*, 2011b).

Gemcitabine remains the current standard of care for PDAC patients (1.2.3). Due to its hydrophilic properties it needs nucleoside transporters to enter the cell, thus their downregulation causes gemcitabine resistance (Mackey *et al.*, 1998). To exhibit cytotoxicity, three intracellular phosphorylation steps are necessary. Thereby, the rate-limiting mono-phosphorylation is catalyzed by a deoxycytidine kinase, an enzyme whose downregulation can lead to resistance (Costantino *et al.*, 2009; Kroep *et al.*, 2002; Nakano *et al.*, 2007). The deregulation of other enzymes involved in gemcitabine metabolism e.g. in its inactivation is also associated with resistance (Amrutkar and Gladhaug, 2017). Attenuation of EMT increased gemcitabine sensitivity by upregulation of its transporters and enhanced proliferation of the tumor cells in a

GEMM of PDAC (Zheng *et al.*, 2015). In 2017, Geller and colleagues hypothesized that intratumoral bacteria found in 75 % of the tested PDAC samples could inactivate gemcitabine by their cytidine deaminase and thereby confer resistance (Geller *et al.*, 2017).

In contrast to gemcitabine, MEK_is target specifically the KRAS downstream kinases MEK1 and MEK2 thereby providing a rationale for treating PDACs that harbor an undruggable activating *KRAS* mutation in more than 90 % of the cases (Waddell *et al.*, 2015). Despite promising pre-clinical results, several clinical trials evaluating various MEK_i could not show any benefit for PDAC patients (Chung *et al.*, 2017; Infante *et al.*, 2014; Van Cutsem *et al.*, 2018; Van Laethem *et al.*, 2017). *In vitro* and in cell line-based PDAC xenografts, inhibition of KRAS upstream tyrosine phosphatase SHP2A abolishes acquired MEK_i resistance (Fedele *et al.*, 2018; Ruess *et al.*, 2018). Knock-down of YAP1, an effector of the Hippo pathway, lowered the IC50 of trametinib in pancreatic and other KRAS-driven cancer cell lines (Lin *et al.*, 2015). Recently, protective autophagy was shown to be enhanced during MEK pathway inhibition indicating a potential resistance mechanism (Bryant *et al.*, 2019; Kinsey *et al.*, 2019).

1.5 Aim of the study

Pancreatic ductal adenocarcinoma is an aggressive tumor entity characterized by a tremendous inter- and intraindividual heterogeneity and resistance to all therapeutic strategies evaluated so far. The four genes (*KRAS*, *TP53*, *CDKN2A*, *SMAD4*) that are commonly mutated in PDAC remain undruggable. More than 90 % of the cases harbor an activating *KRAS* mutation as key driver. Thus, targeting of the downstream mitogen-activated protein kinase kinases 1 and 2 seems promising. However, despite positive pre-clinical studies on MEK inhibitors (MEK_is), various clinical trials revealed no benefit to patients. The underlying mechanisms remain poorly understood. As emerging evidence supports treatment-induced resistance to be a multifactorial process, this work focused on a comprehensive characterization of MEK_i resistant PDAC at both the (epi-)genotype and the phenotype level. An *in vitro* model was generated based on primary cell lines derived from a genetically engineered PDAC mouse model. In a multi-omics approach different cell states upon resistance induction followed by drug withdrawal should be compared in order to identify differences that could potentially explain MEK_i resistance. Whole genome sequencing was used to investigate genetic alterations that might confer resistance. Additionally, cell population dynamics during the development of resistance should be examined. A drug screening approach indicated a potential relevance of treatment-induced DNA methylation changes, whereby little is known about this in PDAC so far. To evaluate in detail genomic regions affected by differential DNA methylation upon MEK_i treatment, the methylome of cell states with different MEK_i sensitivity should be investigated by whole genome bisulfite sequencing. Published data of chromatin states in PDAC and normal pancreas should be merged to estimate the methylation impact to regulatory regions active in PDAC. Phenotypically, the MEK_i-induced differential expression of RNAs and proteins should be addressed by RNA-sequencing and mass spectrometry, respectively. Finally, the different data types should be integrated and complemented by functional assays. This might provide a link between the resistant phenotype and an (epig-)genotype and thus lead to a novel strategy for overcoming MEK_i resistance.

Overall, this work should contribute to a better understanding of resistance mechanisms in PDAC with a focus on DNA methylation and tumor cell plasticity using MEK inhibition as an example. The identification of a targetable mechanism may provide a new window of opportunity for the treatment of PDAC patients.

2 MATERIALS AND METHODS

2.1 Materials

Standard consumables were not listed.

2.1.1 Cell lines

Ten different primary murine PDAC cell lines derived from tumors of ten different *Ptf1a*$^{wt/Cre}$*; Kras*$^{wt/LSL-G12D}$*; Trp53*$^{loxP/loxP}$ mice were used. Cell lines were kindly provided by Marija Trajkovic-Arsic (Institute for Developmental Cancer Therapeutics & Division of Solid Tumor Translational Oncology (DKTK/DKFZ partner site Essen), West German Cancer Center, University Hospital Essen, Germany). Polymerase chain reaction (PCR)-based mycoplasma testing was performed on a regular basis.

2.1.2 Culture Medium

All cell lines were cultivated in high-glucose Dulbecco's Modified Eagle medium (DMEM) (Life Technologies Europe BV, Bleiswijk, Netherlands) containing 10 % heat-inactivated fetal bovine serum (FBS) (Life Technologies Europe BV, Bleiswijk, Netherlands), 1 % penicillin/streptomycin (Life Technologies Europe BV, Bleiswijk, Netherlands), and 1 % non-essential amino acids (Sigma-Aldrich Chemie GmbH, Taufkirchen, Germany).

2.1.3 Inhibitors

Table 2-1: List of inhibitors used

Inhibitor	*Manufacturer*
Decitabine (5-Aza-2'-Deoxycytidine)	Sigma-Aldrich Chemie GmbH, Taufkirchen, Germany
JQ1	Cayman Chemical Company, Ann Arbor, MI , USA
Mocetinostat	Selleck Chemicals LLC, Houston, TX, USA
Suberoylanilide hydroxamic acid (SAHA)	Selleck Chemicals LLC, Houston, TX, USA
Trametinib (GSK1120212)	LKT Laboratories, St. Paul, MN, USA

2.1.4 Commercially available kits

Table 2-2: List of commercially available kits used

Kit	*Manufacturer*
12 – 230 kDa Wes Separation Module. 25 capillary cartridges	Bio-Techne GmbH, Wiesbaden, Germany
Anti-Rabbit Detection Module for Wes	Bio-Techne GmbH, Wiesbaden, Germany
Anti-Mouse Detection Module for Wes	Bio-Techne GmbH, Wiesbaden, Germany
Caspase-Glo® Assay	Promega GmbH, Madison, WI, USA
DNMT Activity Assay Kit (Fluorometric)	Abcam, Cambridge, UK
EZ DNA Methylation-Gold™ Kit	Zymo Research Europe GmbH, Freiburg, Germany
FITC Annexin V Apoptosis Detection Kit I	BD Bioscience, Franklin Lakes, NJ, USA
Maxwell RSC Cultured Cells DNA Kit	Promega GmbH, Madison, WI, USA
Maxwell® RSC simplyRNA Cells Kit	Promega GmbH, Madison,WI, USA
Nuclear Extraction Kit	Abcam, Cambridge, UK
SuperScript™ IV First-Strand Synthesis System	Thermo Fisher Scientific, Waltham, MA, USA
TET Hydroxylase Activity Quantification Kit (Fluorometric)	Abcam, Cambridge, UK

2.1.5 Chemicals, reagents and enzymes

Table 2-3: List of chemicals, reagents and enzymes used

Reagent	*Manufacturer*
0.05 % Trypsin - ethylenediaminetetraacetic acid (EDTA) (1 x), phenol red	Thermo Fisher Scientific, Waltham, MA, USA
2-Propanol	AppliChem GmbH, Darmstadt, Germany

50 x Tris-acetate-EDTA (TAE) Buffer	Carl Roth GmbH + Co. KG, Karlsruhe, Germany
Accutase solution	Sigma-Aldrich Chemie GmbH, St. Louis, MO, USA
Agarose	Biozym Scientific GmbH, Hess. Oldendorf, Germany
AMPure XP beads	Beckman Coulter, Inc., Indianapolis, IN, USA
Bovine serum albumin, fraction V	Carl Roth GmbH + Co. KG, Karlsruhe, Germany
CellTiter-Glo® Luminescent Cell Viability Assay	Promega GmbH, Madison, WI, USA
cOmplete™, Mini Protease Inhibitor Cocktail	Roche Diagnostics GmbH, Mannheim, Germany
Crystal violet	Sigma-Aldrich Chemie GmbH, St. Louis, MO, USA
Dimethyl sulfoxide (DMSO)	Sigma-Aldrich Chemie GmbH, Taufkirchen, Germany
Dulbecco's phosphate-buffered saline (DPBS)	Thermo Fisher Scientific, Waltham, MA, USA
Ethidium bromide solution, 1 % (w/v) in water	Carl Roth GmbH + Co. KG, Karlsruhe, Germany
HotStarTaq Master Mix (1000 U)	Qiagen, Germany, Hilden
Invitrogen™ Molecular Probes™ DAPI (4',6-Diamidino-2-Phenylindole, Dihydrochloride)	Thermo Fisher Scientific, Waltham, MA, USA
LightCycler ® 480 SYBR Green I Master	Roche Diagnostics GmbH, Mannheim, Germany
Loading dye, 6 x	VWR International GmbH, Darmstadt, Germany
Methanol	AppliChem GmbH, Darmstadt, Germany
Optiblot Bradford Reagent	Abcam, Cambridge, UK
Paraformaldehyde solution 4 % (w/v) in PBS	Santa Cruz Biotechnology, Inc, Dallas, TX, USA
peqGOLD 100 bp DNA Ladder	VWR International GmbH, Darmstadt, Germany

PhosSTOP, Phosphatase Inhibitor Cocktail Tablets	Roche Diagnostics GmbH, Mannheim, Germany
Pierce™ BCA Protein Assay Kit	Thermo Fisher Scientific, Waltham, MA, USA
ProLong™ Diamond Antifade Mountant	Thermo Fisher Scientific, Waltham, MA, USA
RIPA Buffer (10 x)	Cell Signaling Technology, Inc., Danvers, MA, USA
SignalStain® Antibody Diluent	Cell Signaling Technology, Inc., Danvers, MA, USA
TC10 Trypan blue dye	Bio-Rad Laboratories GmbH, München, Germany
Triton® X 100	Carl Roth GmbH + Co. KG, Karlsruhe, Germany

2.1.6 Devices

Table 2-4: List of devices used

Device	*Manufacturer*
Analytical balance Entris® 224i-1S	Sartorius Lab Instruments GmbH & Co. KG, Göttingen, Germany
Autoclave V-150	Systec GmbH, Linden, Germany
Barnstead™ GenPure™ Pro Ultrapure water system	Thermo Fisher Scientific, Waltham, MA, USA
BD FACSCelesta™	BD Bioscience, Franklin Lakes, NJ, USA
Bead Bath™ Mini M714	Lab Armor, LLC., Cornelius, OR, USA
CO_2 Incubator HERAcell 240 i	Thermo Fisher Scientific, Waltham, MA, USA
D300e Digital Dispenser.	Tecan Group Ltd., Männedorf, Switzerland
Diaphragm Pump BVC control	VACUUBRAND GMBH + CO KG, Wertheim, Germany
Ecotron Incubation Shaker	Infors AG, Bottmingen, Switzerland

EV 265 Consort Power Supply	Consort bvba, Turnhout, Belgium
Fluorescence Microscope Axio Observer.Z1	Carl Zeiss Microscopy GmbH, Jena, Germany
Gel Doc XR Gel Documentation System	Bio-Rad Laboratories GmbH, München, Germany
Heraeus Fresco 17 Microcentrifuge	Thermo Fisher Scientific, Waltham, MA, USA
Heraeus Megafuge 16R Centrifuge	Thermo Fisher Scientific, Waltham, MA, USA
Heraeus Megafuge 8R Centrifuge	Thermo Fisher Scientific, Waltham, MA, USA
Incubator BD115	Fa. BINDER GmbH, Tuttlingen, Germany
Inverse Microscope Primovert	Carl Zeiss Microscopy GmbH, Jena, Germany
Laboratory pH Meter 766	Knick Elektronische Messgeräte GmbH & Co. KG, Berlin, Germany
LightCycler® 480 Instrument	Roche Diagnostics GmbH, Mannheim, Germany
Maxwell® RSC Instrument	Promega GmbH, Madison, WI, USA
Multidrop™ Combi Reagent Dispenser	Thermo Fisher Scientific, Waltham, MA, USA
Multipette E3	Eppendorf AG, Hamburg, Germany
Multiskan™ FC Microplate Photometer	Thermo Fisher Scientific, Waltham, MA, USA
Nalgene® Mr. Frosty® Cryo 1 °C Freezing Container	Thermo Fisher Scientific, Waltham, MA, USA
NanoDrop 2000c Spectrophotometer	Thermo Fisher Scientific, Waltham, MA, USA
PerfectBlue™ Horizontal Maxi S Plus Gel System	VWR International GmbH, Darmstadt, Germany
Pipettes PIPETMAN Classic P2, P10, P20, P100, P200 and P1000	Gilson Incorporated, Middleton, WI, USA

pipetus® Pipette Filler	Hirschmann Laborgeräte GmbH & Co. KG, Eberstadt, Germany
Platform Shaker Duomax 1030	Heidolph Instruments GmbH & CO. KG, Schwabach, Germany
Quantus™ Fluorometer	Promega GmbH, Madison, WI, USA
Safe 2020 Class II Biological Safety Cabinet	Thermo Fisher Scientific, Waltham, MA, USA
Simple Western System Wes™	ProteinSimple, San Jose, CA, USA
Sunlab® Mini Centrifuge SU1550	Labdiscount GmbH, Mannheim, Germany
T100™ Thermal Cycler	Bio-Rad Laboratories GmbH, München, Germany
TC20™ Automated Cell Counter	Bio-Rad Laboratories GmbH, München, Germany
Tecan Spark® 10 M Multiplate Reader	Tecan Group Ltd., Männedorf, Switzerland
ThermoMixer™ C	Eppendorf AG, Hamburg, Germany
Ultrasonic Bath Sonorex RK 158 M	BANDELIN electronic GmbH & Co. KG, Berlin, Germany
Vortex Mixer Vortex Genie 2	Scientific Industries, Inc., Bohemia, NY, USA

2.1.7 Software and databases

Table 2-5: List of software and databases used

Software/Database	*Developer/Reference*
amplikyzer2 v. 1.2.0	Sven Rahmann, Genome Informatics, Institute of Medical Genetics, University Duisburg-Essen, Essen, Germany
BD FACSDiva v. 8.0.1.1	BD Bioscience, Franklin Lakes, NJ, USA
Combenefit v. 2.02.	Di Veroli *et al.*, 2016
Compass for SW v. 4.1.0	ProteinSimple, San Jose, CA, USA

D300eCONTROL v. 3.3.0	HP Development Company, L.P., Palo Alto, CA, USA
Ensembl release 93	Zerbino *et al.*, 2018
Excel 2016 v. 2001	Microsoft Corporation, Redmond, WA, USA
FlowJo v. 10.5.3	FlowJo, LLC, Ashland, OR, USA
GSEA v. 3.0	Subramanian *et al.*, 2005
Inkscape v. 0.92.4	Free Software Foundation, Inc, Boston, MA, USA
Integrative Genome Viewer v. 2.4.4	Robinson *et al.*, 2011
MethPrimer	Li and Dahiya, 2002
NCBI Primer-BLAST	Ye *et al.*, 2012
Prism v. 7.03	GraphPad Software, San Diego, CA, USA
R v. 3.6.0	The R Foundation for Statistical Computing, Vienna, Austria
RStudio v. 1.2.5001	R Studio, Inc., Boston, MA, USA
Zen Blue Edition v. 2.6	Carl Zeiss Microscopy GmbH, Jena, Germany

2.2 Methods

If nothing else indicated, methods were performed at room temperature.

2.2.1 Cell culture

2.2.1.1 Cultivation, counting and freezing of primary murine PDAC cell lines

Cell lines were incubated at 37 °C and 5 % CO_2. Upon a confluency of 60-80 %, cells were split or used for experiments. For detachment, medium was removed and cells were washed with DPBS. Afterwards, 0.05 % trypsin - EDTA (1 x) was added and the enzymatic reaction was stopped after 3-5 min by the addition of culture medium. Cells were recovered by centrifugation for 5 min at 400 g.

Cell counting was performed with the TC20™ automated cell counter using 10 µl of an equally mixed suspension of cells dissociated in medium and trypan blue to distinguish viable from dead cells.

For freezing, cells were detached by 0.05 % trypsin - EDTA (1 x) and pelleted for 5 min at 400 g. The pellet was resuspended in freezing medium containing 50 % culture medium, 40 % FBS and 10 % DMSO and $1x10^6$ cells per vial were aliquoted. The vials were immediately transferred into a freezing container (Mr. Frosty™) filled with 2-propanol enabling a slow and controlled freezing rate of approximately -1 °C/min and frozen at -80 °C overnight. For long-term storage, frozen vials were transferred into liquid nitrogen.

2.2.1.2 MEK inhibitor resistance induction in primary murine PDAC cell lines

MEK inhibitor (MEK_i) resistance was induced by treatment with increasing doses of the MEK_i trametinib. Induction was started with 5 nM and concentration doubling was continued until the cells grew in 100 x of their initial IC50 (800 nM to 4200 nM trametinib). One batch of each line was cultivated with 100 x IC50 of trametinib in the culture medium (in the following named as resistant). Medium exchange was performed every 2-3 days together with the addition of fresh trametinib. A second batch was cultivated without MEK_i and samples were named according to their passage number after drug withdrawal (Px; x means passage number).

2.2.1.3 Cell harvest for nucleic acid or protein isolation

For harvesting, cells were cultivated in 10 cm dishes up to 80 % confluency. The medium was removed and the cell layer was washed twice carefully on ice with ice-cold DPBS. Afterwards, 1 ml of DPBS was added and cells were harvested using a cell scraper. For pellets intended for protein isolation, DPBS was additionally mixed with protease- and phosphatase-inhibitor cocktails (1 tablet per 10 ml DPBS each).

2.2.1.4 Cell viability assay

Cell number optimization for 80 % confluency after 72 h of incubation was performed in 96- or 384-well plates in 100 µl or 30 µl volume, respectively. The D300e Digital Dispenser was used to pre-print DMSO-dissolved drugs in the indicated logarithmic concentration ranges. The DMSO content per well was normalized to the highest concentration on the plate and if possible, kept below 0.1 % of the assay volume. A maximal DMSO content of 0.5 % of the assay volume was allowed in synergism

measurements. Until use, plates were sealed with parafilm and frozen at -80 °C. Before cell seeding, the plates were thawed and warmed to room temperature. After cell harvest and counting (2.2.1.1), the Multidrop Combi Dispenser was used to seed previously optimized cell numbers per well onto the drug-containing plates. After 72 h incubation at 37 °C and 5 % CO_2 cell viability was determined using the CellTiter-Glo® Luminescent Cell Viability Assay according to manufacturer's instruction. The luminescence signal was measured with a Tecan Spark® 10 M multiplate reader for 500 ms. The signal of DMSO treated cells was used for normalization. IC50 values were determined with the 'log(inhibitor) vs. response (three parameters)' equation implemented in Prism. The Loewe method of Combenefit (Di Veroli *et al.*, 2016) was applied to assess synergy.

2.2.1.5 CASP3/7 activity assay

CASP3 activity was measured with the Caspase-Glo® Assay. Test compounds were pre-printed in 96-well plates using the D300e Digital Dispenser. The following concentrations were used: trametinib 100 x IC50 of each individual cell line, decitabine 0.5 µM, trametinib 0.3 µM + decitabine 0.5 µM. Cell numbers per well were optimized for 80 % confluency after 72 h incubation. 100 µl cell suspension per well were seeded with the Multidrop Combi Dispenser. After incubated for the indicated time points the Caspase-Glo® Assay was applied according to manufacturer's instructions. After cell lysis, the CASP3/7-specific proluminogenic substrate is cleaved by the enzymes. Thereby, aminoluciferin is released serving as a substrate for a luciferase contained in the assay. A Tecan Spark® 10 M multiplate reader was used to detect luminescence. Signals were corrected for viable cells measured by CellTiter-Glo® Luminescent Cell Viability Assay on a second plate as described in 2.2.1.4.

2.2.1.6 Immunofluorescence

For immunofluorescence, cells were grown on 8-chamber slides to 80 % confluency and washed twice with DPBS. Fixation was performed in 4 % paraformaldehyde for 20 min. Cells were washed with DPBS and permeabilized using 0.3 % Triton X 100 for 10 min. After washing with DPBS, 5 % bovine serum albumin (BSA) was used for blocking followed by 1 h incubation of primary antibodies (Table 2-6). Slides were washed 3 x 5 min with DPBS containing 1 % Tween. Fluorescence-labeled secondary antibodies (Table 2-6) and DAPI were diluted 1:1,000, respectively and incubated on the slides for 1 h protected from light. Slides were washed with DPBS and mounted.

Microscopy was performed on an Axio Observer.Z1 (Carl Zeiss) using the indicated magnifications.

Table 2-6: Antibodies for the immunofluorescence

Antibody	*Manufacturer*	*Dilution*
Rabbit IgG Isotype Control	R&D Systems, Inc., Minneapolis, MN, USA	1:100
Mouse IgG1 Isotype Control	R&D Systems, Inc., Minneapolis, MN, USA	1:200
E-Cadherin (CDH1) (24E10) Rabbit mAb	Cell Signaling Technology, Inc., Danvers, MA, USA	1:100
N-Cadherin (CDH2) (13A9) Mouse mAb	Bio-Techne GmbH, Wiesbaden, Germany	1:200
Goat anti-Rabbit IgG Cross-Adsorbed Secondary Antibody, DyLight 488	Life Technologies Europe BV, Bleiswijk, Netherlands	1:1,000
Goat anti-Mouse IgG Cross-Adsorbed Secondary Antibody, DyLight 550	Life Technologies Europe BV, Bleiswijk, Netherlands	1:1,000

2.2.1.7 Flow cytometric quantification of cell death

Appropriate cell numbers were determined individually for each cell line in order to achieve 80 % confluence after 84 h. Afterwards, 2 ml cell suspension per well were seeded in 12-well plates pre-printed with the indicated drug concentrations (trametinib 100 x IC50 in each individual cell line, decitabine 0.5 µM, trametinib 0.3 µM + decitabine 0.5 µM) using the D300e Digital Dispenser. DMSO concentrations per well were normalized to the highest concentration on the plate and thereby kept below 1 % of the assay volume. After incubation for 84 h, cells were detached by accutase solution and stained with the FITC Annexin V Apoptosis Detection Kit I according to the manufacturer's protocol. Differently, Annexin V-FITC and propidium iodide (PI) were both diluted 1:40. Fluorescence was analyzed by flow cytometry on a FACSCelesta system. The percentage of each cell population was determined with the FlowJo software.

2.2.1.8 Crystal violet staining

Cells were seeded and incubated as previously described in 2.2.1.7. Cells were washed twice with DPBS and then fixed for 10 min with ice-cold methanol. Afterwards, staining with crystal violet solution (0.1 % (w/v) crystal violet, 25 % methanol, 75 % ultrapure water) was performed for 30 min. Plates were washed with ultrapure water and dried overnight.

2.2.1.9 Cytogenetic analysis

The cytogenetic analysis of parental cells #3 and #9 was performed by Elke Jürgens and Regina Kubica (both Department for Human Genetics, Essen). Cells were seeded and incubated 24 h to reach 30-40 % confluency. Prior to harvest, cells were treated with colcemid for 4 h. After centrifugation, cell pellets were resuspended in a hypotonic 75 mM KCl-solution and incubated for 20 min at 37 °C. The solution was removed by centrifugation and cells were fixed 3 x 10 min with ice-cold 3:1 methanol:acetic acid and dropped onto a fat-free and watered glass slide that was then air-dried overnight at 60 °C. Chromosomes were stained with Giemsa and examined under the microscope using 140 x magnification.

2.2.2 Protein analytics

2.2.2.1 Total protein extraction and quantification

Cell pellets (2.2.1.3) were lysed in 1 x RIPA buffer containing protease- and phosphatase-inhibitor cocktails (1 tablet per 10 ml DPBS each) for 20 min on ice. Lysates were centrifuged for 15 min at 4 °C and 17,000 g to remove cell debris. The protein concentration in the retained supernatant was determined using the Pierce BCA Protein Assay Kit in 96-well plate format. For quantification, the absorbance of a BSA dilution series was measured on the same plate using a Multiskan™ FC microplate photometer.

2.2.2.2 Simple western analysis

Simple western analysis was performed on the Wes instrument using the manufacturer’s protocol. Antibody dilutions were optimized to be saturating and linear according to different protein concentrations (Table 2-7). HSP90 or VCL were used for normalization of protein input. When the size difference between housekeeping and target protein was at least 20 kDa, the normalization was carried out by antibody multiplexing in the same capillary.

Table 2-7: Optimized antibody dilutions for the applied protein concentration in a simple western analysis

Antibody	*Manufacturer*	*Dilution*	*Applied protein concentration [µg/µl]*
E-Cadherin (CDH1) (24E10) Rabbit mAb	Cell Signaling Technology, Inc., Danvers, MA, USA	1:1,000	0.1
c-Jun (60A8) Rabbit mAb	Cell Signaling Technology, Inc., Danvers, MA, USA	1:50	0.2
p44/42 MAPK (Erk1/2) (137F5) Rabbit mAb	Cell Signaling Technology, Inc., Danvers, MA, USA	1:50	0.2
HSP 90α/β Rabbit Antibody (H-114)	Santa Cruz Biotechnology, Inc., Dallas, TX, USA	1:250/1:500	0.05 and 0.2/0.1
N-Cadherin (CDH2) (13A9) Mouse mAb	Bio-Techne GmbH, Wiesbaden, Germany	1:100	0.2
Phospho-c-Jun (Ser73) Rabbit mAb	Cell Signaling Technology, Inc., Danvers, MA, USA	1:5	0.2
Phospho-p44/42 MAPK (Erk1/2) (Thr202/Tyr204) (20G11) Rabbit mAb	Cell Signaling Technology, Inc., Danvers, MA, USA	1:15	0.2
Vinculin (E1E9V) XP® Rabbit mAb	Cell Signaling Technology, Inc., Danvers, MA, USA	1:30,000	0.2

2.2.2.3 Nuclear protein extraction and quantification

Nuclear protein extracts were generated with Abcam's Nuclear Extraction Kit according to manufacturer's instructions with the following exception: the extraction was performed for 15 min in an ultrasonic bath filled with ice water. For quantification, 150 µl Optiblot Bradford Reagent were used to quantify 10 µl of nuclear extract in triplicates compared to a BSA standard curve. Absorbance was measured with a Tecan Spark® 10 M multiplate reader.

2.2.2.4 DNMT and TET enzyme activity assay

The activity of DNMT and TET enzymes was determined in triplicates using the DNMT Activity Quantification Kit and the TET Hydroxylase Activity Quantification Kit according to manufacturer's instructions. Per well 7.5 ng of nuclear extracts (2.2.2.3) were applied. Fluorescence was measured with a Tecan Spark® 10 M multiplate reader. Relative fluorescence units (RFU) were blank corrected and divided by the product of protein amount and incubation time.

2.2.2.5 Mass spectrometry

Mass spectrometry (MS) was performed by Kristin Fuchs and Kathrin Witzke (Medizinisches Proteom-Center für Protein-Diagnostik, Ruhr-Universität Bochum, Bochum, Germany). The method section was kindly provided by Kathrin Witzke.

Cell pellets were resuspended in 100 µl 50 mM ammonium bicarbonate and 0.1 % sodium deoxycholate (NaDOC) for cell lysis. Samples were sonicated on ice for 10 min and centrifuged (16,000 g, 15 min, 4 °C). The protein concentration was determined via Bradford assay. Due to a very low concentration, technical replicates were pooled. The samples were ridded of remaining viscosity with 10 impulses at 5 % power by ultrasonic homogenization via Sonopuls HD 200 MS 72 (Badelin) and centrifuged (16,000 g, 15 min, 4 °C). Protein amount was determined via amino acid analysis. Dithiothreitol (5 mM) was added to the sample for reduction (30 min, 60 °C), followed by iodoacetamide (15 mM) for alkylation (30 min, room temperature, in the dark). Lysed proteins were tryptically digested over night at 37 °C (trypsin/protein ratio 1/24). For acidification, trifluoroacetic acid (TFA) (0.5 %) was added (30 min, 37 °C), samples were centrifuged (10 min, 16,000 g) for removal of NaDOC and supernatant transferred to glass vials, dried in a vacuum centrifuge, and dissolved in 0.1 % TFA. A sample amount corresponding to 275 ng was used for one liquid chromatography tandem-mass spectrometry (LC-MS/MS) measurement.

LC–MS/MS analysis was performed on an LTQ Orbitrap Elite instrument (Thermo Fisher Scientific) coupled online to an upstream-connected Ultimate 3000 RSLCnano high-performance liquid chromatography system (Dionex). Samples were measured in a shuffled manner. Peptides dissolved in 0.1 % TFA were pre-concentrated on a C18 trap column (Acclaim PepMap 100; 100 µm × 2 cm, 5 µm, 100 Å; Thermo Fisher Scientific) within 7 min at a flow rate of 30 µl/min with 0.1 % TFA. Peptides were then transferred to an in-house packed C18 analytical column (ReproSil®-Pur from Dr. Maisch HPLC GmbH, Ammerbuch, Germany, 75 µm × 40 cm, 1.9 µm, 120 Å).

Peptides were separated with a gradient from 5 %–40 % solvent B over 98 min at 300 nl/min and 65 °C (solvent A: 0.1 % formic acid=FA; solvent B: 0.1 % formic acid, 84 % acetonitrile). Full-scan mass spectra in the Orbitrap analyzer were acquired in profile mode at a resolution of 60,000 at 400 m/z and within a mass range of 350-2000 m/z. MS/MS spectra were acquired in data-dependent mode at a resolution of 5,400. For MS/MS measurements, the 20 most abundant peptide ions were fragmented by collision-induced dissociation (normalized collision energy of 35) and measured for tandem mass spectra in the linear ion trap.

Proteins were identified with Proteome Discoverer v. 1.4 (Thermo Fisher Scientific). Spectra were searched against the UniProtKB/Swiss-Prot database (Release 2018_11; 53,780 entries) using Mascot v. 2.5 (Matrix Science, London, UK). Taxonomy setting was *Mus musculus* and mass tolerance was 5 ppm and 0.4 Da for precursor and fragment ions, respectively. Dynamic and static modifications were considered for methionine (oxidation) and cysteine (carbamidomethyl), respectively. The false discovery rate (FDR) was calculated with the Proteome Discoverer Target Decoy PSM Validator function, and identifications with an FDR > 1 % were rejected. The software Progenesis QI v. 2.0.5387.52102 (Nonlinear Dynamics) was used for label-free quantification. The obtained .raw files were aligned to a reference run and a master map of common features was applied to all experimental runs to adjust for differences in retention time. Ion charge states of 2+, 3+, and 4+ with a minimum of three isotope peaks were considered, and raw ion abundances were normalized for automatic correction of technical or experimental variations between runs. Quantified features were identified using the obtained Proteome Discoverer identifications. All non-conflicting peptides were considered for protein quantification.

Progenesis calculates statistical significance of measured differences (ANOVA p-value) and ratios of means (fold changes). However, when more than two different groups are processed with the software, the resulting p-values only state that a significant difference between two of those groups exists. Similarly, only maximal fold changes are calculated. Application of a post-hoc test was therefore necessary. This statistical analysis was performed with the software R v. 3.4.0. Normalized protein abundances were obtained from Progenesis and analyzed by applying ANOVA followed by Tukey's honest significant difference (HSD) method. Fold changes between groups were determined based on normalized abundances while ANOVA was calculated using asinh-transformed data for consistency with the Progenesis QI software. The FDR was controlled by adjusting ANOVA p-values using the method of

Benjamini and Hochberg (Benjamini and Hochberg, 1995). For proteins with ANOVA p-values below the significance level of α=0.05, the Tukey HSD method was applied to further characterize the identified differences in abundance levels between groups. Proteins were considered differentially abundant between groups with an absolute fold change ≥ 2 and a p-value ≤ 0.05.

2.2.3 Nucleic acid analytics

2.2.3.1 Isolation of nucleic acids

DNA and RNA were isolated using the Maxwell® RSC Cultured Cells DNA and the Maxwell® RSC simplyRNA Cells Kit according to manufacturer's instruction. Differently, DNA was eluted in nuclease-free water.

2.2.3.2 Reverse transcription

Complementary DNA (cDNA) synthesis by reverse transcription was performed with the SuperScript IV First-Strand cDNA Synthesis Reaction Kit using oligo-dT primers. Where possible, 5 µg total RNA (2.2.3.1) served as template. Until use, cDNA was stored at -20 °C.

2.2.3.3 Semi-quantitative real-time PCR

Primers for semi-quantitative real-time PCR (RT-PCR) were designed intron-spanning by NCBI Primer-BLAST (Ye *et al.*, 2012) (Table 2-8). Only primer pairs with an efficiency > 90 % were used. Specificity was checked by melting curve and agarose gel electrophoresis.

Table 2-8: Primers for semi-quantitative real-time PCR

Target	*Primer*	*Sequence 5´-3´*	*Product size [bp]*
Dnmt1[1]	forward reverse	CCTAGTTCCGTGGCTACGAGGAGAA TCTCTCTCCTCTGCAGCCGACTCA	137
Dnmt3a	forward reverse	GACGCCAAAGAAGTGTCTGCT CACTTTGCTGAACTTGGCTATTCT	150
Dnmt3b	forward reverse	CGGCTGTCTAAGAGGGAGGT AGGTCCCATTGCTATGTCGG	193
Gusb	forward reverse	TATGGAGCAGACGCAATCCC TTCGTCATGAAGTCGGCGAA	164

Tet1	forward reverse	GGACATCCCACAGACCGAAG CTGGGGTTTTCACTCCTCCC	155
Tet2	forward reverse	CGAGGCTGCTTTCGTAGAGG AGGGCAAGCTGCTGAATGTA	143
Tet3[2]	forward reverse	TGCGATTGTGTCGAACAAATAGTTCCATA CCGATCCTCCATGAG	111

[1] (Feng *et al.*, 2010a)

[2] PrimerBank ID 22766889a1 (Spandidos *et al.*, 2010)

Semi-quantitative RT-PCR was performed on a LightCycler® 480 Instrument. Triplicates of 5 µl cDNA (described in 2.2.3.2; 1:11.5 diluted in H_2O) were amplified in 20 µl total reaction volume containing 600 nM primers and 10 µl LightCycler® 480 SYBR Green I Master Mix. The thermocycling conditions used are listed in Table 2-9. Gene expression was quantified using the ΔΔCt-method as previously described (Livak and Schmittgen, 2001). *Gusb* served as a housekeeping gene for normalization of cDNA input.

Table 2-9: Thermocycling conditions for semi-quantitative RT-PCR

Step	*Temperature [°C]*	*Time*	*Cycles*
Initial DNA Denaturation	95	10 min	1
Denaturation Primer annealing Elongation	95 60 72	10 s 20 s 20 s	40
Melting Curve	95 65-97 (2.5 °C/s)	5 s continuous	1 1

2.2.3.4 Agarose gel electrophoresis of PCR products

Depending on the product size 1.5 % or 2 % agarose gels were used for separation. Agarose was dissolved in 1 x TAE-buffer and 6 µl ethidium bromide solution (1 % (w/v)) per 100 ml was added. Samples were mixed with 6 x loading dye and 10 µl each were separated at 100 V for 90 min. As size reference, a 100 bp ladder was used. DNA bands were visualized by UV light in the Gel Doc XR Gel Documentation System.

2.2.4 Next generation sequencing and bioinformatic analyses

Sequencing was performed by the specified facilities. Bioinformatic analysis were in parts carried out by Jan Forster, Johannes Köster and Christopher Schröder from the Department of Genome Informatics, Institute of Human Genetics, University Duisburg-Essen, Germany. For each section, individual contributions are indicated.

2.2.4.1 RNA-sequencing

RNA-sequencing (RNA-seq) of cell lines #3, #7 and #9 in parental, resistant, P5 and P12 cell states together with parental, resistant and P12 states of lines #4, #6 and #10 was performed by the CeGaT GmbH (Tübingen, Germany). For library preparation the TruSeq Stranded mRNA Kit (Illumina) was used with 100 ng input RNA (2.2.3.1) and 2 x 100 bp were sequenced on a HiSeq 4000 (Illumina) or a NovaSeq 6000 system (Illumina). Demultiplexing of the sequencing reads was performed with Illumina CASAVA v. 2.17 or bcl2fastq v. 2.19. Adapters were trimmed with Skewer v. 0.1.116 or 0.2.2 (Jiang *et al.*, 2014).

The analysis was continued by Jan Forster. Transcripts were quantified by salmon v. 0.12 (Patro *et al.*, 2017). TXImport v. 1.6 (Soneson *et al.*, 2015) and DESeq2 v. 1.18 (Love *et al.*, 2014) were used to import transcript-level counts, convert them to gene-level counts and perform differential expression analysis between all four cell states (parental, resistant, P5, P12). The resulting p-value was corrected according to the Benjamini-Hochberg procedure (Benjamini and Hochberg, 1995).

Normalized gene-level counts and differential gene lists were provided to Laura Godfrey. Principal component analysis was performed on the normalized read counts. Hierarchical clustering of significantly differentially expressed genes (Benjamini-Hochberg adjusted p-value < 0.01; $\log_2$ fold change > 1 or $\log_2$ fold change < -1) between parental versus the union of resistant, P5, P12 and resistant versus the union of parental, P5 and P12 was computed by the ward.D2 method. Additionally, samples were clustered based on the PDAssigner genes for the classical and the quasi-mesenchymal subtype (Collisson *et al.*, 2011) as well as for the pancreatic-progenitor/classical and squamous/basal-like PDAC subtypes as defined by Bailey *et. al.* (Bailey *et al.*, 2016) and Moffitt *et al.* (Moffitt *et al.*, 2015).

Gene Set Enrichment Analysis (GSEA) (Subramanian *et al.*, 2005) was performed using default settings (1000 permutations, weighted enrichment statistics, signal2noise ranking, real value sorting mode, gene set sizes between 15 and 500) and gene set permutation. For the analysis of a potential PDAC subtype switch, the metagenes

defined by the above-mentioned studies were each defined as an individual gene set and incorporated into the C.6.all (oncogenic signatures) gene set database.

In order to identify differentially expressed genes between parental and resistant cells that show a similar expression pattern in parental and P12 samples, a score s was defined by Jan Forster based on the $\log_2$ fold change between parental/P12 and resistant samples:

$$s = \begin{cases} 0, & \text{if } -1 < log_2FC(P,R) < 1 \\ 0, & \text{if } log_2FC(P,R) \cdot log_2FC(P12,R) < 0 \\ \dfrac{max(|\,log_2FC(P,R)\,|,|\,log_2FC(P12,R)\,|)}{min(|\,log_2FC(P,R)\,|,|\,log_2FC(P12,R)\,|)}, & \text{otherwise} \end{cases}$$

where $log_2FC(A,B)$ describes the $\log_2$ fold change between A and B. Genes were only considered if the $\log_2$ fold change between parental and resistant cell state was reasonably large.

2.2.4.2 Whole genome sequencing

Whole genome sequencing (WGS) was performed of parental and resistant cells of lines #3 and #9. DNA isolated from the tail tip of the donor mouse of #3 served as a normal control (2.2.3.1). The Genomics and Proteomics Core Facility of the German Cancer Research Center (GPCF DKFZ, Heidelberg) performed the library preparation with the TruSeq DNA PCR-free Kit (Illumina) and the 150 bp paired-end sequencing on a HiSeq X (Illumina). Reads were aligned to the mouse reference genome GRCm38 using BWA-MEM v. 0.7.15 (Li, 2013). Duplicate reads were marked with sambamba v. 0.6.5 (Tarasov *et al.*, 2015).

Jan Forster and Johannes Köster performed variant calling and annotation. Variants and small insertions and deletions (InDels) were called in a two-step process. First, candidate variants were called using freebayes v. 1.1.0 (Garrison and Gabor, 2012), with parental and resistant tumor samples as well as the normal control. In a second step, variants were validated and readjusted by Varlociraptor v. 1.1.1 (Köster *et al.*, 2019).

These variants were divided into three groups based on their variant allelic fraction (VAF) in the respective cell states of each cell line:

- Variant present in parental (VpP): Drop of VAF to 0 from parental to resistant cells
- Variant present in resistant (VpR): VAF rises above 0.1 in resistant compared to 0 parental cells
- Variant present in parental and resistant (VpPR): VAF > 0 in parental and resistant samples

VpPs and VpRs were validated in P5 and P12 samples using the available whole genome bisulfite sequencing (WGBS) data. Since the technical differences between WGBS and WGS affect the comparability of results from both methods, validation was performed solely on WGBS samples (2.2.4.3).
Data management and visualization was performed using bcftools v. 1.9 (Li, 2011) and python v. 3.7 libraries seaborn v. 0.9 and pandas v. 0.24.
Variants were annotated using Jannovar v. 0.25 (Jager *et al.*, 2014) with the GRCm38 annotation database as well as sorting intolerant from tolerant (SIFT) scores (Ng and Henikoff, 2003) (Download source: http://sift.bii.a-star.edu.sg/sift4g/public//Mus_musculus/GRCm38.83.zip).
To compare variants between both cell lines, the closest variant positions between both variant calls were identified using the closest algorithm from BEDtools v. 2.27 (Quinlan and Hall, 2010).

2.2.4.3 Whole genome bisulfite sequencing

The DNA methylome of cell lines #3 and #9 in parental, resistant, P5 and P12 cell states was analyzed by WGBS. Library preparation of DNA (2.2.3.1) using the TruSeq DNA PCR-free Methyl protocol (Illumina) and 150 bp paired-end WGBS on a HiSeq X were performed at the Genomics and Proteomics Core Facility of the German Cancer Research Center (GPCF DKFZ, Heidelberg, Germany). Reads were mapped by the facility using bwa-meth v. 0.2.0 (Pedersen *et al.*, 2014) on the GRCm38 assembly with added PhiX genome as a sequencing control.
The following analyses were performed by Jan Forster and Christopher Schröder. CpG methylation levels were computed using an in-house script. Reads with a mapping quality < 30 and bases with base quality < 17 were filtered.
The BSmooth algorithm of bsseq v. 1.10 (Hansen *et al.*, 2012) was used to detect differentially methylated regions (DMRs) between parental and resistant samples with a minimum CpG-count of four and a minimal difference in methylation level of 0.4.

For each DMR, the nearest flanking genes were determined by finding the nearest transcription start sites (TSSs) to each region BEDTools closest v. 2.27 (Quinlan and Hall, 2010).

The localization of DMRs relative to genes and CpG islands was performed using BEDTools intersect v. 2.27 (Quinlan and Hall, 2010). Reference data were taken from Ensembl build 93 (Zerbino *et al.*, 2018) (genes) and the University of California, Santa Cruz (UCSC) database (CpG islands).

Reference data for shore and shelf regions were created using BEDTools flank v. 2.27 (Quinlan and Hall, 2010). Shores were defined as regions up to 2000 bp away from CpG islands and shelfs as regions up to 2000 bp away from shores. Expression changes of the two nearest genes of every DMR were assessed from RNA-seq data as described above (2.2.4.1). Genes with a $\log_2$ fold change between resistant and parental cells > 1 were defined as upregulated in resistant cells, those with a $\log_2$ fold change < -1 as downregulated in resistant cells.

To model the methylation changes between parental, resistant and P12 cells a score s_2 was developed by Jan Forster and Laura Godfrey:

$$s_2 = \begin{cases} 0, & \text{if } \Delta(P,R)\cdot\Delta(P,P12) < 0 \\ 1, & \text{if } \Delta(P,R)\cdot\Delta(R,P12) < 0 \\ \dfrac{|\Delta(P,P12)|}{|\Delta(P,R)|}, & \text{otherwise} \end{cases}$$

where $\Delta(A,B)$describes the difference in methylation between A and B. A score > 0.5 means a P12 methylation level closer to the parental than the resistant level, while scores < 0.5 indicate that the P12 methylation is closer to the resistant level. The 90 % quantile is represented by 0.44. Thus, the DMRs scoring > 0.44 were defined as reverting DMRs.

The following analyses were performed by Jan Forster. The UCSC liftOver tool (Kent *et al.*, 2002) was used together with the mm10ToHg38 liftOver chain in order to identify regions in the human genome that are associated with the murine DMRs. The minimum ratio of bases that need to remap to define a region as valid liftOver was set to 0.5. DMR overlaps with miRNA target regions, VISTA enhancers and transcription factor binding sites (TFBS) derived from reference data of the Ensembl regulation build 93 (Zerbino *et al.*, 2018) were computed using BEDTools intersect v. 2.27 (Quinlan and Hall, 2010). Additionally, methylated TRE-like sequence (mTRE) motif positions were

taken from MEME suite v. 5.1.1. (Grant *et al.*, 2011) and BEDTools intersect v. 2.27 (Quinlan and Hall, 2010) was used to compute their overlap with DMRs.

The findMotifsGenome script from HOMER v. 4.9 (Heinz *et al.*, 2010) was used in order to find enrichment of known binding motifs from the HOMER library. The script was used with standard parameters (-size 200 -cpg) on the GRCm38 assembly, comparing the reverting DMRs to random background sequences.

Chromatin immunoprecipitation and sequencing (ChIP-seq) for H3K27me and assay for transposase-accessible chromatin and sequencing (ATAC-seq) organoid data available from Roe *et al.* (Roe *et al.*, 2017) were used in order to check whether DMRs overlap with open chromatin or enhancer regions. Analysis was performed on the following organoids:

ChIP-seq:

H3K27ac:

- N5, N6 – normal pancreatic organoids – (Boj *et al.*, 2015)
- T3, T6, T19, T23, T33, T34 – tumor organoids

H3K4me1:

- T3, T6, T23 – tumor organoids

ATAC-seq:

- N5, N6 – normal pancreatic organoids – (Boj *et al.*, 2015)
- T3, T6, T23 – tumor organoids

Reads were aligned with BWA-MEM v. 0.7.17 (Li, 2013) against the GRCm38 assembly and duplicated reads were removed using Samtools v. 1.9.

Identification of ChIP-seq and ATAC-seq peaks was performed using MACS2 v. 2.1.2 (Gaspar, 2018; Zhang *et al.*, 2008) callpeak function with default settings. Resulting narrowPeak files were further merged with BEDtools v. 2.27 (Quinlan and Hall, 2010) merge and overlapped with the DMRs using BEDtools intersect to analyze how many peaks from tumor and normal organoids are located within the DMRs.

In order to detect possible enrichment of TFBS, mTRE as well as ATAC-seq and ChIP-seq peaks in DMRs compared to the remaining genome, every DMR was matched with 1 million randomly picked genomic regions with similar length and CpG-count. The occurrence of the features of interest was then compared between DMRs and the average of the randomly chosen regions. A feature was defined as significantly

enriched if its occurrence in the DMRs was larger than in the average of random regions in at least 95 %, 99 % or 99.9 % of all comparisons (significance level < 0.05, < 0.01 or < 0.001).

VpPs and VpRs defined by WGS (2.2.4.2) were validated in the WGBS data of the same cell lines. To adjust for bisulfite conversion, only A > T and T > A variants covered > 15 x were assessed using Varlociraptor v. 1.1.1 (Köster *et al.*, 2019).

2.2.4.4 Targeted deep bisulfite sequencing

WGBS results were validated by targeted deep bisulfite sequencing of 15 DMRs as described elsewhere (Leitao *et al.*, 2018). Selection criteria of the validated DMRs were:

- Proportion of hypo- and hypermethylated DMRs reflects that of the whole WGBS data set
- Reversion in P12 (reversion score > 0.44, see 2.2.4.3)
- Sequence conservation in humans based on UCSC liftover (Kent *et al.*, 2002)
- Preferentially with at least one flanking transcript showing reverted expression in P12

Primers for the first PCR were designed with MethPrimer (Li and Dahiya, 2002) as described by Leitao *et al.* (Leitao *et al.*, 2018). Their sequences are listed in Table 2-10.

Table 2-10: Primers used in the first PCR of targeted deep bisulfite sequencing

During oligonucleotide synthesis the following tag sequences were added to the 5´end of each forward and reverse primer: CTTGCTTCCTGGCACGAG (forward) and CAGGAAACAGCTATGAC (reverse).

DMR	*Primer*	*Sequence 5´-3´*	*Location in mm10*	*bp*	*CpGs*
247	forward reverse	ATTTTATGGGTTAGTTGTTTGATTT CAACTAATAACACTTTTAACACCC	chr10:99266158-99266419	262	9
422	forward reverse	GTTTGTTTGTAATTGGGGATTAGG TCTAAAATACAACCCTACATATAAATC	chr11:113060998-113061290	293	11
513	forward reverse	TTGTTAAATGGAATTGTTGTTGAGA AAAACTCTTACATAAACTACCAAAC	chr12:85859330-85859634	305	3
711	forward reverse	TAAAGTAGTGGGATAAATTTTTTTT CTAATCTTCTTATTCTTAACAAATCC	chr15:27467984-27468252	269	6

825	forward reverse	AGATTAGTGTTTTTAATTATTTTGA CCAAACAAAAAACATCATACTTTC	chr16:23272009-23272213	205	6
869	forward reverse	TTTTTTGTTTAAGGAAAGGATA CCATTCTCAAAACAAATTTTAC	chr16:92620511-92620772	262	8
929	forward reverse	TTGTAAGGTTGTATTTTTTTTGATGTTT CAACCCTTAAATACTAAAACTCAACTC	chr17:44718034-44718321	288	6
963	forward reverse	TGGGAGGTAGTGTGGGATATAGTAG CTTCCCAAAAACAAAAACACTCTAA	chr17:84141583-84141880	298	5
1144	forward reverse	AGGAGTGTGTTAATTTTTAGGGGTTA CCCAACCAAATAAAACCTACCTAA	chr2:26501667-26501948	282	8
1211	forward reverse	ATTTGTTAGTATAGAAGAAGGTTGGTAGT AACAAATTCTAAAAAAAATTCCCTC	chr2:102873250-102873543	294	4
1232	forward reverse	TTTGTTTAGGTTTTGTTTTTTGTTG ATTCACACCATTTACAAATCACAC	chr2:127336828-127337044	217	5
1463	forward reverse	GTTGATTATTAGTTTTTTTTGTAGTT CACATTTACACTAATATCCCAACC	chr4:119244934-119245233	300	13
1602	forward reverse	TAGTAATATAAGATGTTTAAGTATTGAA AAAACCCCACAAAACTCTCTCTAA	chr5:98943301-98943589	289	8
1823	forward reverse	AAAAGTTTTAGAGTGAGTAGAATAGGT CTTACAACCCAAAAACCACAAC	chr7:24370317-24370596	280	10
1998	forward reverse	TAATTTTAGTATATGGGGAGTGGGA TAACCATTCCCTTAAAAACACTACC	chr8:34813921-34814236	316	9

Primer sequences for the second PCR were taken from Leitao *et al.* (Leitao *et al.*, 2018). The purified amplicons were quantified and pooled. The library was sequenced on a MiSeq (Illumina) by the BioChip-Laboratory of the Essen University Hospital. amplikyzer2 was used for analysis. Due to the multiplicative coverage compared to WGBS, DMRs were classified as positively validated at a minimum methylation difference of 0.2. The reversion score was applied as described in 2.2.4.3.

2.2.5 Patient-derived xenografts

All mice experiments were carried out by the EPO GmbH, Berlin-Buch, and performed according to the German Animal Protection Law with approval from the responsible authorities. The *in vivo* procedures were consistent and in compliance with the United Kingdom Coordinating Committee of Cancer Research (UKCCCR) guidelines. Diana Behrens (EPO GmbH, Berlin-Buch, Germany) kindly provided this method section.
Already established patient-derived xenografts (PDX) of PDAC at passage number 2 were received from ARC-NET, University of Verona. The materials used have been

collected under Program 1885 protocol 52438 on 23/11/2010 and Program 2172 protocol 26773CE 23/05/2012. The protocols include informed consent of the patients and were approved by the local ethics committee of the Integrated University Hospital Trust of Verona. At the time of surgery patient 1 was 59 years old, patient 2 65 years and patient 3 53 years. Tumor pieces of 3 mm^3 were transplanted subcutaneously into non-obese diabetic/severe combined immunodeficiency (NOD/SCID)-mice with knocked IL2γ receptor (NSG)-mice within 24 h after explant from donor mice. Remaining tumor tissue was preserved in DMSO or snap-frozen for later propagation or analyses. Engrafted tumors at a size of about 1 cm^3 were surgically excised and fragments of 2 - 3 mm^3 re-transplanted into immune deficient Naval Marine Research Institute (NMRI:nu/nu)-mice for further passage. Tumors were passaged not more than 10 times.

For drug screening studies tumor material was implanted subcutaneously into appropriate cohorts of NMRI:nu/nu-mice (n=3 per treatment group). At advanced tumor size (200 mm^3), mice were randomized and treated with 1 mg/kg trametinib (per os, daily), 0.2 mg/kg decitabine (subcutaneous, three times weekly). To further mouse cohorts the combinations of trametinib and decitabine were applied. Tumor size was measured with a caliper instrument and monitored during the entire experiment with the measurements of two perpendicular tumor diameters using the spheroid equation: tumor volume = [(tumor width)^2 x tumor length] x 0.5. Treatment was continued over a period of two weeks unless tumor size exceeded 1 cm^3 or animals showed loss of more than 15 % body weight. Six hours after last treatment animals were sacrificed and tumor samples preserved for further analyses.

Mice were maintained in the pathogen-free animal facility following institutional guidelines and with approval from the responsible authorities. The animals were housed under pathogen-free conditions in individually ventilated cages under standardized environmental conditions (22 °C room temperature, 50 ± 10 % relative humidity, 12 h light-dark rhythm). They received autoclaved food and bedding (Ssniff) and acidified (pH 4.0) drinking water *ad libitum*.

2.2.6 Statistics and reproducibility

Replicates were performed as indicated in the method section or figure legends. For statistical analyses RStudio and Prism were used. The applied test is described in the figure legends.

2.3 Data availability

Proteomics data have been deposited as a complete submission in the ProteomeXchange Consortium via the PRIDE partner repository (http://www.proteomexchange.org; data set identifier: PXD018093 and 10.6019/PXD018093). The .msf files obtained in Proteome Discoverer were converted into the mzIdentML standard format using ProCon PROteomics Conversion tool version 0.9.718 (PubMed ID 26182917). The RNA-seq generated during this study are available at GEO: GEO: GSE146348. The accession number for WGBS and WGS data deposited on ENA is: PRJEB37018.

3 RESULTS

3.1 Multi-omics characterization of MEK$_i$ resistance in PDAC using a primary *in vitro* model

More than 90 % of pancreatic ductal adenocarcinomas (PDACs) harbor an activating *KRAS* mutation that is known to be a key driver and therefore an unambiguous therapeutic target (Kleeff *et al.*, 2016). However, specific inhibitors are still missing, so that targeting of the downstream kinase kinases MEK1/2 represents a possible alternative (Figure 3-1A).

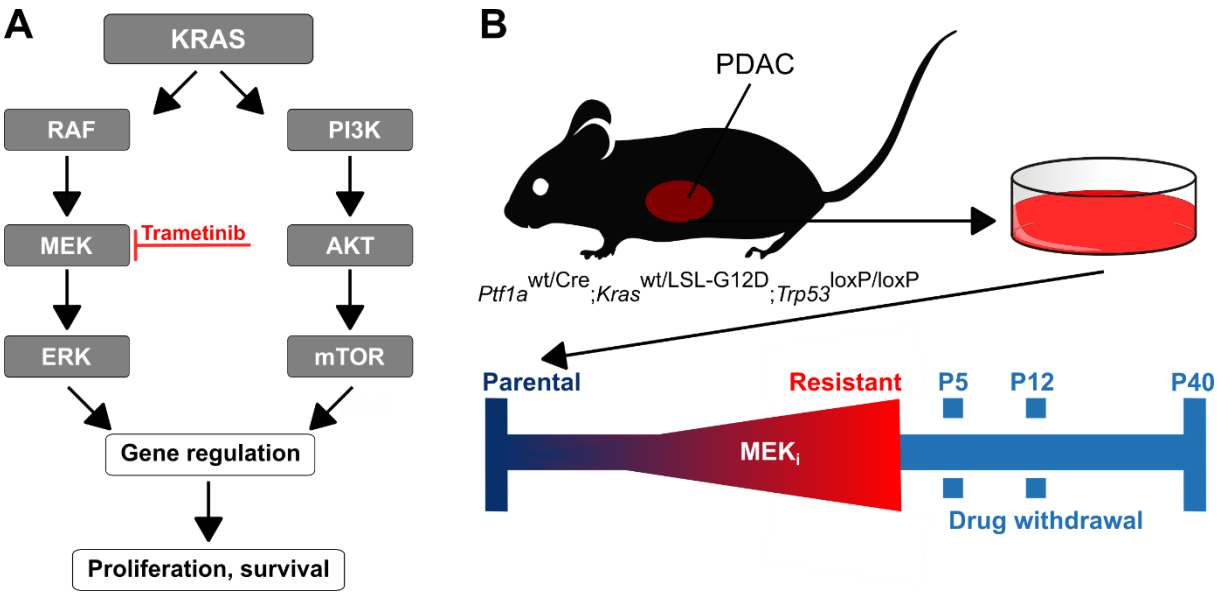

Figure 3-1: Schema of the generated *in vitro* model and MEK$_i$ resistance induction

Simplified overview of KRAS downstream signaling **(A)**. Schema of the generated *in vitro* model and MEK$_i$ resistance induction. Samples taken after drug withdrawal were named according to their passages (P) in drug free medium **(B)**.

Despite promising pre-clinical results, clinical trials failed due to resistance (Chung *et al.*, 2017; Infante *et al.*, 2014; Van Cutsem *et al.*, 2018; Van Laethem *et al.*, 2017). To investigate potential resistance mechanisms, an *in vitro* model was generated based on ten low-passaged (< 4-12 passages) primary cell lines derived from *Ptf1a$^{wt/Cre}$; Kras$^{wt/LSL-G12D}$; Trp53$^{loxP/loxP}$* mice. The pancreas-specific combination of a heterozygous activating *Kras* mutation with a homozygous *Trp53* knock-out results in the rapid formation of aggressive PDACs, which in key aspects are resembling human PDACs (Heid *et al.*, 2016; Mazur *et al.*, 2015a). Initially, all tested cell lines were sensitive to the MEK inhibitor (MEK$_i$) trametinib with IC50s in the low nanomolar range (Table 3-1).

To induce resistance, cells were treated with increasing doses of MEK_i over 3-4 months until they proliferate in 100 x of their initial IC50 dose. One batch was kept under constant drug treatment, termed resistant hereafter, while another batch of each line was cultivated without MEK_i and samples were labeled according to their passages in drug-free medium (Px) (Figure 3-1B).

Table 3-1: IC50 of trametinib in the ten used parental cell lines

The calculation was based on averaged dose response curves of the indicated independent measurements after 72 h of trametinib treatment.

Cell line	*#1*	*#2*	*#3*	*#4*	*#5*	*#6*	*#7*	*#8*	*#9*	*#10*
IC50 [nM]	25.2	9.4	10.9	11.2	12.9	16.3	14.3	5.3	55.2	10.9
Replicates	2	2	3	3	2	3	3	2	3	3

A multi-omics characterization of parental, resistant and reverting cell states was performed and data were integrated if possible (Figure 3-2). Whole genome sequencing (WGS) was used to identify potential resistance mediating mutations as well as to study cell population dynamics. Whole genome bisulfite sequencing (WGBS) provided a global view on the cells methylome, while RNA-sequencing (RNA-seq) and mass spectrometry (MS) were applied to investigate RNA and protein expression, respectively.

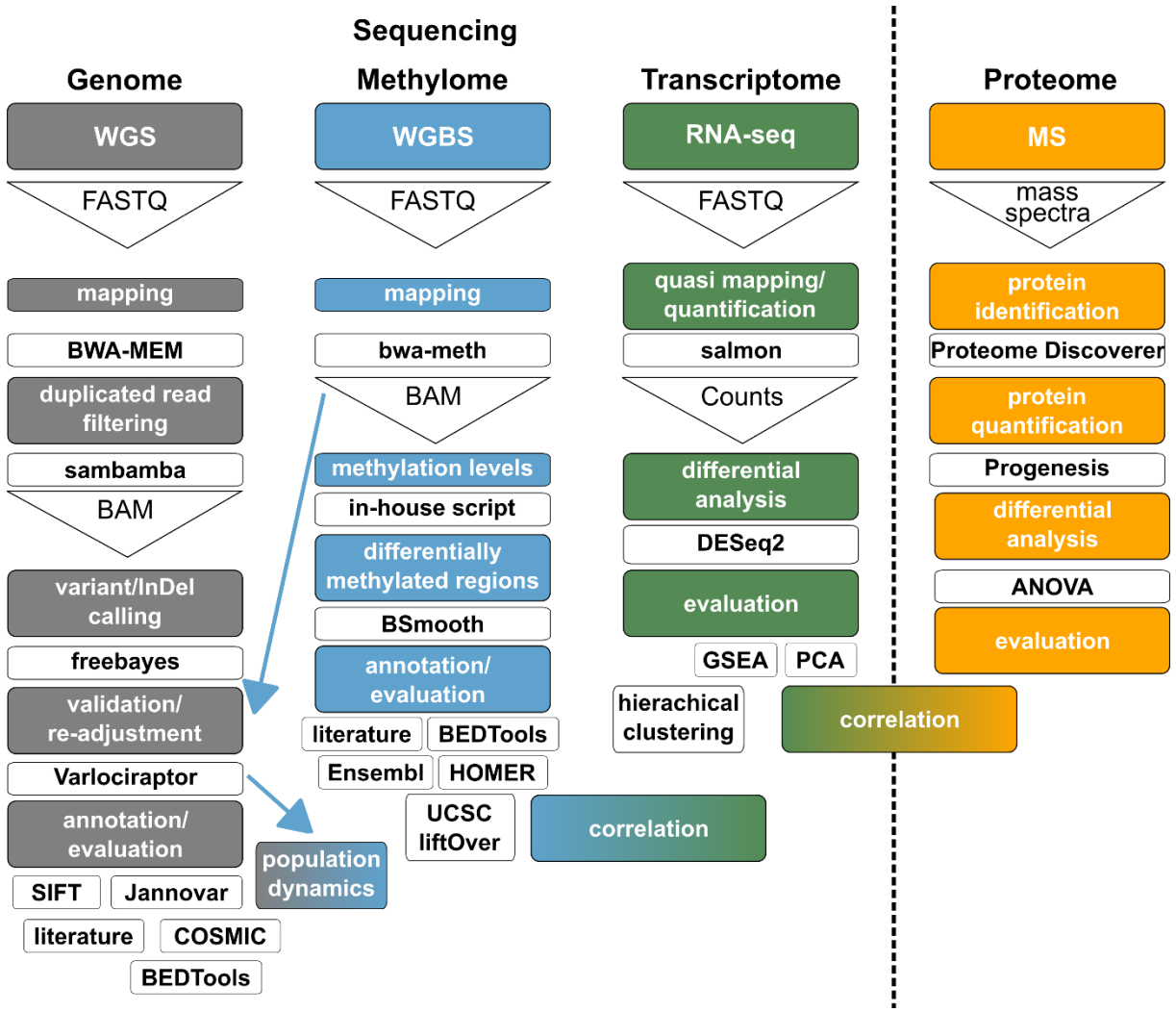

Figure 3-2: Analysis workflow for the multi-omics data of MEK$_i$ resistant PDAC cells

The steps performed for each data type are highlighted in different colors. Data integration is represented by a color gradient. The tools and algorithms used are displayed in white boxes. Triangles describe the output format of the respective analysis step.

3.2 Phenotypic characterization

3.2.1 MEK$_i$ resistance was reversible upon drug withdrawal

All tested cell lines (n=10) developed resistance against MEK$_i$ (Figure 3-3A) accompanied by a strong inhibition of extracellular signal-regulated kinases 1 and 2 (ERK1/2) phosphorylation, which are both direct targets of MEK1/2 (Figure 3-3B). A low remaining ERK1/2 phosphorylation in the resistant cells could only be detected for cell lines #1, #2 and #8. The basal ERK1/2 expression in the parental cells differed up to a factor of three (Figure 3-3C). With about 3.5 relative units, the parental ERK1/2 expression was the highest in cell line #4, while cell lines #3, #6, #7, #9 and #10 demonstrated an intermediate expression level. The lowest ERK1/2 expression in the

parental cells was detected for cells lines #1, #2, #5, #8. In resistant cells, total ERK levels remained stable or slightly decreased compared to their corresponding parental cells.

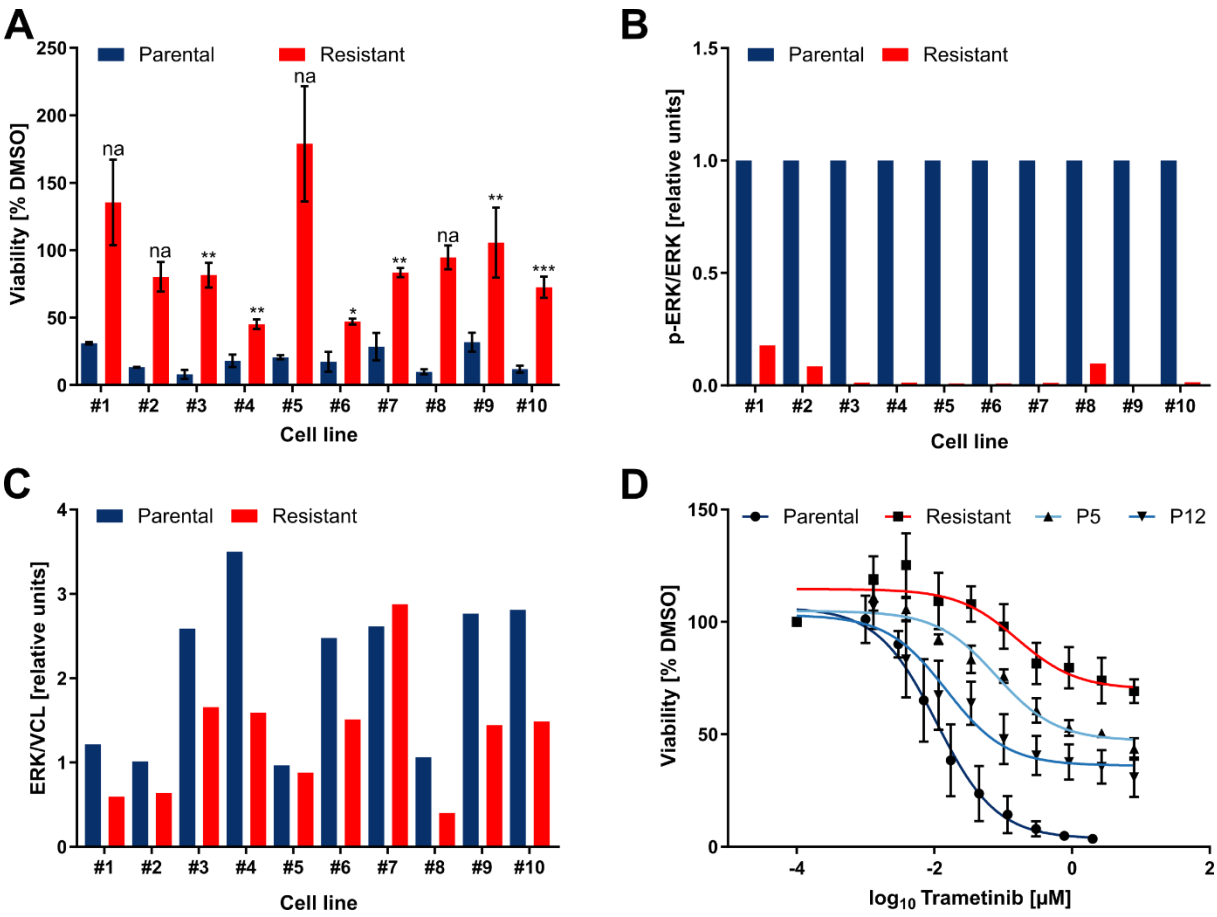

Figure 3-3: ERK1/2 phosphorylation was blocked in MEK$_i$ resistant cells and reversibility of the resistant phenotype occurred after drug withdrawal

MEK$_i$ resistance induction was possible in all ten cell lines tested. Bars represent the mean of two (na, not available) or three independent cell viability measurements after 72 h in 300 nM MEK$_i$ ± SD (*** $p < 0.001$; ** $p < 0.01$; two-tailed unpaired Student's t-test on the log_2 transformed DMSO-normalized values) **(A)**. ERK1/2 phosphorylation analyzed by simple western was blocked in MEK$_i$ resistant cell lines ($p < 0.05$, two-tailed paired Student's t-test on the log_2 transformed ratios) **(B)**. Basal ERK1/2 expression relative to VCL, measured by simple western **(C)**. MEK$_i$ resistance was reversible upon drug withdrawal. The mean of independent dose response curves (n=3) after 72 h incubation ± SD is shown for cell line #3 **(D)**. Results for five additional cell lines are shown in Supplementary Figure 1.

After drug withdrawal a reversibility of the resistant phenotype occurred, the degree of which correlated with the duration of the drug-free cultivation period (Figure 3-3D and Supplementary Figure 1). In most cell lines, after 40 passages (P40) a complete reversion was detected (Supplementary Figure 1).

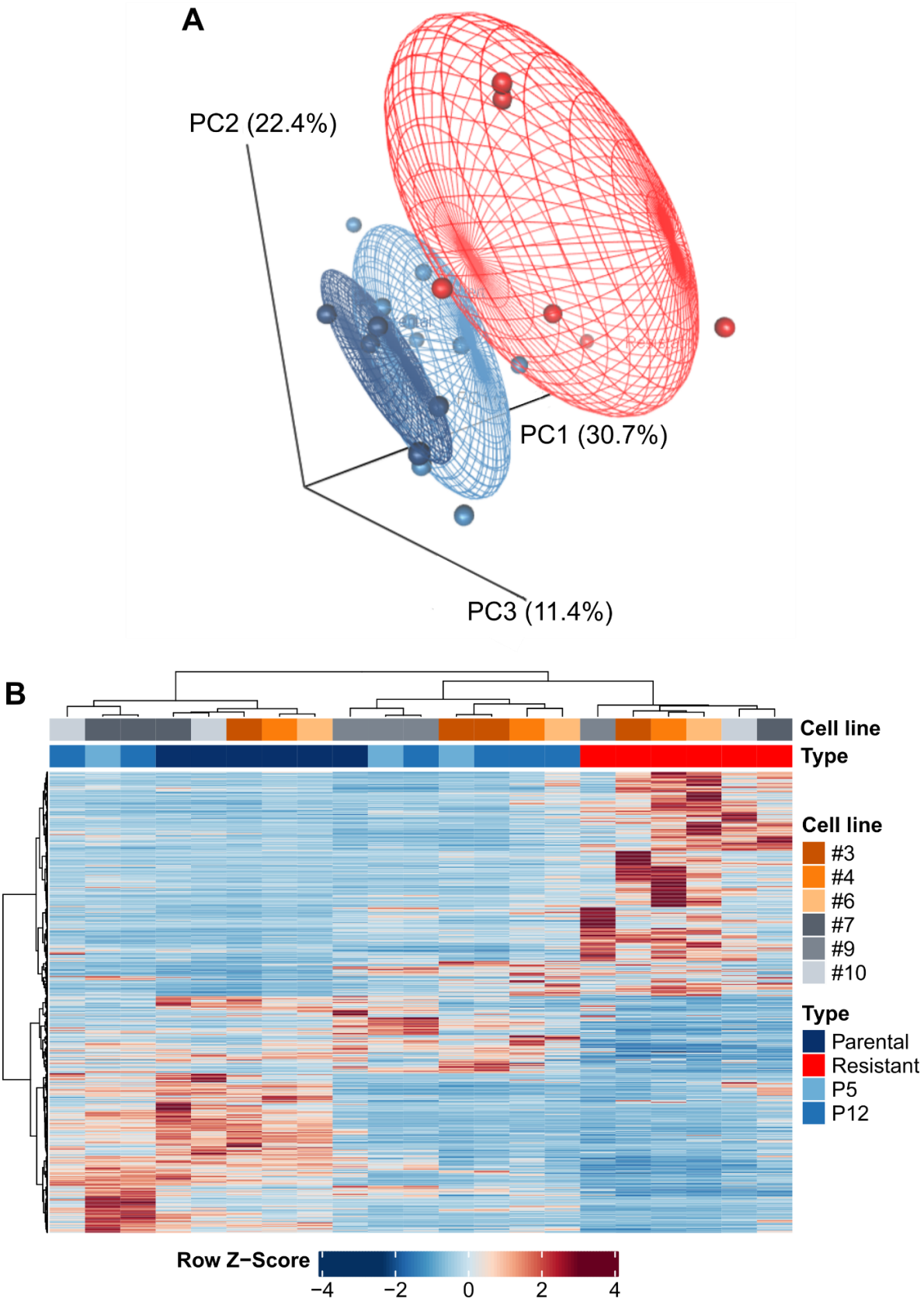

Figure 3-4: Transcriptional variance between parental, resistant and reverting cells underpinned reversibility after drug withdrawal

Principal component analysis of all expressed genes based on RNA-seq revealed a larger difference between the parental (dark blue) and resistant (red) rather than the reverting (P5 and P12; light blue) cell states **(A)**. Hierarchical clustering of genes differentially expressed in parental or resistant cells each compared to the remaining three states separated parental from resistant cells while the reverting states shared characteristics of both **(B)**.

A principal component analysis was performed including all expressed genes measured by RNA-seq in six matched parental, resistant and reverting sample pairs collected for three lines even after 5 (P5, only for #3, #7, #9) or for all six lines after 12 (P12) passages of drug withdrawal. While the transcriptional profiles of parental and resistant cell lines were different, the expression pattern of the reverting cell states resembled that of the parental cells (Figure 3-4A). Next, supervised hierarchical clustering based on genes differentially expressed in parental or resistant cells each compared with the remaining three states was computed. As expected, the resulting dendrogram clearly separated the parental from the resistant cells. Of the reverting cells, some grouped together with the parental cells, whereas the expression signature of others was more similar to the resistant cells (Figure 3-4B). Overall, at the transcriptional level, the impact of MEK_i treatment seemed stronger than the interindividual differences between the cell lines.

In addition, the protein expression of the same six parental, resistant and P12 samples pairs was investigated by MS. Consistently, out of 2175 proteins identified with at least two unique peptides, 168 were significantly differentially expressed between parental and resistant cells (Figure 3-5A). Notably, 105 of the 168 proteins differently expressed between parental and resistant cells also varied between P12 and resistant cells, but only 34 proteins displayed an altered expression between parental and P12 cells (Figure 3-5B-D). Thus, the reversibility of the MEK_i resistant phenotype was not only supported on the mRNA but also on the protein level.

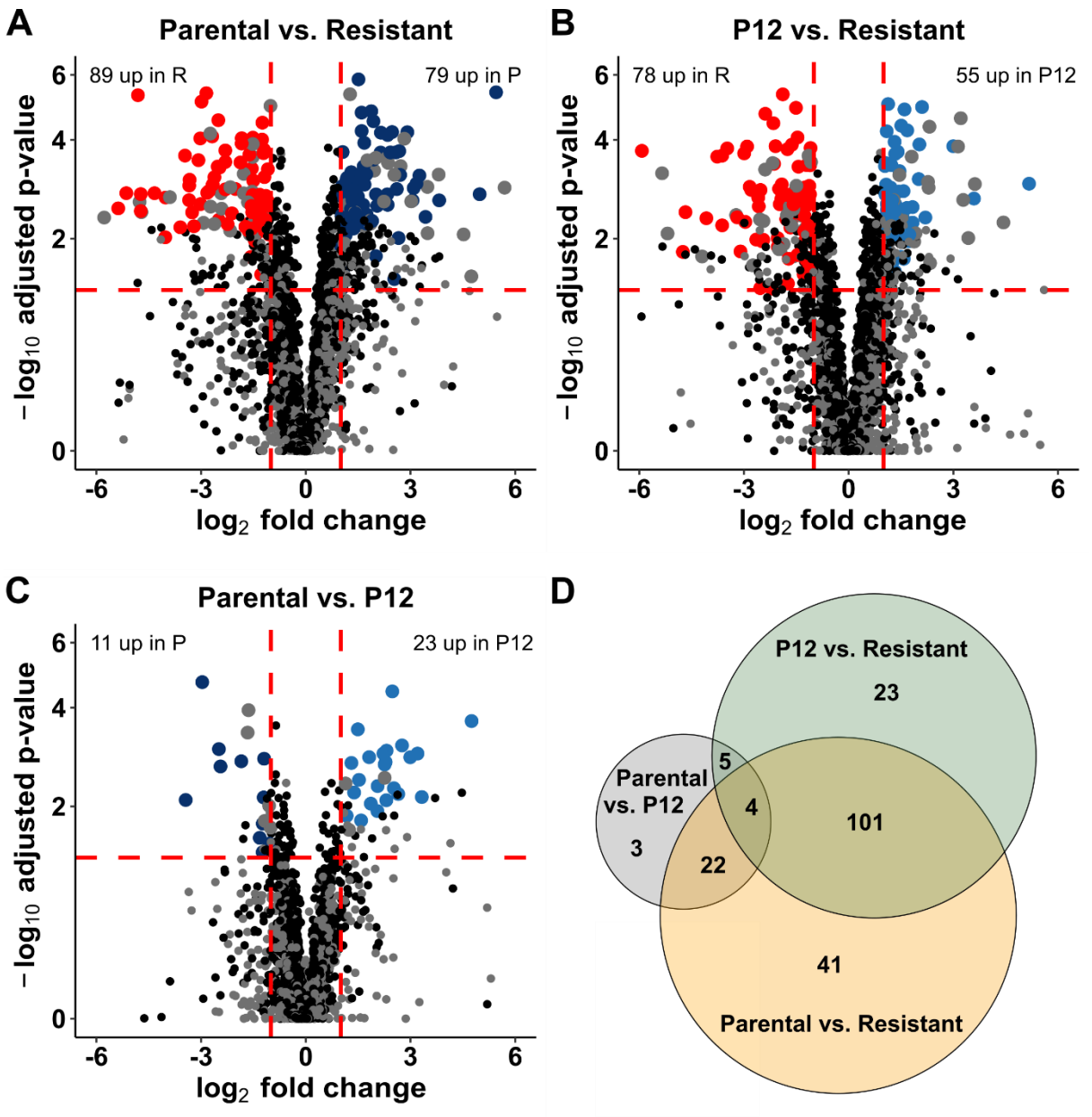

Figure 3-5: Differentially expressed proteins between parental, resistant and reverting cells underpinned reversibility of the induced MEK$_i$ resistance after drug withdrawal

Mass spectrometry unveiled more differentially expressed proteins between resistant and parental **(A)** or P12 **(B)** than between parental and P12 cells **(C)**. Larger colored dots (blue and red) indicate significance ($p < 0.05$ (red horizontal line), $\log_2$ fold change < -1 or > 1 (vertical red lines)) in ANOVA and post-hoc test between the indicated groups and at least 2 unique peptides. Grey dots represent abundances identified by 1 unique peptide. Smaller dots represent abundances that were not significantly different either in ANOVA or post-hoc test or both. In total, 3080 proteins could be quantified by mass spectrometry. Euler diagram displaying the overlap of significantly different abundances per comparison identified with more than 1 unique peptide **(D)**.

3.2.2 MEK$_i$ resistance was associated with EMT and a PDAC subtype switch

Gene Set Enrichment Analysis (GSEA) revealed a significantly enriched signature (normalized enrichment score (NES)=1.73, false discovery rate (FDR)=0.005) which

indicated that the resistant cells underwent epithelial-to-mesenchymal transition (EMT) (Figure 3-6A).

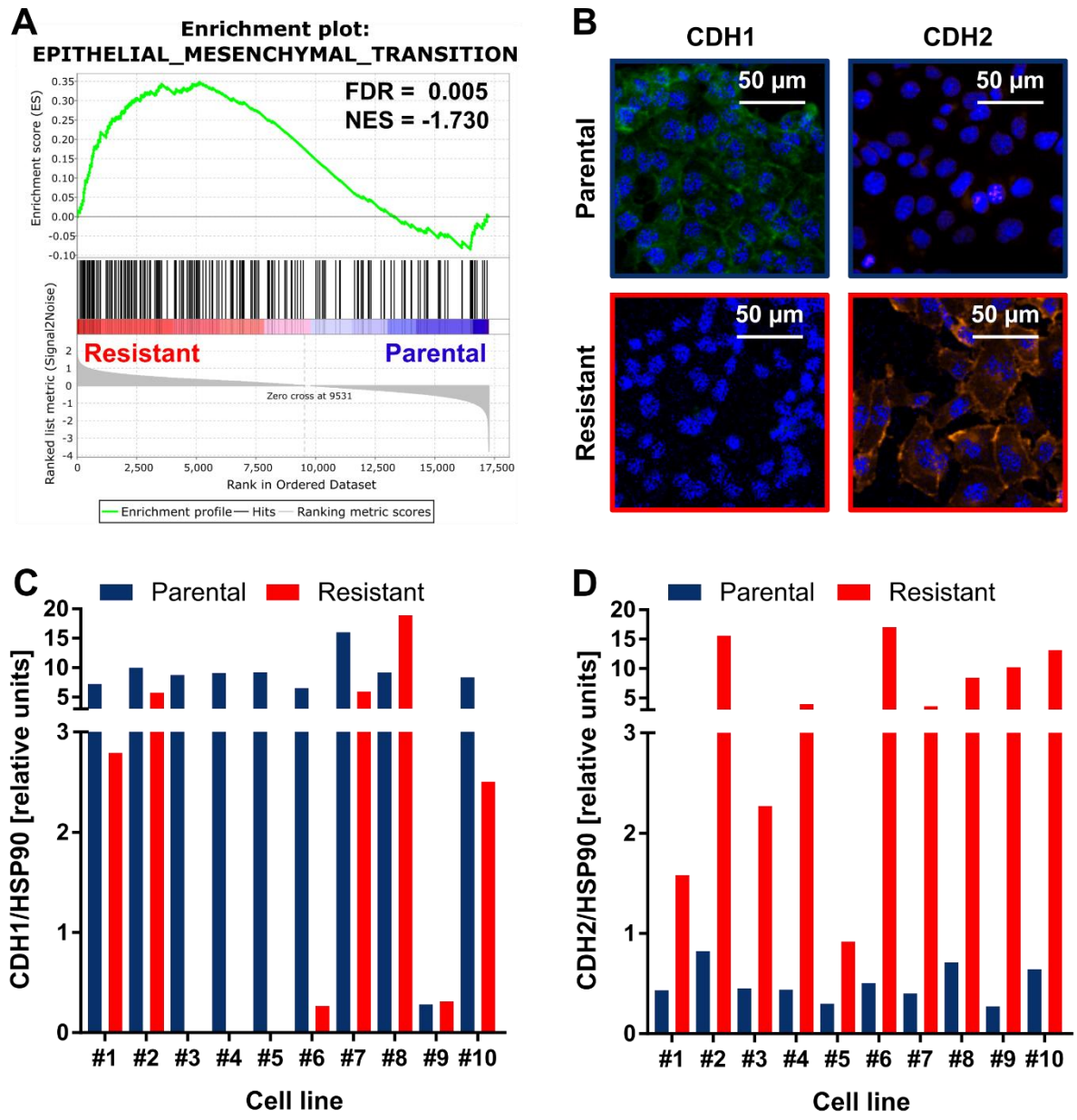

Figure 3-6: MEK$_i$ resistance was accompanied by epithelial-to-mesenchymal transition

Gene Set Enrichment Analysis of RNA-seq from parental compared to resistant cells revealed an enrichment of epithelial-to-mesenchymal transition (EMT)-associated transcripts in the resistant cells **(A)**. Immunofluorescence of CDH1 (green) or CDH2 (orange). DAPI (blue) was used as nuclear counterstain. One representative example (cell line #3) is shown **(B)**. EMT of the resistant cells was further confirmed on the protein level by significantly decreased CDH1 ($p < 0.05$, two-tailed paired Student's t-test on the $\log_2$ transformed ratios between all ten analyzed cell lines) **(C)** and increased CDH2 expression ($p < 0.05$, two-tailed paired Student's t-test on the $\log_2$ transformed ratios between all ten tested cell lines) **(D)**.

The decreased expression of the epithelial marker CDH1 in the resistant cells together with an increase of the mesenchymal marker CDH2 confirmed the association of EMT and MEK_i resistance also on the protein level (Figure 3-6B-D).

While CDH1 expression was completely abolished in the resistant cells of lines #3, #4 and #5, the other cell lines except #8 and #9 displayed a moderate to strong reduction (Figure 3-6C). An increase of CDH1 in the resistant cells could only be observed for cell line #8, in which the expression was 1.5 times higher compared to the parental cells. In contrast to all other tested cell lines, the CDH1 expression was low even in the parental cells of line #9 and was maintained at the same level in the resistant cells. The basal CDH2 expression was similar in all ten cell lines analyzed. The increase in the resistant cells ranged from three times the parental expression in cell line #5 to about 37 times in cell line #9 (Figure 3-6D).

The fact that the resistant cells displayed mesenchymal properties is of particular interest with regard to two PDAC subtypes, which were consistently identified in several different studies (Bailey *et al.*, 2016; Collisson *et al.*, 2011; Moffitt *et al.*, 2015). While the classical/pancreatic progenitor subtype displays a more epithelial-like phenotype, the squamous/quasi-mesenchymal/basal-like subtype is associated with mesenchymal characteristics. Hierarchical clustering based on the RNA expression of known subtype-specific genes defined by Bailey *et al.* (Bailey *et al.*, 2016) showed a perfect separation of the parental from the resistant cells (Figure 3-7A). When repeating the analysis with the subtype-defining genes from Collisson *et al.* (Collisson *et al.*, 2011) or Moffitt *et al.* (Moffitt *et al.*, 2015) a similar result was obtained, albeit parental cells of line #9 clustered with the resistant cells (Figure 3-7B,C). Of the parental cells, cell line #9 displayed the highest IC50 of MEK_i and can be considered the most mesenchymal line of the cohort due to its lack of CDH1 expression (Table 3-1 and Figure 3-6C).

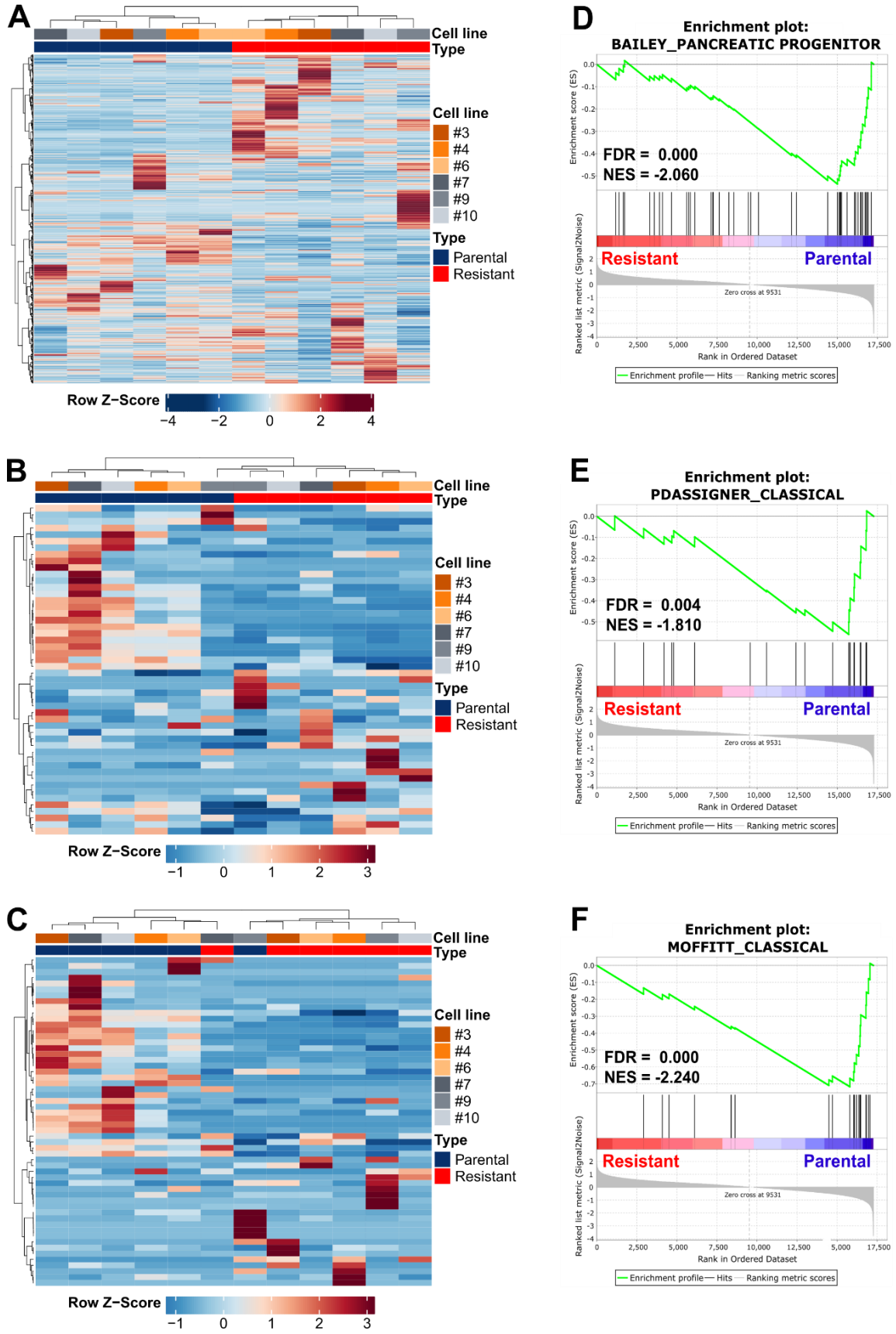

Figure 3-7: MEK$_i$ resistance was accompanied by a subtype switch from classical to basal-like PDAC

Hierarchical clustering **(A-C)** and Gene Set Enrichment Analysis **(D-F)** of the parental and resistant cells based on the expression of metagenes for the epithelial (pancreatic progenitor/classical) and the mesenchymal (squamous/quasi-mesenchymal/basal-like) subtype as defined by Bailey *et al.* (Bailey et al., 2016) **(A,D)**, Collison *et al.* (Collisson *et al.*, 2011) **(B,E)** and Moffitt *et al.* (Moffitt *et al.*, 2015) **(C,F)**.

Unique gene sets were defined based on the subtype-specific genes derived from the mentioned studies and GSEA was performed with the RNA-seq data.

Thereby, all three signatures related to the epithelial subtype (classical or pancreatic progenitor subtype) were significantly enriched in the parental cells with a NES below -1.8 and an FDR < 0.001 (Figure 3-7D-F).

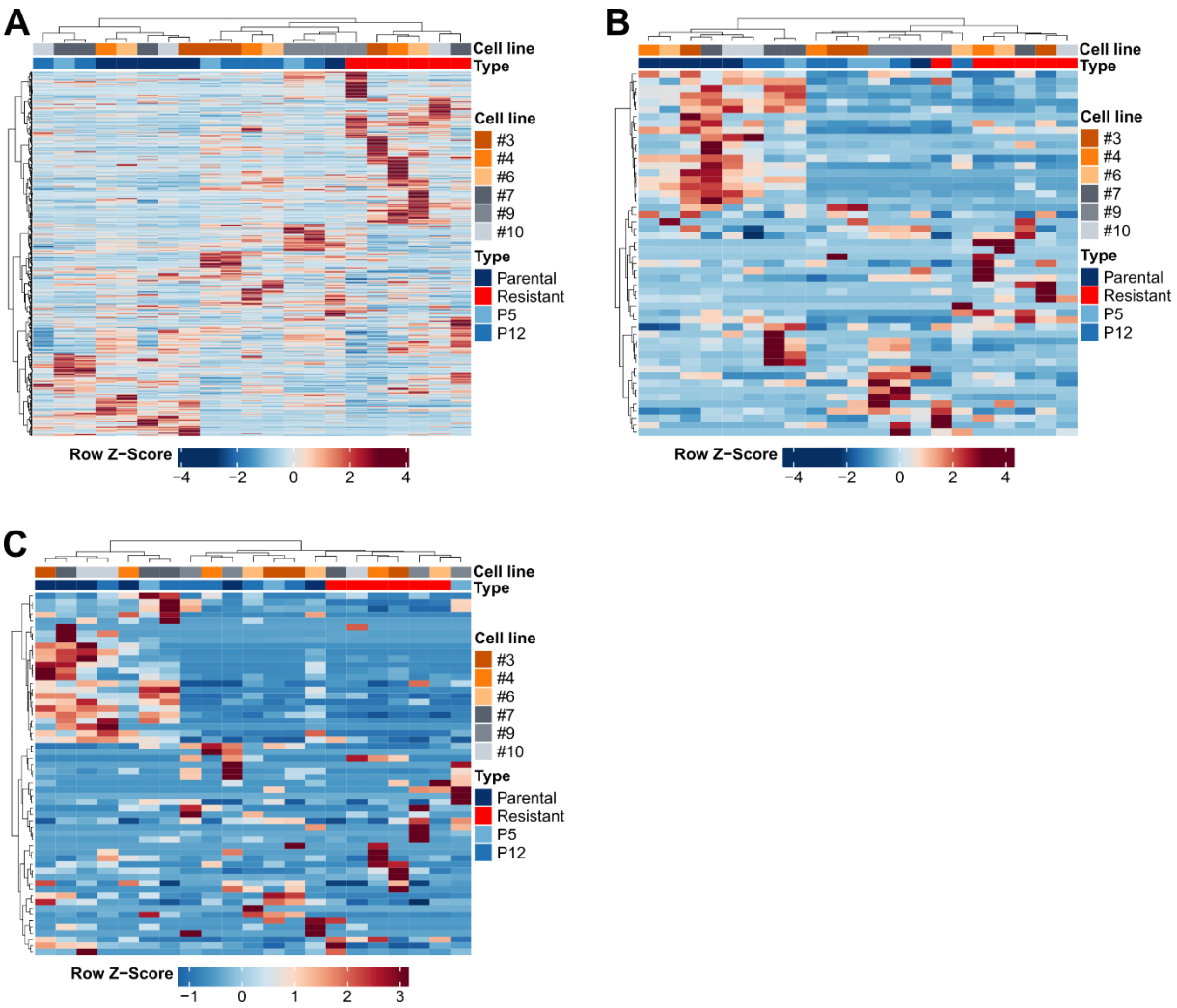

Figure 3-8: Reverting cells displayed transcriptional changes in the subtype-defining genes

Hierarchical clustering of parental, resistant and reverting (P5 and P12) cells based on the expression of metagenes for the epithelial (pancreatic progenitor/classical) and the mesenchymal (squamous/quasi-mesenchymal/basal-like) subtype as defined by Bailey *et al.* (Bailey et al., 2016) **(A)**, Collison *et al.* (Collisson *et al.*, 2011) **(B)** and Moffitt *et al.* (Moffitt *et al.*, 2015) **(C)**.

In light of the observed reversibility of the resistant phenotype, the question arose to which subtype the reverted cell states can be assigned. In a re-clustering based on the gene expression of assigner genes proposed by Bailey *et al.* (Bailey *et al.*, 2016) including the reverting cell states P5 and P12, the clear separation of parental and resistant cells was almost maintained (Figure 3-8A). However, the parental line #9 now

clustered with the resistant ones as previously described for the other gene sets. The reverting samples built separate clusters either adjacent to the parental or the resistant cells. For cell lines #3, #7 and #9 in which a P5 as well as a P12 sample were sequenced, both samples clustered together. Hierarchical clustering based on the expression of genes defined by Collisson *et al.* (Collisson *et al.*, 2011) or Moffitt *et al.* (Moffitt *et al.*, 2015) led to a similar dendrogram (Figure 3-8B,C).

Analyzing the expression pattern of CDH1 and CDH2 as surrogate markers for epithelial and mesenchymal cell characteristics, a significantly reverting mRNA expression was observed for both (Figure 3-9A,B). The strongest decrease of the *Cdh1* expression in the resistant cells was observed for cell line #4 by a $\log_2$ fold chance of 13 while the reduction in cell line #7 was only marginal. On the protein level based on MS, the CDH1 decrease in the resistant cells correlated with the corresponding mRNA expression, but in P12 the CDH1 level P12 remained similar to that in the resistant cells for lines #4, #6 and #7 or further decreased in lines #3 and #10 (Figure 3-9C). A slightly reverting pattern could only be observed for cell line #9, whereas its parental expression had a $\log_2$ fold chance of about 1.6 below the median CDH1 expression across all six parental cells analyzed. For CDH2, a reversion as in the corresponding RNA-seq data was observed in all six cell lines (Figure 3-9D). In contrast to the MS results, in a simple western analysis, the CDH1 expression was restored in P5 and P12 of cell lines #3, #4, #7 to varying degrees, but not in line #9, which already showed a 30 fold lower CDH1 expression in the parental cells compared to the median of the other three tested lines (Figure 3-9E). After drug withdrawal, the expression level of the mesenchymal marker protein CDH2 decreased in all four tested cell lines and thereby independently confirmed the results obtained by MS (Figure 3-9F).

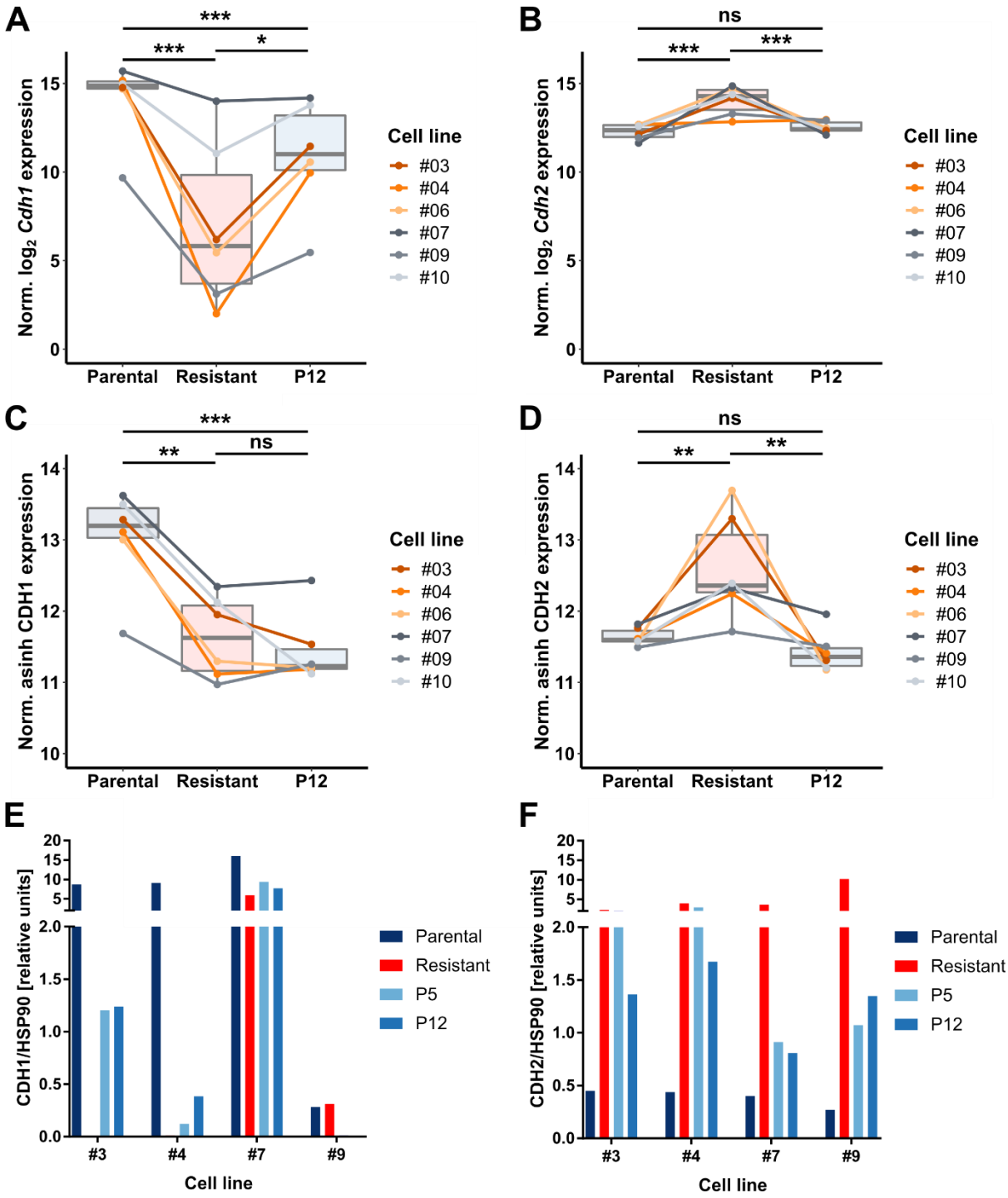

Figure 3-9: Expression of CDH1 and CDH2 partially reverted after drug withdrawal

Normalized (Norm.) and log_2 transformed RNA-seq read counts of *Cdh1* **(A)** and *Cdh2* **(B)** displayed a reverting pattern in P12 samples (*** $p < 0.001$; ** $p < 0.01$; * $p < 0.05$; ns, non-significant; differential expression analysis). Mass spectrometry revealed a significant lower CDH1 **(C)** protein expression in resistant and P12 samples than in parental cells, while CDH2 **(D)** levels increased in the resistant cells and decreased to the parental expression level in P12 (*** $p < 0.001$; ** $p < 0.01$; ns, non-significant; ANOVA with Tukey post-hoc test). Normalized CDH1 **(E)** or CDH2 protein expression **(F)** based on simple western in four matched parental, resistant, P5 and P12 samples.

3.3 Mutational landscape and cell population dynamics

3.3.1 Whole genome sequencing-based mutation analysis of MEK_i resistant cells

As resistance to targeted therapies is frequently mediated by mutations that lead to re-activation or bypassing of the targeted pathway, WGS was performed to assess genetic alterations associated with MEK_i resistance. Parental and resistant samples of lines #3 and #9 as well as tail DNA of the donor mouse for line #3 were sequenced with a median coverage of 40 x. Single nucleotide variants (SNVs) that could be detected with a variant allelic fraction (VAF) of at least 0.1 in the resistant cells but not in their naïve counterparts were termed ‘variant present in resistant’ (VpR). With 3657 and 3204 VpRs a similar order of magnitude was found in the resistant cells of lines #3 and #9 (Figure 3-10A,B). Following the same principle, variants were defined that were only present in parental cells as ‘variant present in parental’ (VpP). Of these, a considerably smaller number could be identified with 131 VpPs in cell line #3 and 837 in cell line #9 (Figure 3-10A,B).

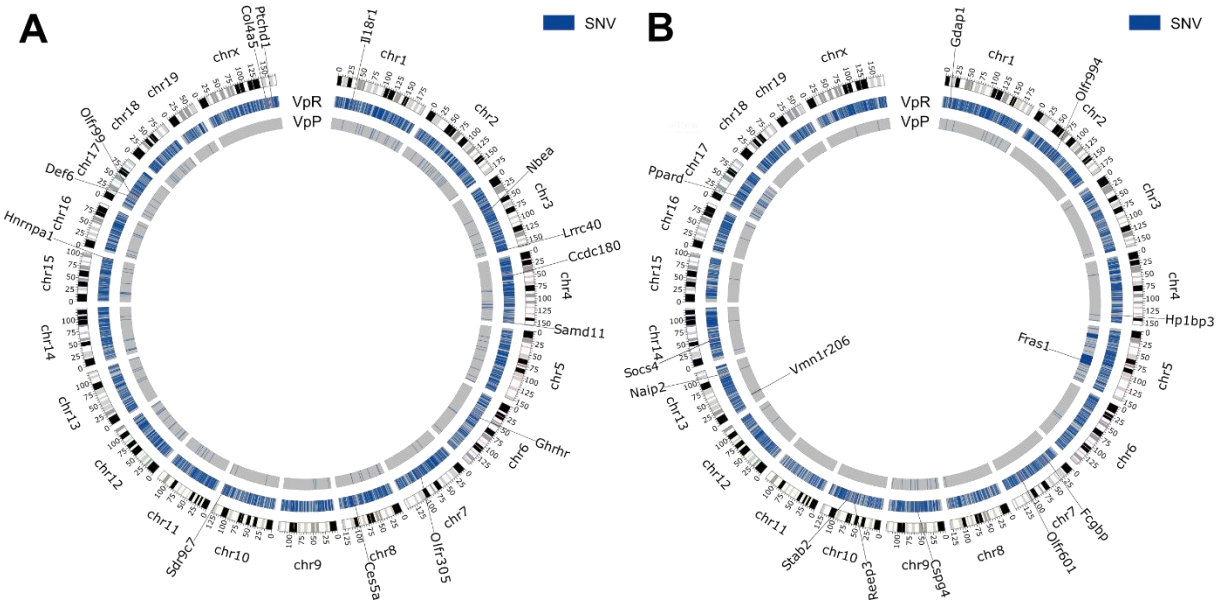

Figure 3-10: Single nucleotide variants of resistant compared to parental cells

Circos plots displaying variants present in resistant (VpRs) or variants present in parental (VpPs) in cell lines #3 **(A)** and #9 **(B)**. Genes predicted as deleterious by SIFT are named. Both graphs were plotted by Jan Forster.

Since it is highly unlikely that MEK_i resistance is associated with a loss of a specific mutation, the following analyses focused primarily on the characterization of VpRs. Less than 1 % of them were located in the coding sequence of the genome (36 in #3 and 23 in #9). Of these, 25 (cell line #3) and 19 (cell line #9) were nonsense or

missense mutations. To estimate their impact on the cell, SIFT prediction was performed revealing 14 and 11 deleterious variants for cell lines #3 and #9, respectively (Figure 3-10A,B and Supplementary Tables 1-3). Using a second approach by Jannovar, the proposed impact of the SIFT deleterious VpRs was only moderate. Furthermore, none of the genes affected by a VpR is known to be involved in the targeted MEK nor the parallel phosphatidylinositol 3-kinase (PI3K) pathway or listed in the COSMIC database to confer therapy resistance to human cancer cells. In addition to SNVs, small insertions and deletions (InDels) were called but none of the genes affected is known to be involved in re-activation or bypassing of the MEK pathway. In particular, the parallel PI3K pathway was not affected by InDels. A comparison between both cell lines showed that neither the same variant occurred, nor the same gene or genes associated with the same pathway were affected.

3.3.2 Whole genome sequencing revealed clonal expansion during acquired MEK_i resistance

In addition to mutational analyses, the high resolution sequencing data on the whole genome level allowed to assess whether the MEK_i resistance of murine PDAC cell lines was the result of a poly-clonal event or based on clonal expansion. Poly-clonality would indicate the existence of an adaptive capacity in most of the different cell clones in the parental cell population. In contrast, clonality relies in theory on a single clone harboring an *a priori* MEK_i resistance or the capability to acquire resistance in presence of the drug.

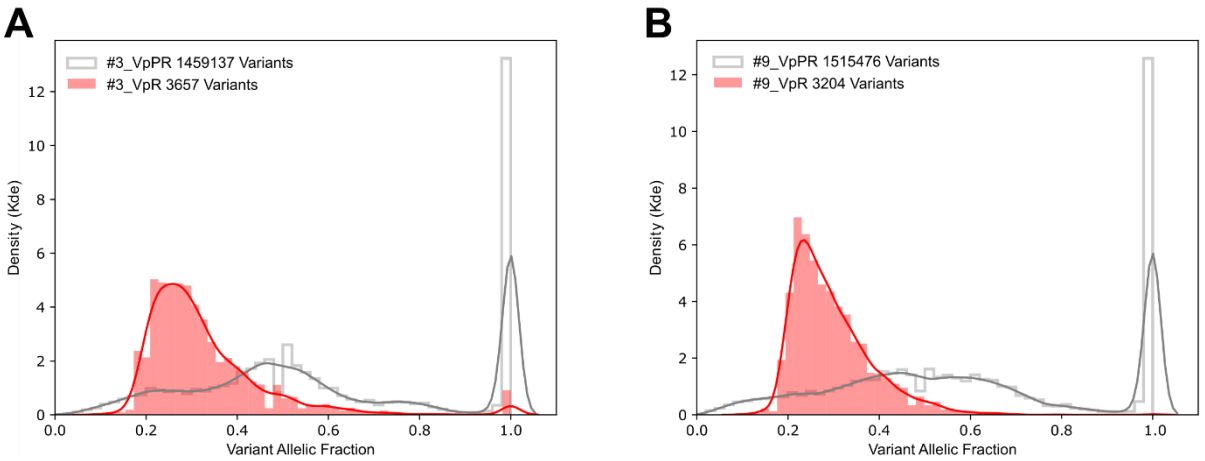

Figure 3-11: Variant allelic fraction of VpRs shifted compared to VpPRs

Kernel density estimation (kde) for the allelic fraction of variants exclusively detected in resistant cells (VpRs) compared to variants present in parental and resistant (VpPRs) for cell lines #3 **(A)** and #9 **(B)**. Both graphs were plotted by Jan Forster.

To address this question, the distribution of the VAF of VpRs was analyzed. Compared to the variants present in both parental and resistant cells (VpPRs), the VAF of VpRs shifted remarkably and peaked around 0.25 in both cell lines (Figure 3-11A,B).

One explanation would be the co-existence of two resistant clones in almost equal proportions. Owing to the fact that similar observations were made in two independent matched-pairs and an equally balanced co-existence of two different cell clones would be an unlikely event, aneuploidy was rather considered. Tumor cells are known to be affected by chromosomal instability that could result in the multiplication of single chromosomes or even the whole set of chromosomes. By performing a cytogenetic analysis of metaphase chromosomes, a numeric anomaly was found already in the parental cells. Instead of 40 chromosomes per diploid cell, 77 chromosomes in line #3 and 70 chromosomes in line #9 were counted in the median indicating a near tetraploidy for both cell lines (Figure 3-12 and Table 3-2).

Figure 3-12: Murine PDAC cell lines harbor a near tetraploidy

Representative example of a mitosis with 63 chromosomes of cell line #9 after Giemsa staining at 140 x magnification. The image was taken by Elke Jürgens.

Table 3-2: Numbers of evaluated mitosis in parental cells after staining with Giemsa

A representative example for 63 mitotic chromosomes pre nucleus in cell line #9 is displayed in Figure 3-12 (na, not available).

Number	*1*	*2*	*3*	*4*	*5*	*6*	*7*	*8*	*9*	*10*	*11*	*12*
Karyotype cell line #3	76	79	78	74	na	na	na	na	na	na	na	na
Karyotype cell line #9	70	70	70	67	59	70	70	60	73	70	63	70

In accordance, the evaluation of the VAF of VpRs per chromosome revealed an incomplete doubling for distinct chromosomes indicated by a VAF peak > 0.25, e.g. for chromosomes 9, 12 or 13 of cell line #3 or chromosomes 5 or 19 of line #9 (Figure 3-13A,B). Taken together, the observed VAF distribution peak at 0.25 in these almost tetraploid cells suggests that the MEK_i resistant cells are the result of a clonal expansion of a single cell clone. Furthermore, most VpRs must have occurred after the tetraploidy.

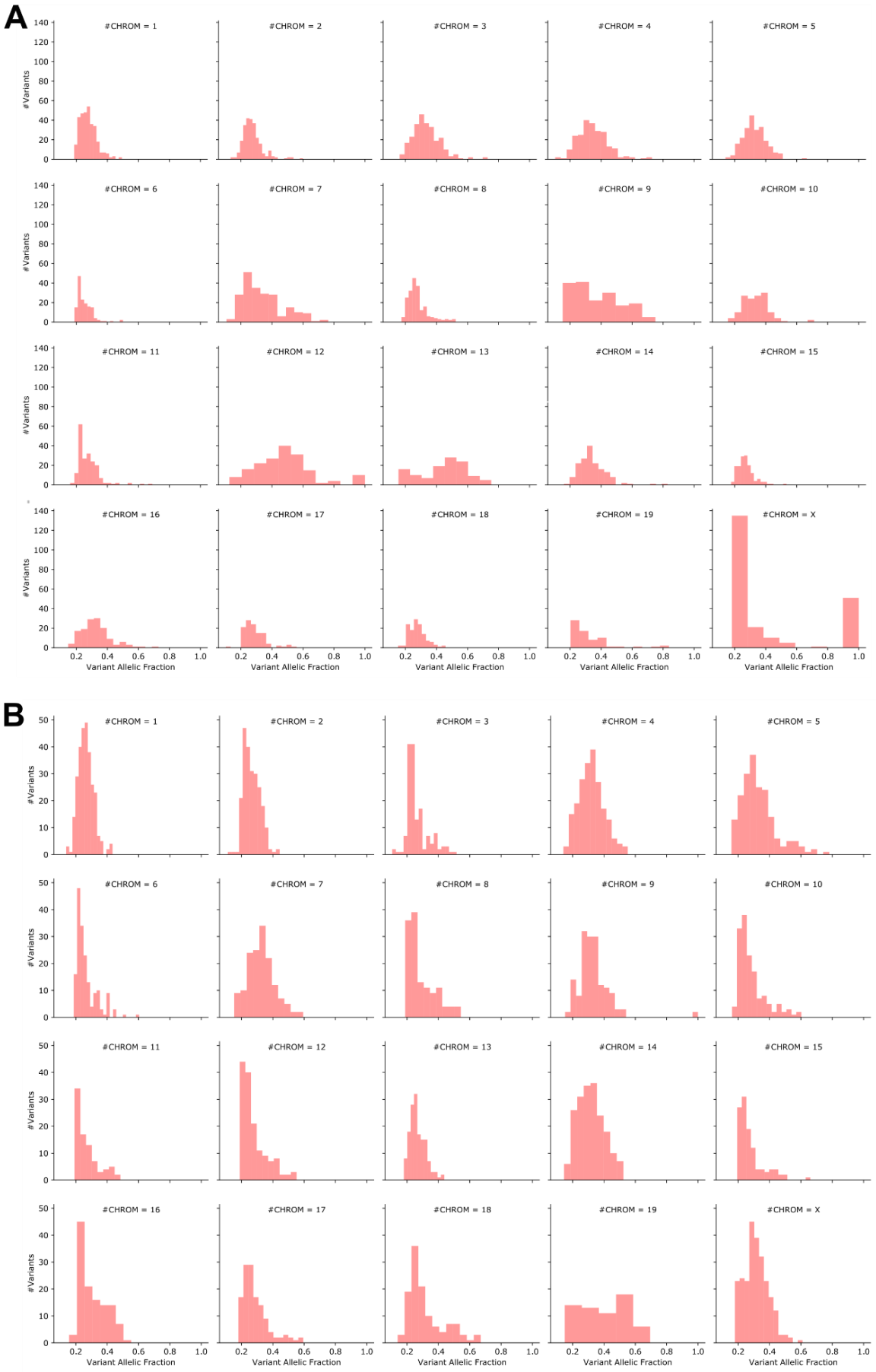

Figure 3-13: Individual chromosomes demonstrated an aneuploidy deviating from a quadrupling

Histogram of the allelic fraction of variants present in resistant (VpRs), separated by chromosome for cell line #3 **(A)** or #9 **(B)**. Both graphs were plotted by Jan Forster.

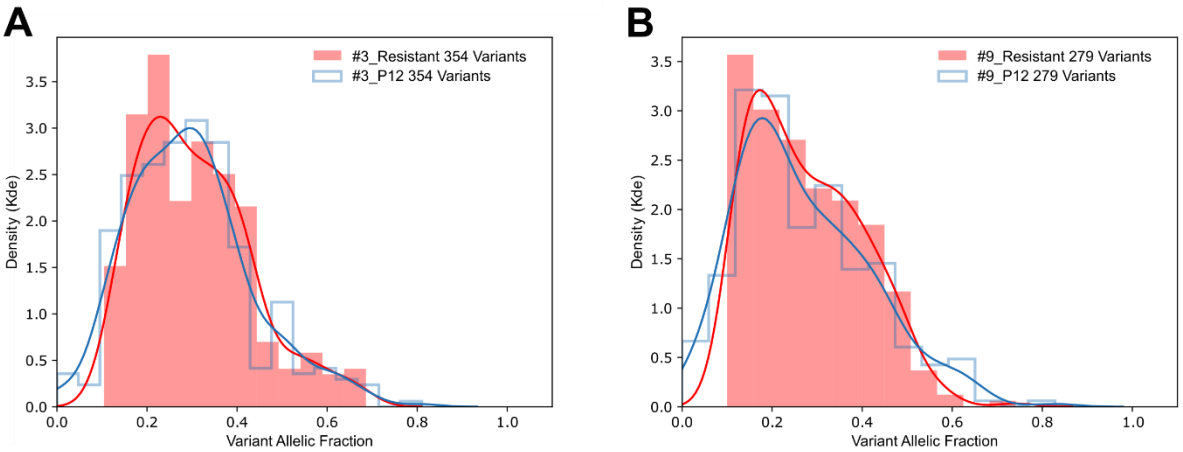

Figure 3-14: Reversion of MEK$_i$ resistance upon drug withdrawal was not due to a parental outgrowth

Based on A > T and T > A, variants called by WGS and validated by WGBS with at least 15 x coverage are shown. Kernel density estimation (kde) of the allelic fraction of variants present in resistant (VpRs) in resistant compared to P12 cells of cell line #3 **(A)** or #9 **(B)**. Both graphs were plotted by Jan Forster.

A question resulting from these data was whether a small fraction of parental cells survived the MEK$_i$ treatment and started to re-grow upon drug withdrawal, thus, outcompeting the resistant cell population over time. Therefore, the available WGBS data of parental, resistant and P12 cells of lines #3 and #9 were analyzed, where the DNA samples of the parental and resistant cells were the same as for WGS. Due to C/T substitutions caused by bisulfite conversion, the analysis was limited to A > T and T > A variants previously identified by WGS. A minimum coverage of 15 was assumed. Thereby, 354 or 279 VpRs and 10 or 36 VpPs could be used for further evaluation. Almost all VpRs were found also in P12 cells with a VAF distribution similar to the resistant cells while all except 2 VpPs, were not detectable in P12 cells (Figure 3-14A,B).

3.4 Global DNA methylation analysis

3.4.1 MEK$_i$ resistance was associated with DNA hypermethylation

The observed transcriptional differences between parental and resistant cells including a phenotypic switch in combination with their mutational landscape suggest that epigenetic regulation may be involved in MEK$_i$ resistance. Therefore, a drug screening was applied to test inhibitors that target chromatin modifiers, chromatin readers and DNA methylation. MEK$_i$ resistant cells but not their naïve counterparts displayed a strong sensitivity for the DNA methyltransferase (DNMT) inhibitor (DNMT$_i$) decitabine (Figure 3-15A-C). While the effect of class I-specific or pan histone deacetylase

(HDAC) inhibition was slightly more pronounced in the resistant cells, the BET protein inhibitor (BET_i) JQ1 revealed an opposite effect (Figure 3-15A,B).

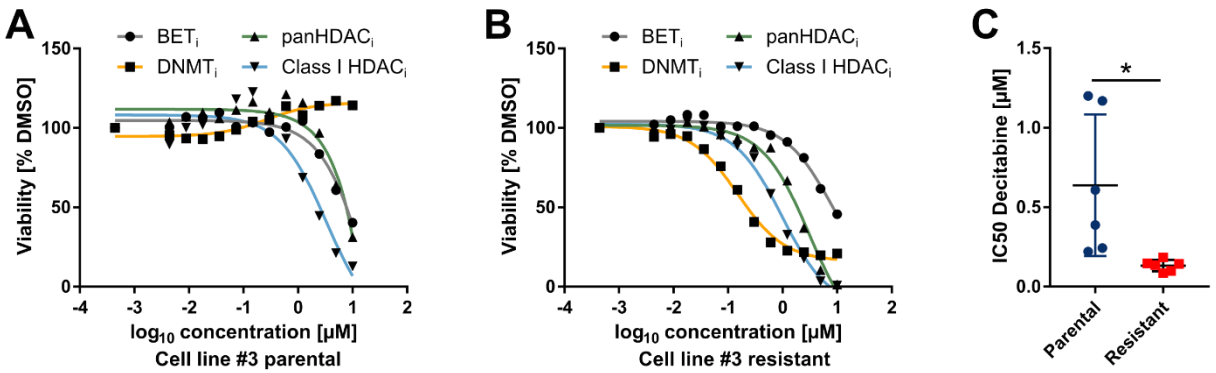

Figure 3-15: MEK_i resistant but not parental cells exhibited a remarkable sensitivity for DNA methylatransferase inhibition

Cell viability screening using inhibitors targeting different epigenetic modulators in parental **(A)** or resistant cells **(B)** shown for cell line #3 as a representative example. The dose response curves determined after 72 h with the CellTiter-Glo® cell viability assay are displayed. The IC50 of the DNA methyltransferase inhibitor ($DNMT_i$) decitabine was significantly lower in six matched-pairs of parental versus resistant cells (* $p < 0.05$; two-tailed paired Student's t-test) **(C)**.

Owing to the remarkable $DNMT_i$ sensitivity for the resistant cells only, genome-wide DNA methylation changes upon MEK_i treatment were assessed by WGBS. Sequencing was performed with cell lines #3 and #9 for the parental, resistant, P5 and P12 samples, respectively. The overall gene body methylation was the same over all four analyzed states and showed a typical drop of DNA methylation at transcription start and end sites (Figure 3-16A). Next, differentially methylated regions (DMRs) were defined as regions of at least four CpGs with a minimal methylation level difference of 0.4. Compared to the parental cells, 2191 DMRs were detected in the resistant cells, covering a total of 38,000 CpGs almost equally distributed over all chromosomes (Figure 3-16B,C). On average, one DMR consisted of 17 CpGs (min=4, max=178) with a mean length of 794 bp (min=12 bp, max=4157 bp).

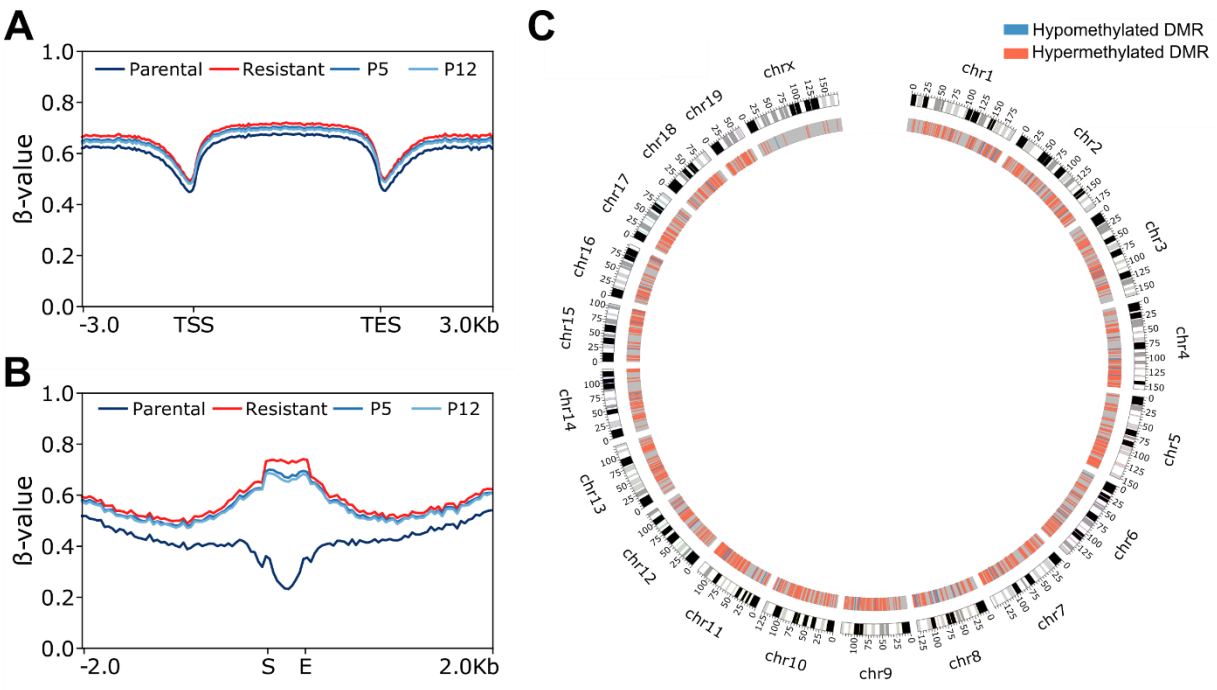

Figure 3-16: MEK$_i$ resistance was accompanied by DNA hypermethylation

Whole genome bisulfite sequencing was performed with cell lines #3 and #9. Mean gene body methylation levels in parental, resistant, P5 and P12 cells. (TSS: transcription start site; TES: transcription end site) **(A)**. Mean methylation levels of all DMRs and their flanking regions (± 2 kb) in the four indicated cell states. (S: start DMR; E: end DMR) **(B)**. Circos plot illustrates the chromosomal location of 2191 DMRs between two parental and resistant cell lines **(C)**. All three graphs were plotted by Jan Forster.

Notably, more than 96 % of the DMRs were hypermethylated in the resistant cells (Figure 3-17A). Since a conserved DNA sequence between mice and humans suggests a potential relevance of the region, the nucleotide sequence conservation of the murine DMRs compared to human was estimated using the UCSC liftover tool. In this approach, about 76 % of DMRs had a conserved underlying DNA sequence (Figure 3-17B). Next, the DMRs were categorized according to their location in the genome either relative to CpG islands or genes. The majority of 43.37 % was located outside of CpG islands in the ocean areas of the genome, while only 8.26 % had a direct CpG island overlap (Figure 3-17C). In the island flanking regions, 39.25 % and 6.12 % were found in the shores and shelfs that were defined as 2000 bp around a CpG island and 2000 bp around shores, respectively. Related to genes, nearly one third (29.53 %) of the DMRs was located intergenically, whereas of the intragenic DMRs, 65.95 % were intronic and 4.52 % exonic (Figure 3-17D).

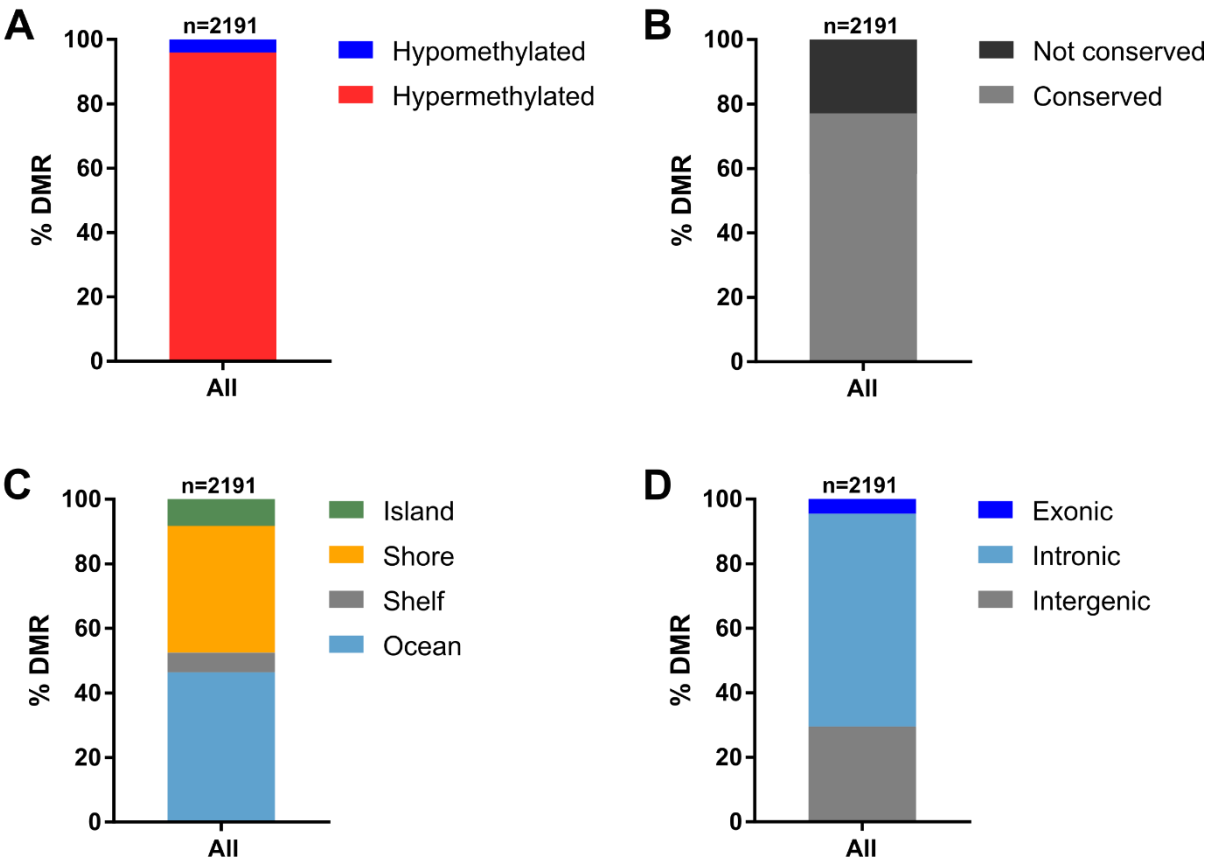

Figure 3-17: Characterization of differentially methylated regions between parental and resistant cells

The majority of DMRs was hypermethylated in resistant cells **(A)**. The sequence of about 76 % of DMRs was conserved between mouse and human according to the UCSC liftover tool **(B)**. Relative location of DMRs compared to CpG islands **(C)** or genes **(D)**.

To investigate a possible correlation of DNA methylation and the expression of certain associated genes, two flanking genes were annotated to each DMR based on the nearest transcription start side (TSS) in both directions. The median distance from the DMR was similar for the left (median=24332 bp, interquartile range=82664.5 bp) and right flanking genes (median=24687 bp, interquartile range=77395.5 bp). Gene expression was correlated using RNA-seq data of the same cell lines. More than half of the flanking genes were not differentially expressed between parental and resistant cells (Figure 3-18A,B). Based on studies of CpG islands in gene promotors, DNA hypomethylation is thought to be associated with active transcription and hypermethylation with gene silencing, but beyond promotors the regulation seems more complex. In the two sequenced cell lines, either one third of hypomethylated DMR flanking genes were upregulated or about 25 % downregulated in case of DMR hypermethylation (Figure 3-18A,B).

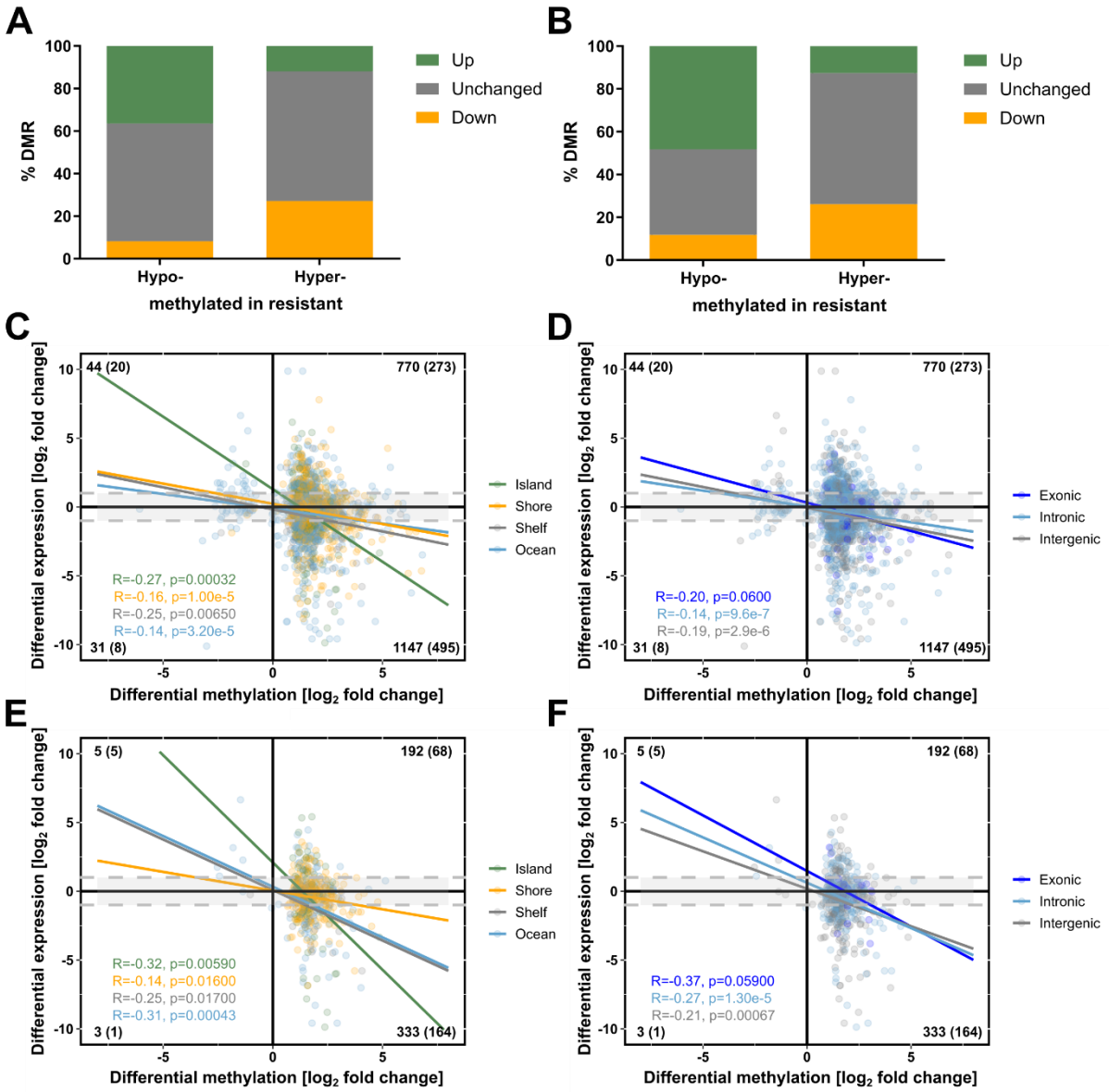

Figure 3-18: Correlation of differentially methylated regions with the expression of flanking genes

Expression changes of the two flanking genes with the nearest transcription start site left **(A)** or right **(B)** from the DMRs in MEK$_i$ resistant cells. (up: adjusted p-value < 0.05 and log_2 fold change resistant vs. parental cells > 1; down: adjusted p-value < 0.05 and log_2 fold change resistant vs. parental cells < -1). Correlation of DMR methylation changes and the expression changes of the nearest downstream gene between parental and resistant cells separated by their location according to CpG islands **(C)** or genes **(D)** was assessed using Pearson correlation. In addition, the analysis was limited to downstream genes with a maximum distance of 7.5 kb from their transcription start site to the DMR **(E,F)**. The number of events is given in each quadrant with the number of significantly differently expressed genes shown in brackets (adjusted p-value < 0.05 and log_2 fold change < -1 or > 1). Dotted grey lines mark log_2 fold changes of 1 and -1.

About 10 % of neighboring genes each showed a direct correlation with the methylation change. Next, the analysis was limited to downstream genes only and DMRs were separated based on their location in the genome. DMRs that overlapped with CpG islands revealed with R=-0.27 and p=0.00032 the highest negative correlation with the

expression of their nearest downstream gene (Figure 3-18C,D). Furthermore, it was investigated whether the correlation depends on the distance of the gene relative to the DMR. Therefore, the 533 DMR were examined exemplarily, which have a downstream gene at a maximum distance of 7500 bp measured from the TSS (Figure 3-18E,F). This led to a stronger negative correlation between DNA methylation and the transcript level of the annotated gene for DMRs overlapping with islands (R=-0.32, p=0.00590), ocean (R=-0.31, p=0.00043) and intragenic regions (intronic: R=0.27, p=0.000013, exonic: R=0.37, p=0.059). However, the correlation coefficient remained weak.

3.4.2 A DMR subset reverted upon drug withdrawal

Due to the resistance reversibility after drug withdrawal, it was investigated whether DMRs exhibit a similar reversibility and are thus likely to be involved in MEK_i resistance. Therefore, a scoring function was developed that reflects the DNA methylation dynamics between parental, resistant and P12 cells (Figure 3-19A). Using the 90 % quantile as a cut-off, 217 DMRs could be identified, whose methylation levels correlated with MEK_i sensitivity (Figure 3-19B-D and Supplementary Tables 4 and 5). Since the P5 cells, which harbored an intermediate MEK_i resistance, were not included in the scoring function, they served as controls. In line with the correlation of methylation and MEK_i sensitivity in the other cell states, the methylation levels of the reverting DMRs of the P5 samples was always between the resistant and the P12 methylation beta-values (Figure 3-19E).

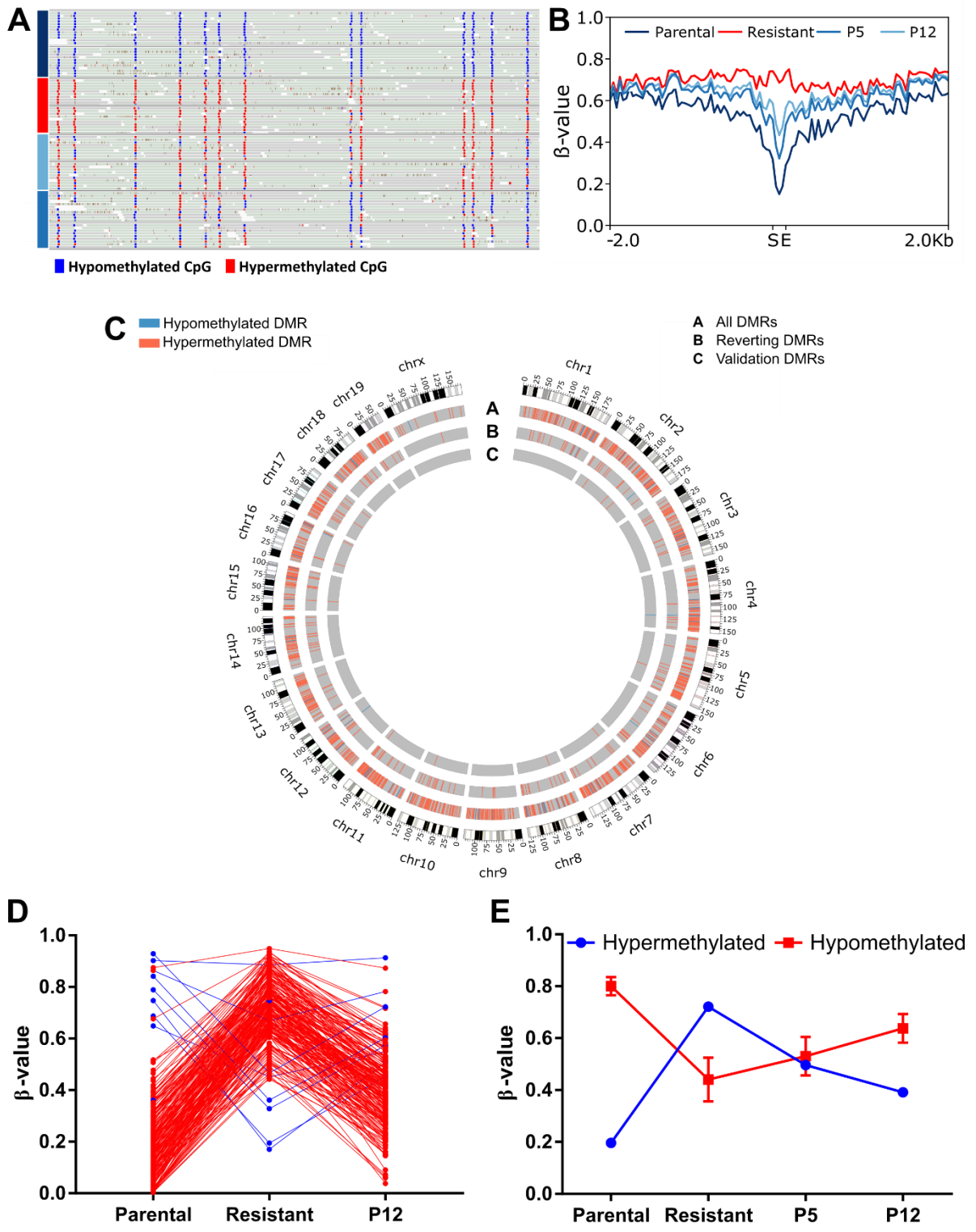

Figure 3-19: Distinct differentially methylated regions reverted after MEK$_i$ withdrawal

Representative Integrative Genomics Viewer snapshot of the reverting DMR_1716 in the parental (dark blue), resistant (red), P5 (light blue) and P12 (blue) cell states of cell lines #3 and #9 (upper row and lower row, respectively). 13 of 16 CpGs are shown **(A)**. Mean methylation levels of the reverting DMRs and their 2 kb up- and downstream regions of cell lines #3 and #9 in the parental, resistant and reverting P5 and P12 cells (S: start DMR; E: end DMR) **(B)**. Circos plot displaying the chromosomal location of all 2191 DMRs between the two parental and resistant cell lines (circle A) or 217 defined reverting DMRs whose methylation pattern in P12 resembles that of parental cells (circle B). Circle C illustrates 15 DMRs that were validated by targeted deep bisulfite sequencing **(C)**. Methylation pattern of 217 reverting DMRs separated into hypo- (blue) and hypermethylated (red) regions **(D)**. Mean methylation ± SEM of 217 reverting DMRs including P5 **(E)**. Graphs A-C were plotted by Jan Forster.

A group of 15 selected DMRs was validated by targeted deep bisulfite sequencing in parental, resistant and P12 samples of four additional cell lines (Figure 3-19C, Figure 3-20A-C and Figure 3-21).

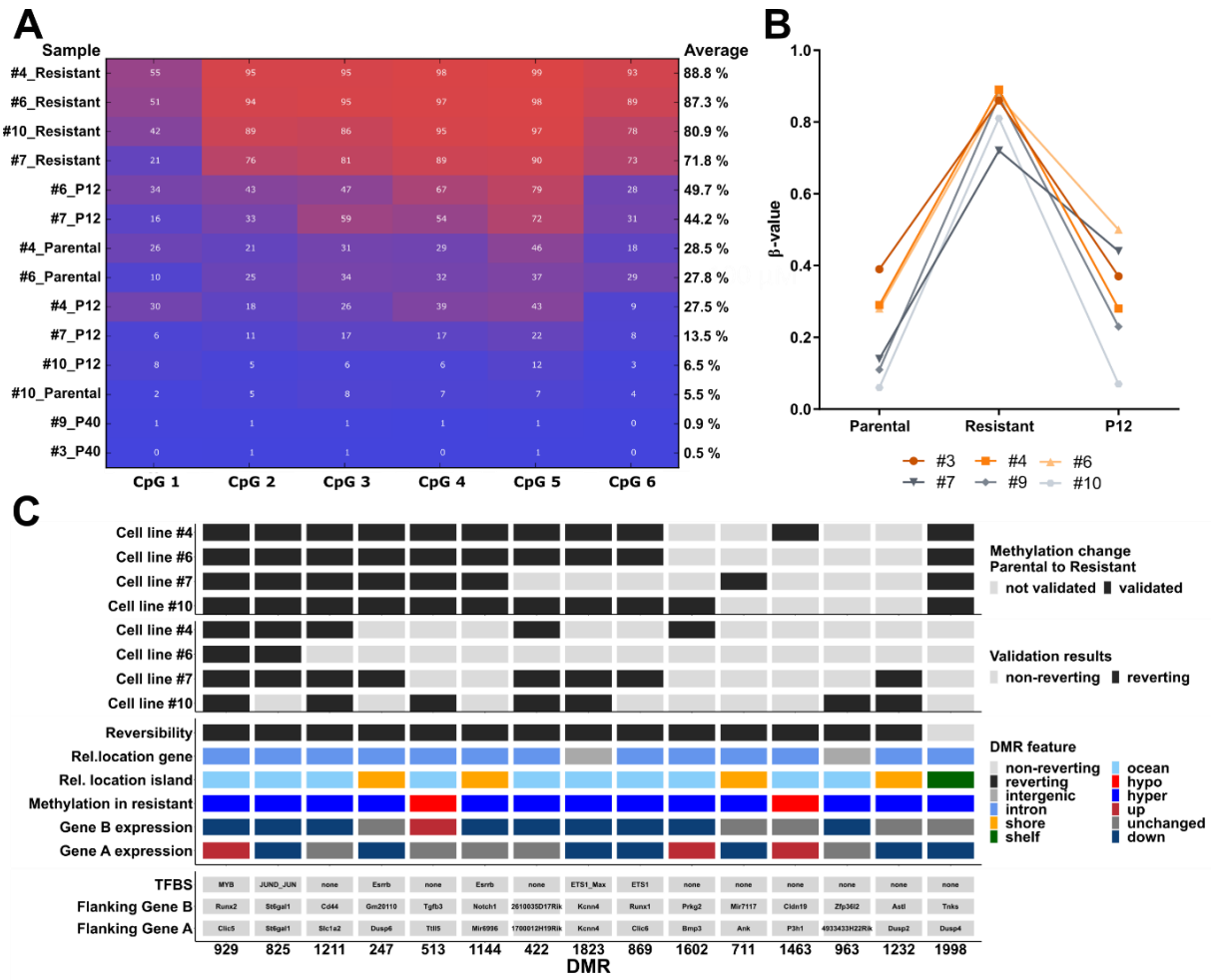

Figure 3-20: Validation of representative reverting differentially methylated regions by targeted deep bisulfite sequencing

Methylation pattern of DMR_929 in four independent cell lines compared to the WGBS samples #3 and #9 based on the b-value per CpG **(A)** and averaged over the entire region **(B)**. Overview of the validation results for 15 selected DMRs with their corresponding annotations **(C)**. Except DMR_1998 all DMRs were defined as reverting in the WGBS dataset.

In at least two of these cell lines, 10 out of 15 DMRs were differentially methylated between parental and resistant cells (Figure 3-20C and Figure 3-21). In at least one of the cell lines used for validation, a reverting pattern in P12 samples was observed for eight of these 10 DMRs. However, DMR1998 was also not reverting in the WGBS data set and served as a negative control.

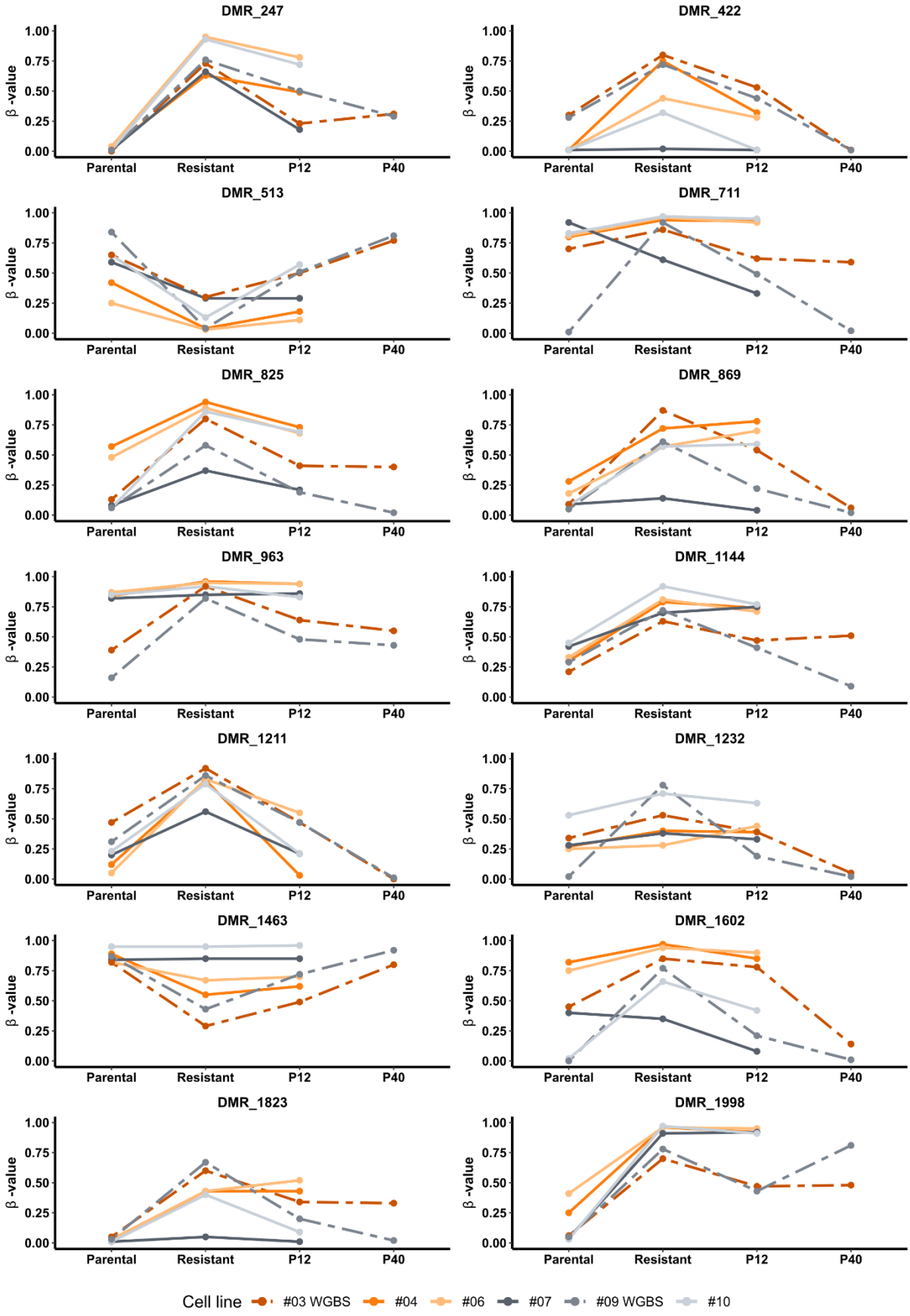

Figure 3-21: Dynamics of reverting DMRs in different cell lines

Individual methylation patterns of 14 DMRs, validated by targeted deep bisulfite sequencing in four independent cell lines compared to cell lines #3 and #9 analyzed by WGBS. In addition, samples after 40 passages of drug withdrawal (P40) of #3 and #9 were measured by targeted deep bisulfite sequencing.

In addition to the independent cell lines, samples taken after 40 passages of drug withdrawal (P40) were sequenced for cell lines #3 and #9 that were previously analyzed by WGBS up to P12 samples. Except for the non-reverting DMR_1998, the methylation levels of the 14 tested reverting DMRs in P40 remained at the P12 level or below (Figure 3-21).

It was investigated whether the observed methylation dynamics during gain and loss of MEK_i resistance were due to a regulation of their catalyzing enzymes.

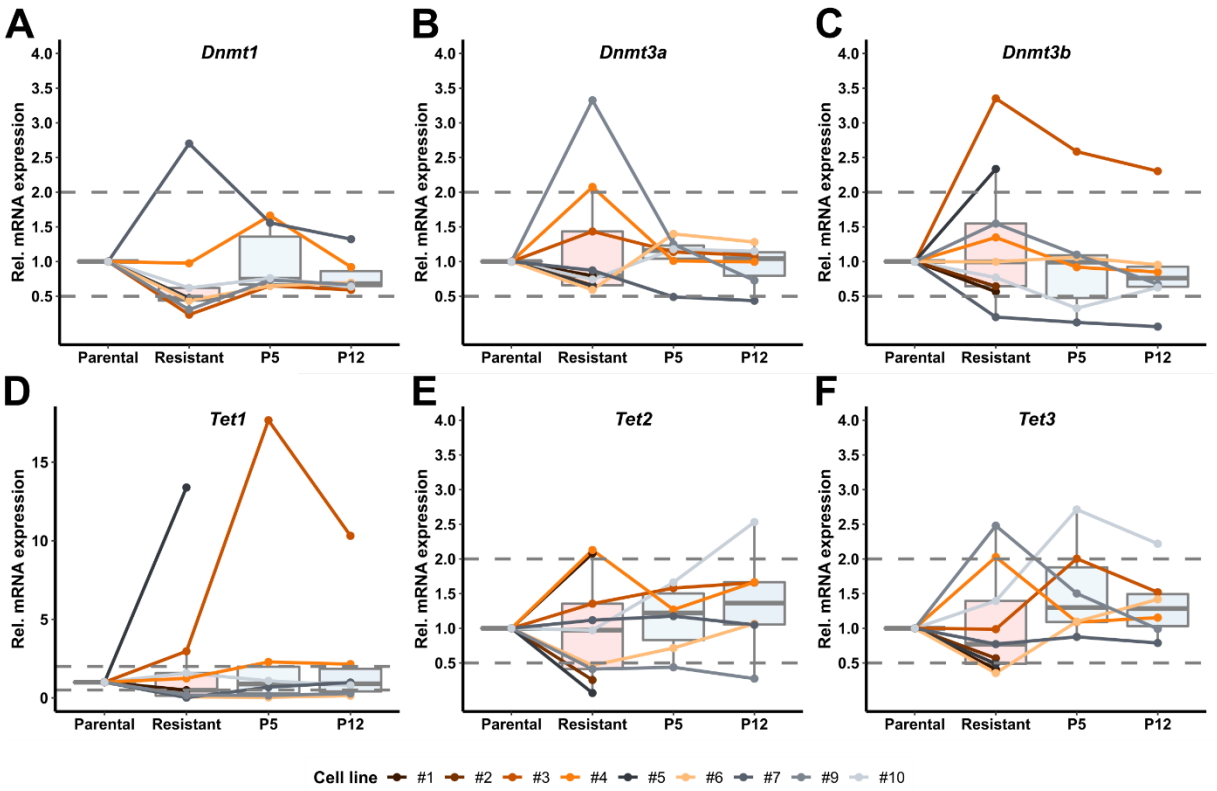

Figure 3-22: Neither DNMTs nor TET enzymes were differently expressed in MEK_i resistance and reversion

Relative (Rel.) mRNA expression was measured by RT-PCR and quantified using the ΔΔCt-method (Livak and Schmittgen, 2001). *Gusb* served as reference. Dotted grey horizontal lines indicate a relative expression of 0.5 or 2. (* $p < 0.05$; two-tailed paired Student's t-test on the ΔCT values).

While DNMT1 maintains DNA methylation after replication, DNMT3a and DNMT3b are required for *de novo* methylation. The demethylation of DNA depends on the activity of TET enzymes of which three different ones are known that exhibit partially redundant functions. With the exception of outliers, no general trend of a differential mRNA expression between parental, resistant P5 or P12 cells could be observed for any of the genes tested (Figure 3-22A-F). Solely *Dnmt1* seemed to be downregulated in the resistant compared to parental cells (Figure 3-22A). These results were not significant in an ANOVA testing the ΔCT values between the six cell lines that were additionally

measured in P5 and P12 states. Apart from the expression of an enzyme, its activity plays a major role for execution of its function. Therefore, both DNMT and TET enzyme activity were assessed using activity assays based on universal DNMT or TET substrates. Overall, the measured values were widely scattered and highly variable between the six tested matched pairs (Figure 3-23A,B). DNMT activity tended to be highest in the resistant cells, while TET enzyme activity increased slightly in the P12 cells.

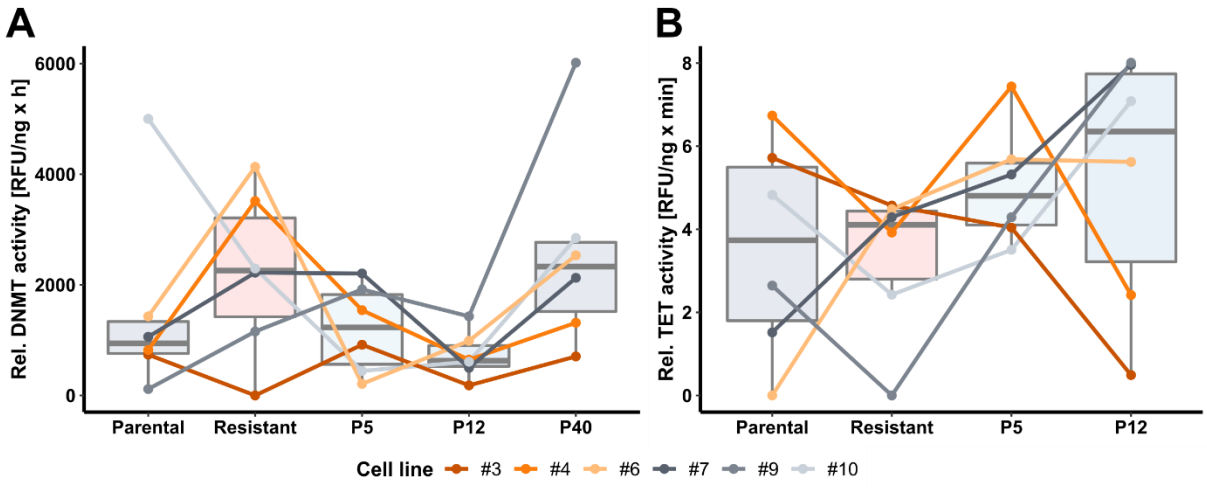

Figure 3-23: While DNMT activity was the highest in resistant cells, TET activity increased in P12 cells

DNMT **(A)** and TET enzyme **(B)** activity were assessed by a fluorogenic activity assay based on universal substrates for each enzyme class. Relative (Rel.) fluorescence units (RFU) were blank corrected and divided by the product of protein amount and incubation time.

The reverting DMRs were annotated and characterized compared to the non-reverting DMRs. While the proportion of hypomethylated DMRs remained low in the reverting regions, the degree of DMR sequence conservation in human slightly decreased (Figure 3-24A,B). The reverting DMRs were located in the ocean nearly twice as often (80.18 % vs. 42.65 % in non-reverting DMRs), but were less frequent in shores or shelfs (Figure 3-24C). Notably, none of the reverting DMRs overlapped with a CpG island. With 0.56 % compared to 4.87 % less reverting than non-reverting DMRs were found in exons (Figure 3-24D).

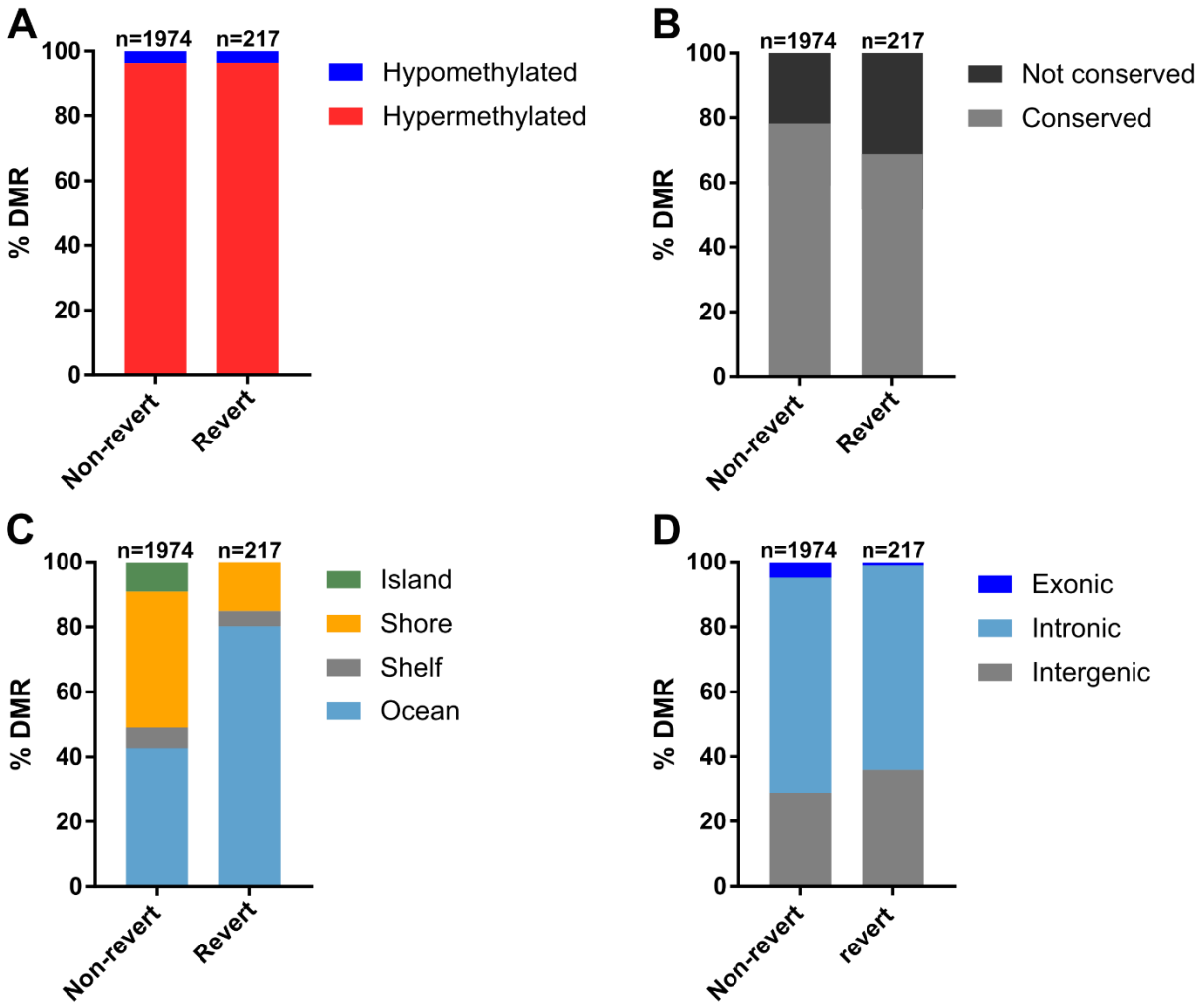

Figure 3-24: Characterization of reverting compared to non-reverting differentially methylated regions

Comparison of reverting and non-reverting DMRs based on their methylation change in the resistant cells **(A)**, their sequence conservation in human **(B)** and their relative location according to CpG islands **(C)** or genes **(D)**.

3.4.3 *In silico* assessment of the functional relevance of reverting DMRs

The correlation of dynamic DNA methylation changes in parental, resistant and P12 cells with their MEK_i sensitivity indicated a functional relevance of reverting DMRs for the resistant phenotype. To investigate this relevance, the overlap of DMRs with miRNA target regions, VISTA enhancers and transcription factor binding sites (TFBS) as annotated by Ensembl was computed for the reverting DMRs compared to the total DMRs (Figure 3-25A). An increased co-localization with the reverting DMRs could only be detected for TFBS, where nearly 25 % of the reverting DMRs but only about 15 % of the entire DMRs overlapped with one or more TFBS. Notably, all TFBS-containing reverting DMRs were hypermethylated in the resistant cells. Compared to randomly

selected regions with similar length and CpG content, TFBS were significantly enriched in all 2191 DMRs and even more in the 217 reverting DMRs (Figure 3-25B).

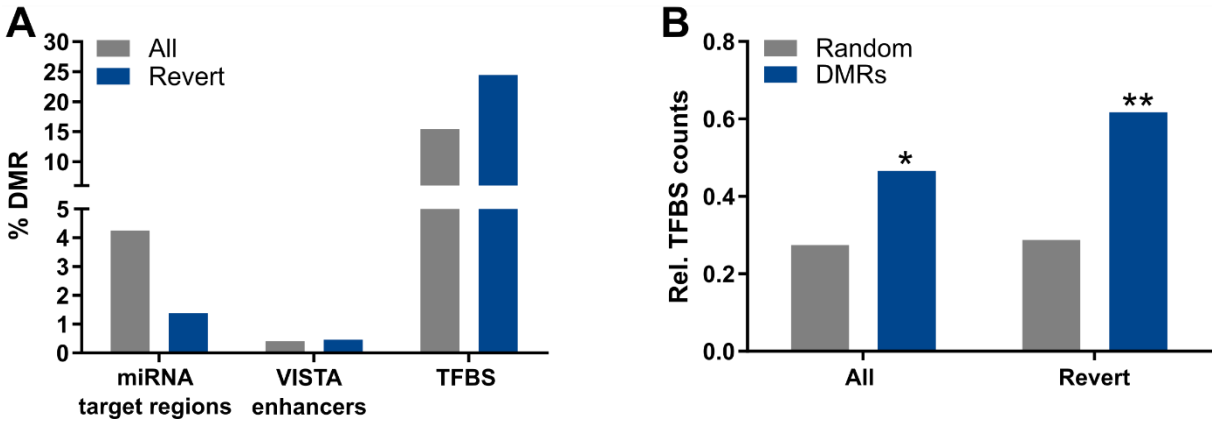

Figure 3-25: Differentially methylated regions were significantly enriched for transcription factor binding sites

Percent of DMRs overlapping with the indicated feature annotated by Ensembl **(A)**. Transcription factor binding sites (TFBS) were significantly enriched in all and even more in reverting DMRs compared to 10^6 random regions of similar length and CpG count (** significance level < 0.01; * significance level < 0.05; Rel., relative) **(B)**.

It is well known that the activity of regulatory elements is highly tissue- as well as context-specific and their deregulation is often associated with cancer (Kundaje *et al.*, 2015). To estimate the state of regulatory elements in PDAC, the DMRs were merged with published data from Roe and colleges (Roe *et al.*, 2017) that indicate open chromatin (assay for transposase-accessible chromatin and sequencing (ATAC-seq)) or potential active enhancer sites (chromatin immunoprecipitation and sequencing (ChIP-seq) for H3K27ac and H3K4me1) in murine pancreas organoids. Their organoid collection consisted of normal pancreas as well as PDAC derived from *Kras*$^{wt/LSL-G12D}$; *Trp53*$^{wt/LSL-R172H}$; *Pdx1-Cre* mice, a similar model to the one used in the present study. The overlap with peaks indicating open chromatin or peaks of both analyzed histone marks was higher for the reverting than the non-reverting DMRs (Figure 3-26A). With nearly 86 % and 69 %, the majority of reverting DMRs co-localized with H3K27ac indicative for active enhancer sites or H3K4me1, found at active or poised enhancers. In addition, more than half (54.3 %) of the reverting DMRs were associated with open chromatin identified by ATAC-seq.

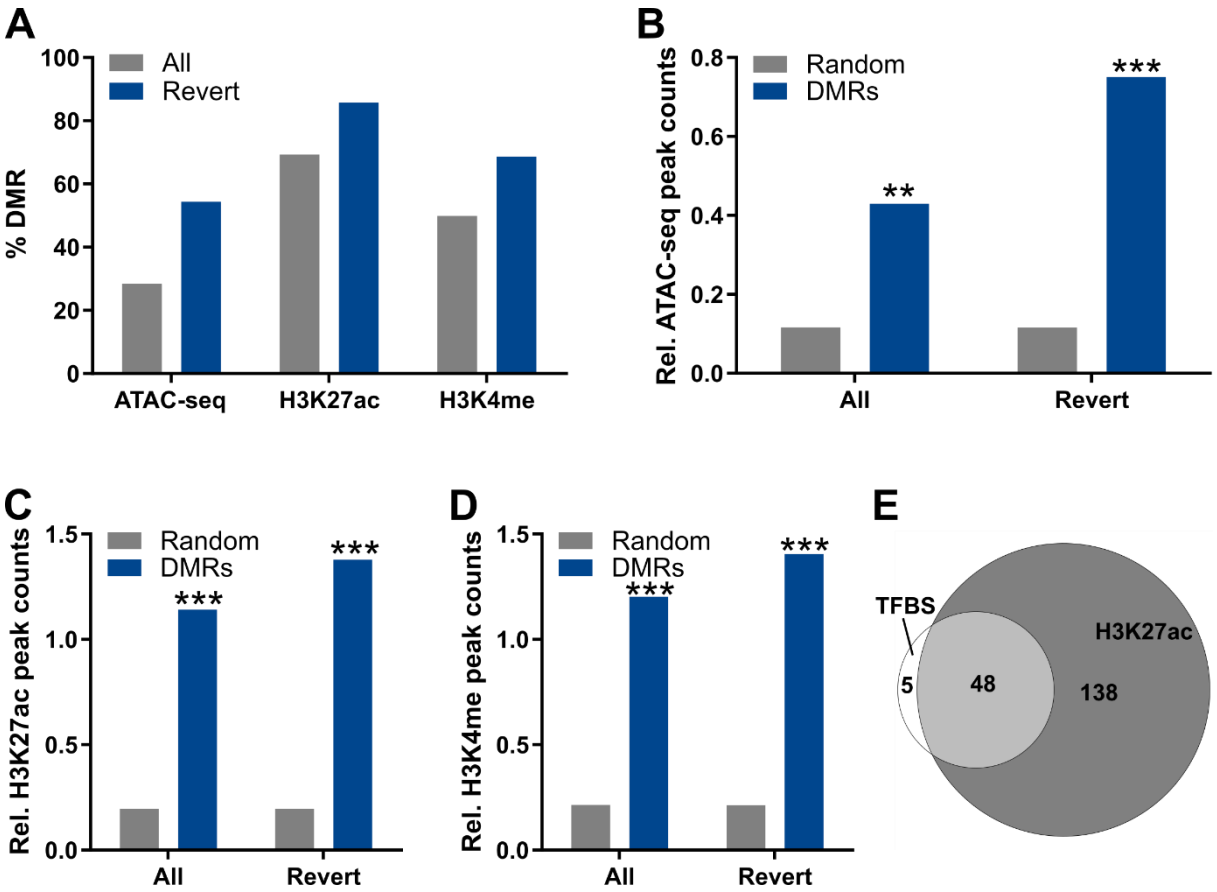

Figure 3-26: Differentially methylated regions overlapped with open chromatin and active enhancers

Percent of DMRs that co-localized with an ATAC-seq or ChIP-seq peak for H3K27ac or H3K4me1 found in at least 2 organoids published by Roe and co-workers (Roe *et al.*, 2017) **(A)**. Enrichment for ATAC-seq **(B)**, H3K27ac **(C)** or H3K4me1 **(D)** peaks in the DMRs relative to 10^6 random regions of similar length and CpG count (*** significance level < 0.001; ** significance level < 0.01; Rel., relative). **(E)** Euler diagram of reverting DMRs that overlapped with transcription factor binding sites (TFBS) and/or H3K27ac peaks. All 149 reverting DMRs that co-localized with a H3K4me1 peak represented a subset of the displayed 186 reverting DMRs overlapping with a H3K27ac peak.

Since open chromatin as well as DNA occupied by H3K27ac or H3K4me1 modified histones comprise only about 0.8 %, 3 % or 2.5 % of the entire genome, they were significantly enriched in all DMRs and even stronger in the reverting DMRs (Figure 3-26B-D). All of the 149 H3K4me1 associated reverting DMRs and 90.5 % of TFBS-containing DMRs also overlapped with H3K27ac peaks (Figure 3-26E). Two different approaches were used to identify the corresponding transcription factors. In both analyses, binding motifs for proteins of the JUN, FOS and activating transcription factor (ATF) families were amongst the top enriched TFBS (Figure 3-27A,B).

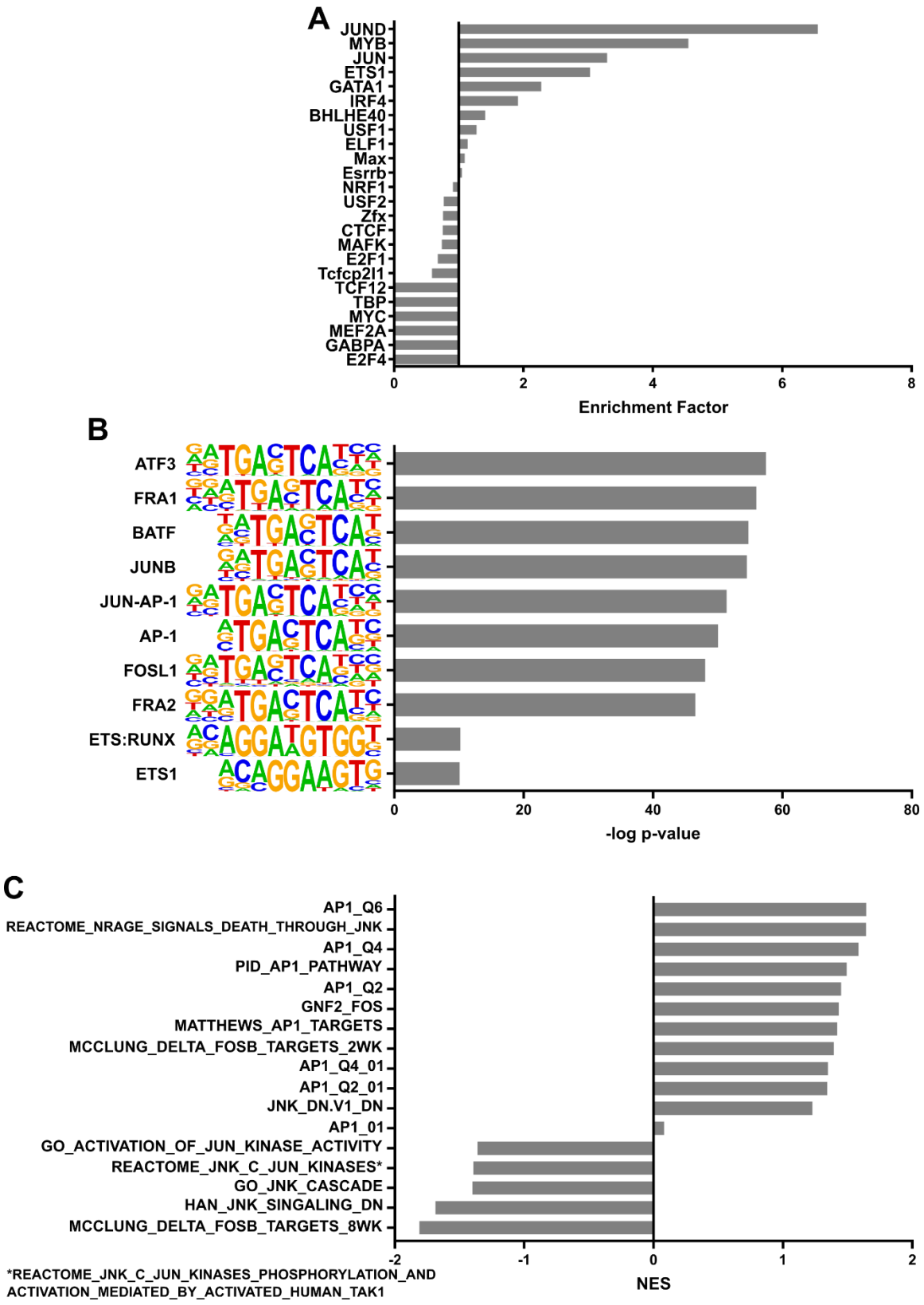

Figure 3-27: Binding sites for AP-1 transcription factor components were enriched in the reverting differentially methylated regions

Enrichment of binding sites for the indicated transcription factors in the 217 reverting DMRs compared to the remaining 1974 non-reverting DMRs **(A)**. Enrichment of the top ten transcription factor binding motifs from the HOMER database between the reverting DMRs and random background sequences **(B)**. Normalized enrichment score (NES) of AP-1 related gene expression signatures that were significantly (FDR < 0.25) different between parental and resistant cells based on Gene Set Enrichment Analysis of RNA-seq data **(C)**. A positive NES indicates an enrichment in the parental cells.

Together, these proteins form the dimeric transcription factor activator protein 1 (AP-1), which can bind DNA at 12-O-tetradecanoylphorbol-12-acetate response elements (TRE) and cyclic adenosine monophosphate response elements (CRE) depending on its exact composition. Recently, DNA methylation was shown to prevent this motif binding (Xuan Lin *et al.*, 2019; Yin *et al.*, 2017).

Correspondingly, various AP-1/JUN expression signatures were enriched in the RNA-seq data of the parental compared to resistant cells (Figure 3-27C). On the protein level, JUN expression was significantly increased in the resistant cells, while the ratio of Ser73 phosphorylated to total JUN was significantly lower compared to parental cells (Figure 3-28A-C).

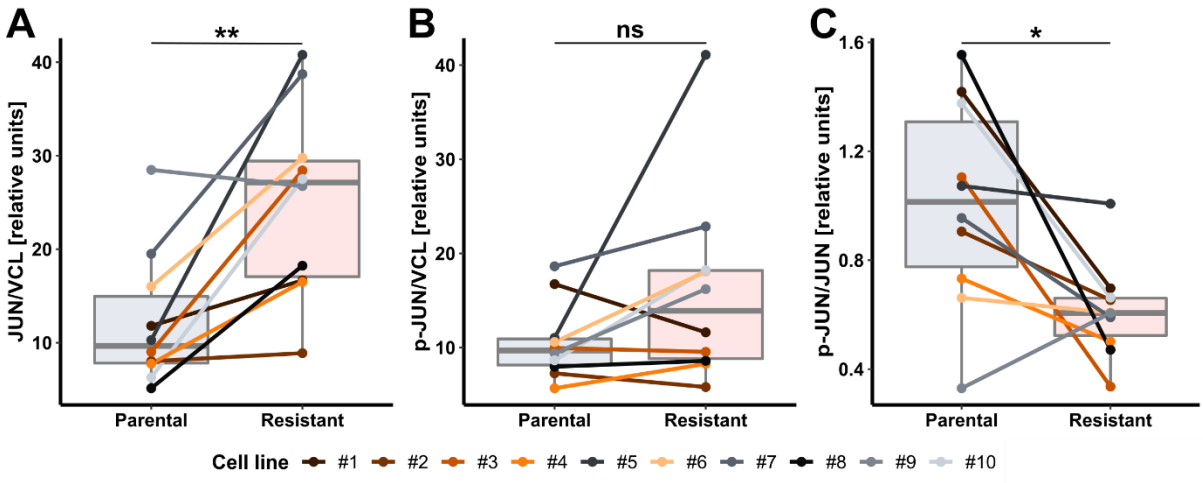

Figure 3-28: JUN protein expression was significantly upregulated in MEK$_i$ resistant cells but the proportion of phosphorylated to total JUN was decreased

Relative protein expression of total JUN **(A)** or p-JUN (Ser73) **(B)** compared to VCL in parental and resistant cells measured by simple western. **(C)** Proportion of p-JUN (Ser73) to JUN. (** $p < 0.01$; * $p < 0.05$; ns, non-significant; two-tailed paired Student's t-test).

Besides the silencing of its canonical binding site by DNA methylation, the generation of a new AP-1 binding motif has been described (Gustems *et al.*, 2014; Hong *et al.*, 2017; Tulchinsky *et al.*, 1996).

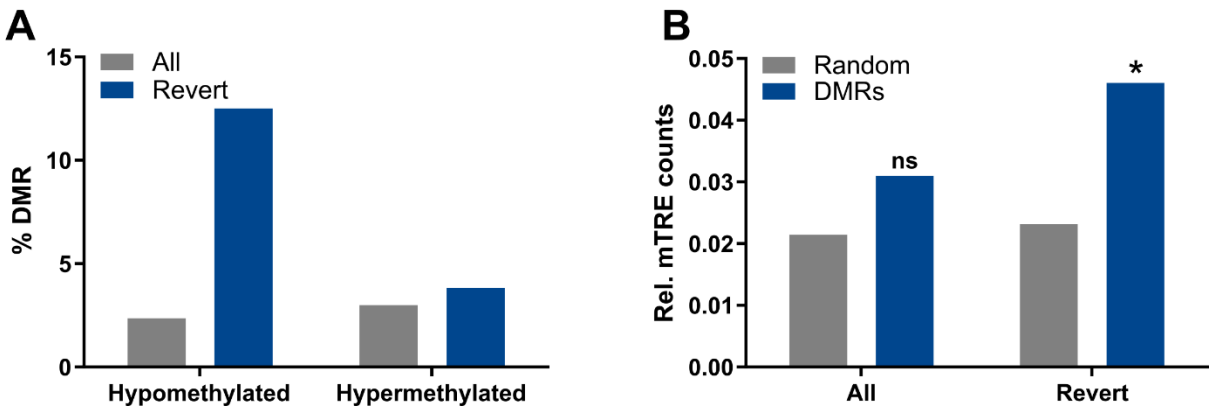

Figure 3-29: mTRE motifs were significantly enriched in the reverting DMRs

Percent of DMRs with an internal mTRE motif separated by the methylation change between parental and resistant cells **(A)**. Enrichment for mTRE motifs in the DMRs relative to 10^6 random regions of similar length and CpG count (* significance level < 0.05; ns, non-significant; Rel., relative) **(B)**.

The so-called mTRE motif is created by DNA methylation of a TRE-like sequence containing a C instead of a T at its 5´end (Hong *et al.*, 2017). Both hypo- and hypermethylated DMRs contained an underlying sequence motif for mTRE (Figure 3-29A). The percentage increase in comparison between all and the reverting DMRs was significantly greater for the hypomethylated DMRs from 2.4 % to 12.5 % than for the hypermethylated DMRs (from 3.0 % to 3.8 %). However, in absolute numbers, only two DMRs with an internal mTRE motif were hypomethylated and one of them was classified as reverting. A significant enrichment compared to random regions of similar length and CpG content was only found for the reverting DMRs (Figure 3-29B). In the entire genome, 0.2 % of all CpGs are located in the beginning of a mTRE motif.

3.5 Data integration and target validation

3.5.1 Reversible CASP3 downregulation attenuated treatment-induced apoptosis in MEK_i resistant cells

The previous analyses focused on the identification and characterization of global changes in MEK_i resistant cells. Transcriptional and phenotypic variance as well as adaptive DNA hypermethylation could be found. The integration of the different data types enabled the identification of individual targets whose deregulation was potentially relevant for the resistant phenotype.

Since AP-1 is involved in apoptosis, the identified co-localization of its binding sites with hypermethylated DNA regions provided first evidence for a possible modulation of apoptosis in the resistant cells. Furthermore, among the reverting DMRs defined by WGBS, two regions were found in proximity downstream of the *Casp3* gene, whose

encoded protein is essential for the execution of apoptosis (Figure 3-30A). Notably, *Casp3* mRNA as well as CASP3 protein expression inversely correlated with the DMR methylation (Figure 3-30B,C). Both were significantly downregulated in the resistant cells but returned to parental levels in P12 cells. Concordantly, in comparison to resistant cells, the parental cells showed an enriched expression signature for genes involved in apoptosis (FDR < 0.05, NES=-1.827) (Figure 3-30D).

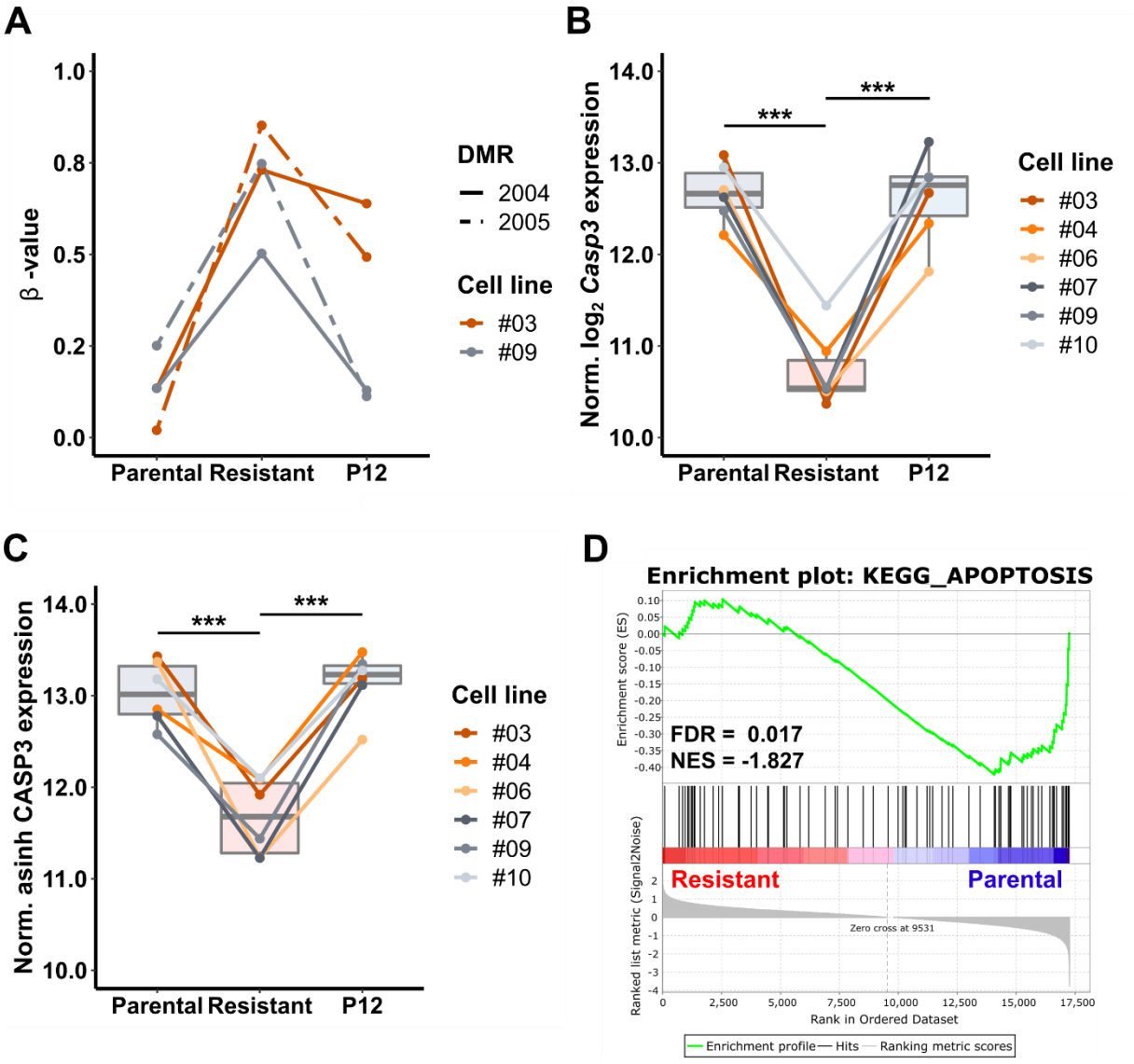

Figure 3-30: DNA methylation of a *Casp3* associated region correlated negatively with its expression and an apoptosis gene expression signature

DMR_2004 and DMR_2005 were hypermethylated in resistant cells and reverted upon MEK_i withdrawal in P12. Both were located intergenically downstream of *Casp3* **(A)**. Normalized (Norm.) *Casp3* mRNA expression measured by RNA-seq in six matched pairs of parental, resistant and P12 cells inversely correlated with DMR methylation (*** adjusted $p < 0.001$) **(B)**. Mass spectrometry revealed a reverting CASP3 protein expression in six matched pairs of parental, resistant and P12 cells (*** $p < 0.001$; ANOVA with Tukey post-hoc test) **(C)**. The KEGG pathway apoptosis gene set was significantly enriched in parental compared to resistant cells (FDR < 0.05). Gene Set Enrichment Analysis was performed on the normalized read counts of RNA-seq **(D)**.

Functional annotation revealed an overlap of both DMR_2004 and DMR_2005 with active enhancers (H3K27ac and H3K4me1 marked) and open chromatin suggesting their relevance for *Casp3* transcriptional regulation (Table 3-3). Notably, in the sequence of DMR_2004 in total 6 binding sites for the three different AP-1 proteins JUN, JUND and MAFK were found (Table 3-3).

Table 3-3: Overlap of the *Casp3* associated DMRs with chromatin marks and TFBS

Organoid data of ATAC-seq and ChIP-seq from Roe *et al.* (Roe *et al.*, 2017) were used. The number of analyzed organoids is listed in brackets. For DMRs, the number of organoids that exhibited at least one peak for the indicated chromatin mark is displayed.

DMR	*DMR position (mm10 coordinates)*	*ATAC-seq (5 organoids)*	*H3K27ac (8 organoids)*	*H3K4me (3 organoids)*	*TFBS*
2004	chr8:46639157-46640247	2	8	2	JUN:3 MAFK:1 JUND:2
2005	chr8:46641220-46641654	3	8	2	BHLHE40:1 ETS1:1

In order to analyze whether CASP3 activity was altered in MEK$_i$ resistant cells in addition to the CASP3 expression, a luminescence-based activity assay was performed in three different cell lines. Upon MEK$_i$ treatment, CASP3 activation was induced in all parental cells tested but attenuated in the resistant cells (Figure 3-31A-C).

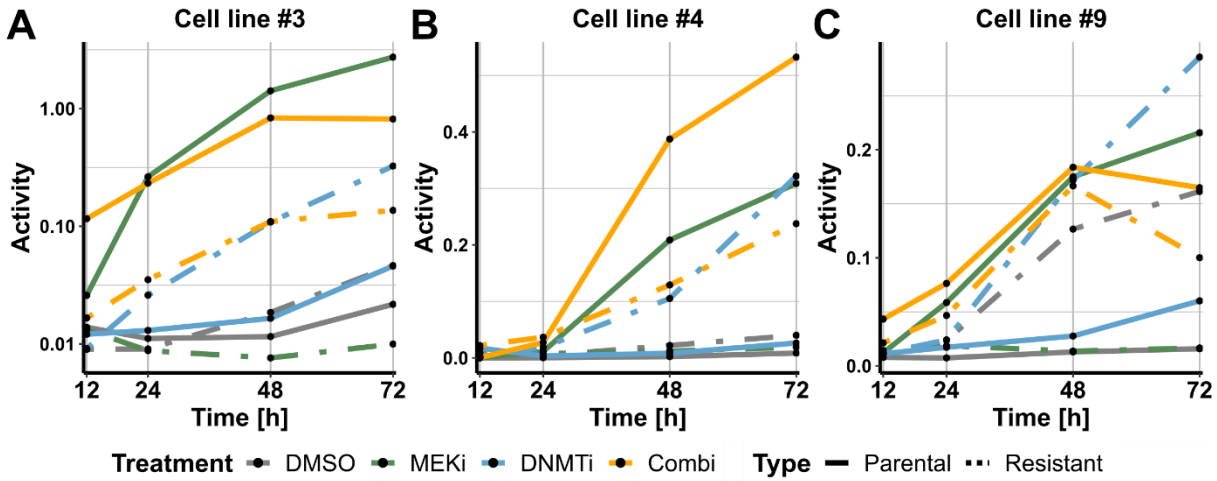

Figure 3-31: CASP3 activity induced by MEK$_i$ was attenuated in the resistant cells

CASP3 activity after incubation with the indicated compounds in cell lines #3 **(A)**, #4 **(B)** and #9 **(C)** measured with the Caspase-Glo® Assay. Signals were corrected for viable cells.

In contrast, MEK$_i$ withdrawal was accompanied by an increasing basal CASP3 activity in the resistant cells, which could be further enhanced by DNMT$_i$ treatment. The DNMT$_i$ effect on the CASP3 activity of the parental cells was only marginal, which is in accordance with the previously shown cell viability data (Figure 3-15). While a combined treatment with MEK$_i$ and DNMT$_i$ induced the activity of CASP3 in MEK$_i$ resistant cells similar as DNMT$_i$ alone, the impact on the parental cells was comparable to MEK$_i$ single treatment (cell lines #3 and #9, Figure 3-31A,C) or even stronger (cell line #4, Figure 3-31B).

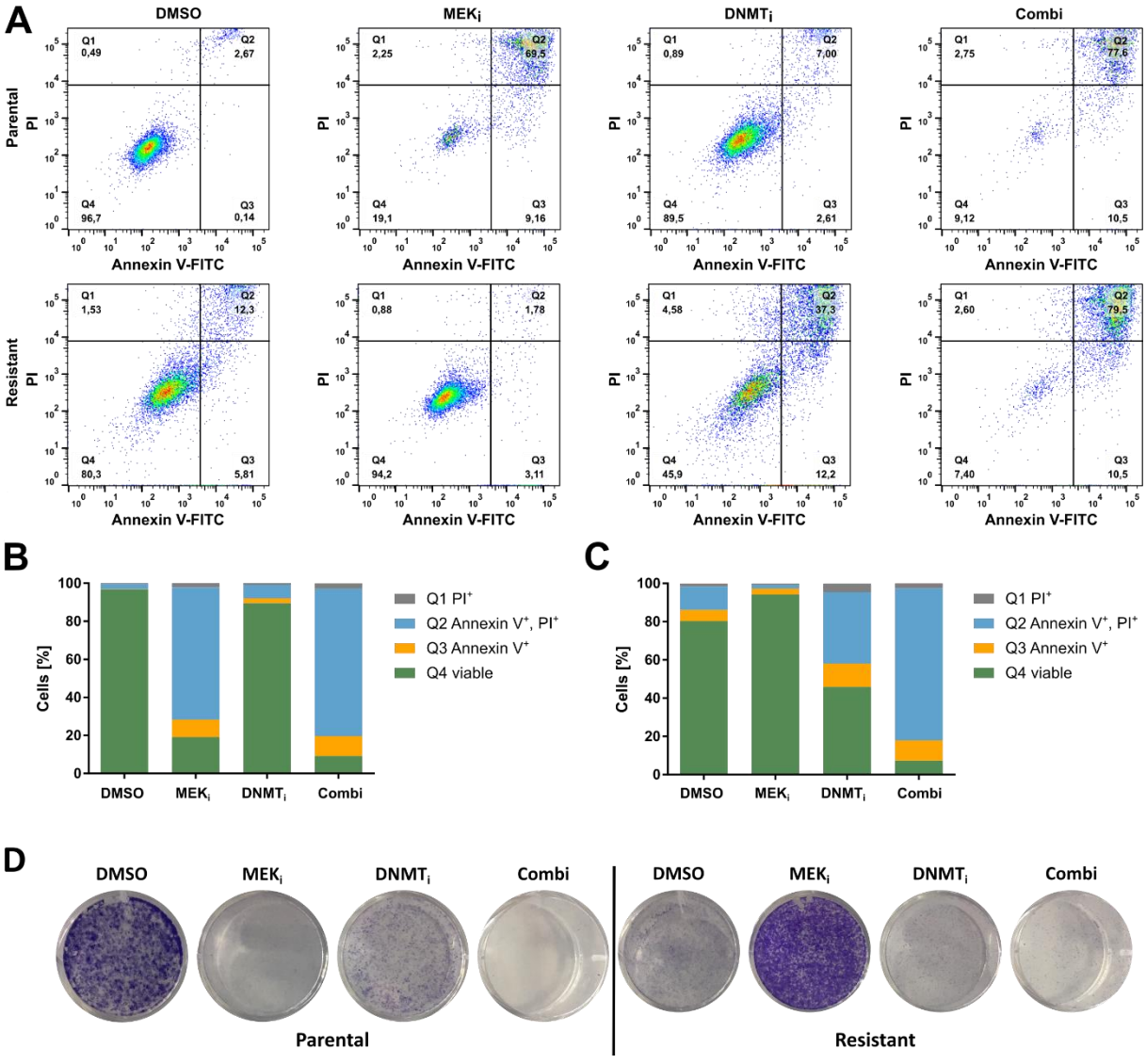

Figure 3-32: Apoptosis induced by MEK$_i$ was attenuated in the resistant cells

Annexin V-FITC/PI co-staining of parental (upper row) or resistant cells (lower row) of line #9 upon 84 h of the indicated treatment measured by FACS **(A)**. Data of two additional cell lines are displayed in Supplementary Figure 2. Quantification of FACS results shown in (A) separated for parental **(B)** or resistant cells **(C)**. Crystal violet staining of cell line #9 after 84 h incubation with indicated compounds **(D)**.

Fluorescence activated cell sorting (FACS) analysis using an Annexin V/PI co-staining confirmed the attenuation of treatment-induced apoptosis by CASP3 inactivation as a potential resistance mechanism in PDAC (Figure 3-32A-C and Supplementary Figure 2). Furthermore, crystal violet staining visualized the treatment-induced cell death (Figure 3-32D). As expected, MEK_i induced cell death in all analyzed parental cells, but not in the resistant cells, whereas the latter were affected by MEK_i withdrawal, $DNMT_i$ treatment and the combination of both.

3.5.2 MEK_i and $DNMT_i$ acted synergistically *in vitro* and *in vivo*

The pronounced $DNMT_i$ sensitivity of the resistant cells and their observed CASP re-activation after $DNMT_i$ treatment supported a possible functional association between MEK_i resistance and DNA methylation. Thus, a synergistic approach would provide a window of opportunity to avoid treatment-induced MEK_i resistance.

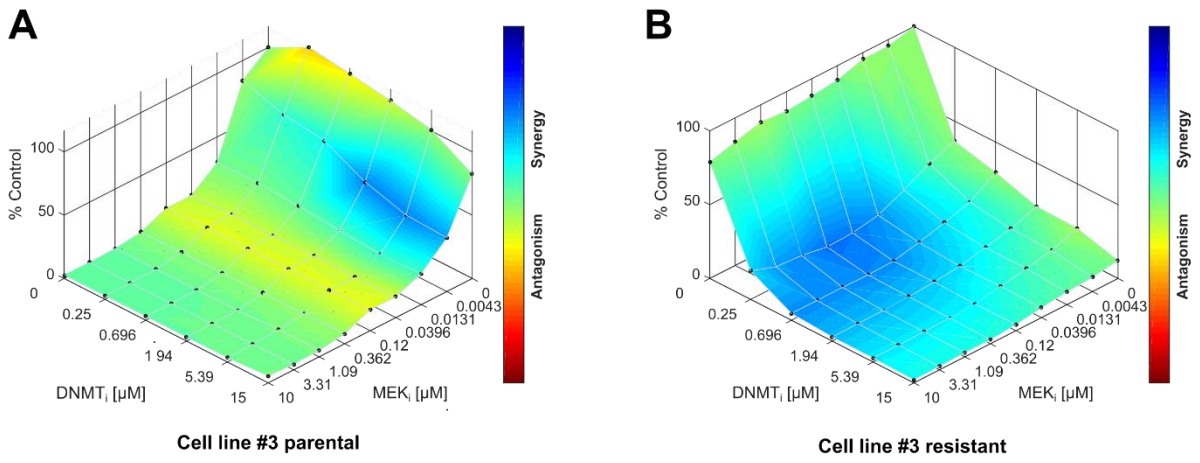

Figure 3-33: Synergism of MEK_i and $DNMT_i$ was more pronounced in the MEK_i resistant than in parental cells

Synergy analysis of MEK_i and $DNMT_i$ applying the Loewe method implemented in the Combenefit software. Cell line #3 in the parental **(A)** and resistant **(B)** cell state is shown as an example. Data for three additional cell lines are displayed in Supplementary Figure 3.

In order to quantify the synergism between MEK_i and the $DNMT_i$ a detailed cell viability assay approach was performed and analyzed based on the Loewe additivity model (Loewe, 1953). In the resistant cells, a synergistic effect of MEK_i and $DNMT_i$ was observed even at low doses of $DNMT_i$ while synergisms in the parental cells was only observed at high $DNMT_i$ concentrations (Figure 3-33A,B and Supplementary Figure 3).

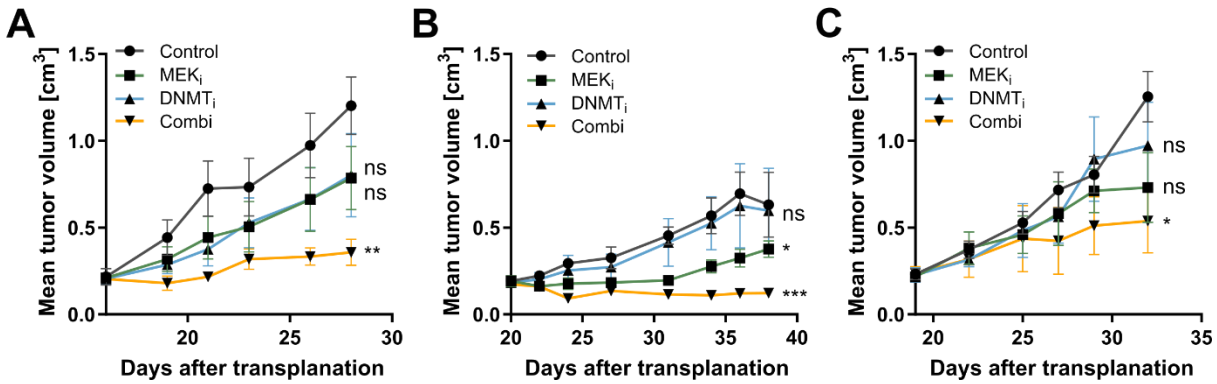

Figure 3-34: Synergism of MEK_i and $DNMT_i$ could also be observed in patient-derived xenografts of PDAC

(A-C) The mean tumor volume of three mice per treatment group is shown ± SEM for three different PDX (** $p < 0.01$; * $p < 0.05$; ns, non-significant; two-tailed unpaired Student's t-test).

Finally, in order to to prove if the observed effect is also true for human PDAC, three different patient-derived xenograft (PDX) models were treated in a proof of principle *in vivo* experiment (Figure 3-34). A synergistic effect of MEK_i and $DNMT_i$ was observed in all three models leading to a partial remission according to the response evaluation criteria in solid tumors (RECIST), criteria in one case and a stable disease in the two others.

4 DISCUSSION

Intratumoral heterogeneity and the mostly late detection of PDACs favor the presence of resistant cells leading to therapeutic failure and a dismal prognosis for PDAC patients (Kleeff *et al.*, 2016; Vasan *et al.*, 2019; Wang *et al.*, 2011b). Thus, there is an urgent need to better understand the underlying molecular mechanisms of therapy resistance. As resistance development is understood as a multifactorial and heterogeneous process, undersampling represents one of the biggest challenges for its investigation (Konieczkowski *et al.*, 2018). On the one hand, the applied methodologies of many studies lead to a focus on few possible mechanisms only and lack functional validations of their results (Konieczkowski *et al.*, 2018). On the other hand, availability of comparable treatment-naïve and resistant patient samples is limited.

In order to counteract undersampling, the present study aimed at characterizing the treatment-induced alterations of pancreatic tumor cells at different regulatory levels using a multi-omics approach. Targeting of oncogene-driven signaling pathways is a validated strategy for cancer therapy (Chapman *et al.*, 2011; Demetri *et al.*, 2002; Lynch *et al.*, 2004). Given that mutant KRAS represents the key driver of more than 90 % of PDACs as well as that the most common variants cannot be inhibited so far, the KRAS downstream kinase kinases MEK1/2 represent a promising target for the treatment of RAS/RAF driven cancers. First, their unique hydrophobic pockets enable a specific, allosteric and non-ATP-competitive inhibition (Ohren *et al.*, 2004). Second, in contrast to many other kinases, only two direct MEK1/2 substrates, ERK1/2, are known, so that fewer off-target effects can be expected when inhibiting MEK1/2 (Caunt *et al.*, 2015; Shaul and Seger, 2007). However, in clinical trials no benefit of MEK_i treatment was achieved for PDAC patients (Chung *et al.*, 2017; Infante *et al.*, 2014; Van Cutsem *et al.*, 2018; Van Laethem *et al.*, 2017). Despite prolonged survival observed with MEK_i monotherapy or in combination with $BRAF_i$ in *BRAF* mutant melanoma, tumors develop resistance in almost all cases (Flaherty *et al.*, 2012a; Flaherty *et al.*, 2012b). Overall, these results underline the importance of understanding and overcoming MEK_i resistance. Therefore, an *in vitro* model was generated based on primary cell lines derived from pancreatic tumors of *Ptf1a*$^{wt/Cre}$*; Kras*$^{wt/LSL\text{-}G12D}$*; Trp53*$^{loxP/loxP}$ mice, a well-established mouse model that is frequently used in pre-clinical studies. Due to the introduced genetic modifications in *Kras* and *Trp53*, the developing tumors recapitulate key features such as desmoplasia

and resistance of human PDAC (Gopinathan *et al.*, 2015; Mazur *et al.*, 2015a). Furthermore, the inbred strain background of *Ptf1a*$^{wt/Cre}$*; Kras*$^{wt/LSL-G12D}$*; Trp53*$^{loxP/loxP}$ mice minimizes interindividual heterogeneity, which in turn reduces complexity and thus enables a clearer evaluation of genome-wide data in the context of therapy resistance (Konieczkowski *et al.*, 2018). However, non-tumor cells influence the evaluation of global analyses, so that the use of GEMM-derived primary cell lines representing a pure tumor cell population was advantageous for the presented multi-omics characterization. Especially DNA methylation is highly cell type-specific so that contamination with stroma cells that make up most parts of PDAC bulk tissue may cause misleading results (Moffitt *et al.*, 2015; Nicolle *et al.*, 2017; Schubeler, 2015). The same applies to mutation analyses, in which variants of contaminating non-tumor cells cannot be distinguished from mutations that have occurred in tumor cells (Robasky *et al.*, 2014).

As a limitation of the chosen cell line-based *in vitro* model, any impact of non-cell-intrinsic mechanisms such as the tumor microenvironment currently discussed to be involved in resistance of PDAC (Hanahan and Coussens, 2012) cannot be addressed. Despite these constraints, resistance induction was possible in all ten cell lines treated with increasing doses of the MEK_i trametinib. This clearly demonstrated that, at least in the analyzed model, MEK_i resistance in PDAC relies on a cell-intrinsic mechanism. The phosphorylation of the ERK1/2 kinases catalyzed by MEK1/2 remained blocked which underpinned the on-target effect of trametinib and most likely excluded decreased drug uptake or increased efflux as a cause of resistance.

Therefore, further analyses were necessary, which not only examine potential changes in components of KRAS signaling e.g. in the MEK_i or the parallel PI3K pathway but also are interpreted without preconceived conclusions. Re-activation or bypassing of the targeted pathway represents a common mechanism of tumor cells to evade drug-mediated signaling ablation (Konieczkowski *et al.*, 2018). MEK_i disturbs the entire pathway regulation involving several feedback loops, so that re-activation of ERK or other kinase-mediated pathways frequently occurs (Caunt *et al.*, 2015). For example, MEK_i resistance *in vitro* and in cell line-based PDAC xenografts could be prevented by inhibition of the KRAS upstream tyrosine phosphatase SHP2A (Fedele *et al.*, 2018; Ruess *et al.*, 2018). However, the authors found a re-activation of ERK, which could be refuted in this study, suggesting that resistant cells of the model system used here probably lost their dependence on ERK downstream signals. Also other studies describe MEK_i resistance in PDAC and other RAS/RAF driven tumors independent of

an ERK rebound, e.g. by protective autophagy or via YAP, a Hippo pathway effector (Bryant *et al.*, 2019; Kinsey *et al.*, 2019; Lin *et al.*, 2015). Trametinib is one of the MEKis that not only inhibits the kinase activity but also leads to weaker re-activation of ERK by limiting the association between MEK1/2 and RAF (Lito *et al.*, 2014). Possibly this rather favors the emergence of ERK independent resistance mechanisms. Notably, both Lin et al. (Lin *et al.*, 2015) and Kinsey et al. (Kinsey *et al.*, 2019) used trametinib, while Bryant and colleges (Bryant *et al.*, 2019) used binimetinib, whose mode of action was not analyzed by Lito and co-workers (Lito *et al.*, 2014).

4.1 MEKi resistance was based on clonal expansion but not the direct consequence of existing or acquired mutations

Resistance to targeted therapies is frequently mediated by the emergence of a distinct cell fraction within the tumor cell population that exhibits mutations to re-activate or bypass the targeted pathway (Engelman and Jänne, 2008; Nardi *et al.*, 2004). Upon MEK inhibition, both *MEK1* mutations (p.P124L, p.F129L) (Emery *et al.*, 2009; Hatzivassiliou *et al.*, 2012; Wang *et al.*, 2011a) in the kinase domain leading to increased activity as well as *MEK1* (p.L115P) and *MEK2* (p.Q60P, p.V215E) mutations (Hatzivassiliou *et al.*, 2012; Villanueva *et al.*, 2013) that prevent inhibitor binding have been described in cell lines and refractory tumors of melanoma, colon and breast cancer. Using WGS, no mutation was found either in the MEK or the parallel PI3K signaling pathway or other receptor tyrosine kinases. Furthermore, there was no evidence of direct resistance mediation even for the few potentially deleterious classified variants. It should be noted that the sample size with two matching parental and resistant pairs was small and the interpretability of non-coding variants is limited, especially for murine data. Besides mutations, structural variants such as *BRAF* and *KRAS* amplifications have been reported to confer acquired MEKi resistance to colorectal cancer (Corcoran *et al.*, 2010; Little *et al.*, 2011), however copy number variations due to larger chromosomal re-arrangements were not investigated in this thesis. Since a near tetraploidy has already been detected in the parental cells, its influence on the development of resistance is unlikely.

Overall, MEKi resistance does not seem to be the result of direct resistance-conferring mutations. This hypothesis is further supported by a study that induced resistance to the small molecule tyrosine kinase inhibitor (TKi) gefitinib in the non-small-cell lung cancer (NSCLC) cell line PC-9 according to a similar protocol as applied in this thesis (Hata *et al.*, 2016). While sublines derived from a PC-9 pool, containing the well

characterized *EGFR* resistance mutation p.T790M, developed resistance in approximately 6 weeks, cell pools without a detectable p.T790M mutation needed with about 6 months remarkably longer (Hata *et al.*, 2016). Since the doubling time for PC-9 was estimated at around 20 h (Koizumi *et al.*, 2005), the proliferation of the GEMM-derived PDAC cell lines was comparable or even faster. Therefore, the duration of resistance induction of 3-4 months in all 10 tested cell lines indicates that resistance did not previously exist in form of a mutation or other mechanisms, but more likely has developed over time. Furthermore, the transcriptome of the late resistant cells characterized by Hata *et al.* (Hata *et al.*, 2016) differed from the treatment-naïve PC-9 cells while the expression profile of the early resistant cells harboring the p.T790M resistance mutation was similar to their parental cells. Moreover, EMT could only be detected for the late but not the early resistant cells. Concordantly, gene expression in the MEK_i resistant cells was clearly different from that in their parental counterparts and displayed an enriched EMT signature (4.2). In a NSCLC cell line, a TK_i tolerating cell population arose *de novo* at a frequency higher than mutational events would suggest (Sharma *et al.*, 2010b). The authors could show that altered histone modifications reversibly mediated the resistant cell state (Sharma *et al.*, 2010b). While Sharma and colleagues (Sharma *et al.*, 2010b) performed short-term treatment for several days with lethal drug doses, trametinib resistance was induced with increasing doses over a period of 3-4 months starting with a concentration below the IC50. Thus, the concept of drug persisting cells proposed by Sharma *et al.* (Sharma *et al.*, 2010b) cannot be fully translated to the trametinib resistance model. However, several studies analyzing therapy-induced resistance in PDAC also suggested mechanisms other than mutations as source of resistance (reviewed in (Swayden *et al.*, 2018)). Although the development of PDAC relies on driver mutations, Yachida *et al.* (Yachida *et al.*, 2010) and McDonald *et al.* (McDonald *et al.*, 2017) showed an epigenetic impact on the progression and metastasis of the disease. The transcriptome-based PDAC subtypes were also associated with certain epigenetic changes and chromatin states indicating the importance of epigenetic dysregulation in PDAC (Lomberk *et al.*, 2018; Nicolle *et al.*, 2017). Therefore, in the context of the current literature the WGS results suggest an epigenetic rather than a mutational cause of MEK_i resistance (4.3).

Assuming that resistance was not already present at low frequency in the parental cell population, the question arises whether many or only certain cells had the ability to develop resistance. Using WGS data of parental and resistant cells, it could be clearly demonstrated, that MEK_i resistance in both tested cell lines was based on the

expansion of a single cell clone of which the frequency in the parental cell population lay below the detection limit. The loss of resistance upon drug withdrawal was not due to the outgrowth of parental cells that survived the period of treatment (Figure 4-1).

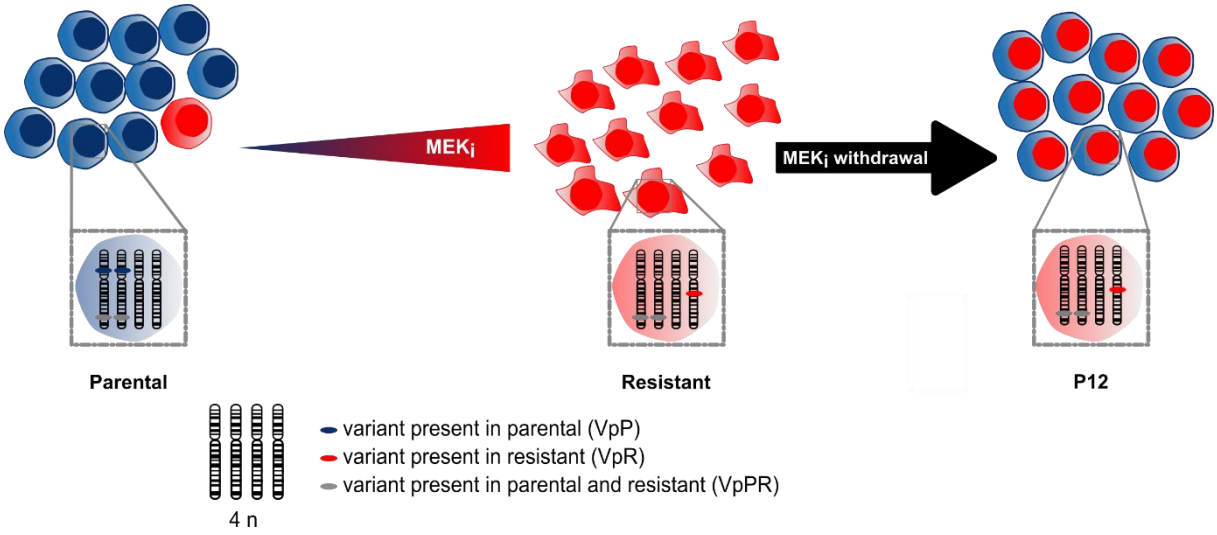

Figure 4-1: Model of the cell population dynamics during gain and loss of MEK_i resistance in PDAC

Thus, despite the remaining VpRs, there was a reversibility of resistance, which further strengthens the hypothesis of an epigenetic cause of resistance. Whether the distinct clone with the ability to adapt to MEK_i was already present in the parental cells or emerged due to MEK_i treatment cannot be distinguished by means of the available data sets due to the limited median coverage of 40 x. If the clone would represent less than 2.5 % of the cell sequenced population it would stochastically not be covered by even one read. In other cancers treated with chemotherapy, both possibilities have been shown, in some studies even with the same treatment in one entity (Ding *et al.*, 2012; Kim *et al.*, 2018; Kurtova *et al.*, 2015; Patch *et al.*, 2015). Some of the chemotherapies used were known to be highly mutagenic, which increases the possibility of acquiring resistant cell clones. In contrast, trametinib is not classified as a mutagenic agent by the U.S. Food and Drug Administration (FDA) (U.S. Food and Drug Administration Center for Drug Evaluation and Research, 2013). In a small cohort of triple-negative breast cancer patients with surviving tumor cells in samples taken after neoadjuvant chemotherapy with low mutagenic taxanes and anthracyclines, the resistant genotypes were already present at low frequencies (0.02 % - 2 %) before treatment in four out of five patients. Notably, the associated transcriptional reprogramming including EMT (4.2) was acquired during treatment but was already primed before treatment (Kim *et al.*, 2018). For their investigation the authors applied

targeted deep sequencing for previously identified variants of the resistant cells at a very high coverage of 1,671,000 x. Considering the mutagenic potential of taxanes and anthracyclines comparable to trametinib, this study rather suggests a pre-existence of a clone that harbors the ability to adapt to drug treatment. Nonetheless, both Sharma *et al.* (Sharma *et al.*, 2010b) and Hata *et al.* (Hata *et al.*, 2016) showed the *de novo* emergence of TK_i resistant cells in cell populations derived from single cell expansion. Overall, the emergence of one resistant clone whose unique variants most likely do not represent a direct cause of resistance suggests that the clone with the greatest potential to epigenetically adapt to the treatment was selected. Whether this clone was already present in the parental cell population remains questionable on the basis of the available data sets.

4.2 MEK_i resistance was associated with phenotypic plasticity

The hypothesis of a cell clone that is capable to epigenetically adapt to MEK_i treatment but lacks a direct resistance mediating mutation is further supported by the phenotypic plasticity of the analyzed cell lines. In contrast to stable genetic alterations such as mutations, epigenetic modifications are reversible and thus allow a more flexible adaptation to environmental stimuli such as drug treatment.

Firstly, the observed resistance reversibility upon drug withdrawal was in line with data of the TK_i tolerating cell state mediated by chromatin alterations in a subpopulation of a NSCLC cell line reported by Sharma *et al.* (Sharma *et al.*, 2010b). The resistant cells displayed a transient stem cell marker expression and after around 30 passages of drug withdrawal, they regained their initial TK_i sensitivity (Sharma *et al.*, 2010b). For patients who initially respond to MEK_i the observed resistance reversibility after drug withdrawal indicates that an alternating treatment regimen could be promising (Kuczynski *et al.*, 2013). A so called ‘drug-holiday’ for a certain time period could potentially prevent the occurrence of treatment-induced resistance. Furthermore, potential side effects of the treatment could be reduced by this strategy. Certainly, the duration of the drug-free interval needs to be determined carefully to get the best effect on tumor shrinkage. For example, patients with secondary EGFR-TK_i resistant NSCLC revealed a benefit of retreatment after a median treatment interruption through chemotherapy for 9.5 months (Becker *et al.*, 2011).

Secondly, MEK_i resistance was accompanied by a transcriptional reprogramming leading to EMT and a switch from the epithelial to the mesenchymal PDAC subtype which is associated with a worse prognosis (Bailey *et al.*, 2016; Collisson *et al.*, 2011;

Moffitt *et al.*, 2015). EMT is known to be linked to stemness enabling tumor cells to develop resistance to a variety of treatments including chemotherapy and targeted agents (Fischer *et al.*, 2015; Hata *et al.*, 2016; Kim *et al.*, 2018; Shibue and Weinberg, 2017; Wang *et al.*, 2011b). In general, cell lines with mesenchymal properties tend to be less sensitive to trametinib treatment than epithelial cells (Jing *et al.*, 2012). In particular, EMT was associated with a reduced dependence on KRAS signals (Singh *et al.*, 2009), which is consistent with the absence of ERK rebound in the MEK_i resistant cells. Hence, of the ten cell lines analyzed, the highest initial IC50 of trametinib was observed in the only cell line (# 9) that lacked expression of the epithelial marker CDH1 already in parental cells and which can therefore be considered the most mesenchymal cell line of the cohort. Suppression of EMT was shown to increase gemcitabine sensitivity in a GEMM of PDAC due to increased cell proliferation and the upregulation of nucleoid transporters (Zheng *et al.*, 2015).

Overall, the frequent occurrence of EMT in resistant tumor cells, regardless of the type of therapy, suggests a general advantage of mesenchymal properties for resistance development. Potentially, tolerance to apoptotic signals and quiescence as cellular attributes of EMT provide a time frame of drug tolerance in which resistances can develop (Boumahdi and de Sauvage, 2020; Francescangeli *et al.*, 2020; Hata *et al.*, 2016; Sharma *et al.*, 2010b; Shibue and Weinberg, 2017). This hypothesis is in line with a study showing that KRAS ablation in a PDAC mouse model was survived by dormant tumor cells with stem cell characteristics (Viale *et al.*, 2014). EMT is thought to be mainly epigenetically controlled (Galle *et al.*, 2020; Shibue and Weinberg, 2017; Skrypek *et al.*, 2017). Arumugam and colleges (Arumugam *et al.*, 2009) provided evidence for EMT as a resistance mechanism for chemotherapy resistant PDAC that could be overcome by $HDAC_i$ treatment. Concordantly, in the study by Sharma *et al.* (Sharma *et al.*, 2010b) described above, the TK_i tolerating cells were sensitive to $HDAC_i$, thus strengthen the hypothesis of epigenetic regulation in therapy resistance. Similarly, MEK_i resistant but not parental cells displayed a remarkable sensitivity for $DNMT_i$.

4.3 MEK_i resistance was associated with adaptive DNA hypermethylation of regulatory regions leading to attenuation of apoptosis

The remarkable $DNMT_i$ sensitivity of resistant but not parental cells indicated a functional importance of DNA methylation for MEK_i resistance. The MEK_i resistant phenotype was associated with more than 2000 mainly hypermethylated DNA regions.

Presumably, stemness properties as part of EMT enable the cells for this extensive modulation of their methylome that usually occurs only during embryogenetic development or differentiation (Feng *et al.*, 2010b; Wallner *et al.*, 2016). Otherwise, the detected DNA methylation changes in the resistant cells could in turn contribute to the development of EMT. A possible causality for altered DNA methylation during EMT was recently provided by Eva Galle and co-workers (Galle *et al.*, 2020) in cell lines from various entities including pancreatic cancer.

In contrast to e.g. DNA methylation arrays, the WGBS approach used in this study allowed an unbiased and comprehensive view on the cells' methylome. Indeed, most DMRs were located outside of CpG islands in non-coding regions and the majority would not have been found with the pre-selected probes on DNA methylation arrays. In 2009, for the first time, DNA methylation changes with relevance for gene regulation in colon cancer were reported to be located outside of promoters and CpG islands in shores (Irizarry *et al.*, 2009). The proportion of an inverse correlation with gene expression in approximately one third of the DMRs was comparable to a study of a large array-based analysis of PDAC methylomes compared to non-malignant pancreatic tissue (Nones *et al.*, 2014). However, the closest linear distance between a DMR and a gene does not necessarily mean a functional relationship. Chromatin folding leads to a DNA topology that could establish a close connection between genes and regulatory regions located far away on the linear DNA strand (Dekker, 2008).

With the inclusion of the reverting cell states, it was possible to define DMRs that reverted after drug withdrawal and thus reflected the phenotypically observed degree of MEK_i resistance. Importantly, a representative selection of reverting DMRs could be validated by deep targeted bisulfite sequencing, which strengthens the hypothesis of dynamic DNA methylation changes during gain and loss of MEK_i resistance. Neither the expression nor the activity of DNMT and TET enzymes was significantly altered over the different cell states analyzed. However, in order to understand the regulation of changes in DNA methylation, the recruitment of DNMTs and TETs to the DNA seems to be the critical step, at least when assuming non-random methylation of DMRs. In addition, defined cell states at which a phenotypic change was already measurable were analyzed in this study. Therefore, a transient increase of expression or activity while acquiring or losing resistance would have been missed.

The high degree of DMR sequence conservation to human which is unexpected for non-coding regions implies their functional relevance (Chinwalla *et al.*, 2002; Yue *et al.*, 2014). Furthermore, their importance for gene regulation is suggested by the fact

that DMRs exhibited a significant overlap with regulatory elements like TFBS and potential active enhancer sites. Notably, more than 90 % of TFBS-containing DMRs coincided with chromatin marks that indicated active enhancers (H3K4me1 and K3K27ac). While the impact of SNVs on enhancer activity and transcription factor binding seems generally low (Sur and Taipale, 2016), the effect of DNA methylation is remarkable (Xuan Lin *et al.*, 2019; Yin *et al.*, 2017). In most cases, the altered DNA structure caused by methyl groups leads to steric hindrance of transcription factor binding although some factors with preference for a methylated motif exist (Yin *et al.*, 2017). As the activity of enhancer sites is highly tissue-specific and context-dependent (Kundaje *et al.*, 2015), published data from Roe and co-workers (Roe *et al.*, 2017) provided a reasonable approximation of enhancers potentially active in PDAC and normal pancreas. They analyzed organoids derived from *Kras*$^{wt/LSL\text{-}G12D}$; *Trp53*$^{wt/LSL\text{-}R172H}$; *Pdx1-Cre* mice. Except for a *Trp53* mutation instead of a knockout and the *Pdx1* instead of the *Ptfa1* promotor to drive *Cre* expression, the model is highly comparable to the one investigated in this study. However, it cannot be excluded that the cultivation as organoids could influence the activity of regulatory elements compared to 2D cell culture. Bhattacharyya *et al.* (Bhattacharyya *et al.*, 2017) used a similar approach based on the analysis of DNA hydroxymethylation by oxidative bisulfite sequencing in PDAC xenografts and cell lines compared to pancreatic controls. Their finding of altered DNA hydroxymethylation preferentially at regulatory regions underlines the functional role of DNA methylation and demethylation at regulatory elements. In contrast, the altered chromatin state described for cells tolerating lethal TK_i doses (Sharma *et al.*, 2010b) was associated with a histone methylation mediated silencing of drug-induced transposable elements rather than affecting regulatory regions (Guler *et al.*, 2017). Consequently, in the case of lethal drug concentrations, maintaining genomic integrity could take precedence over gene regulation. Since the period of drug exposure applied by Guler *et al.* (Guler *et al.*, 2017) was much shorter, they may have observed a transient state that allows the cells to adapt to the treatment. For PDAC, enhancer reprogramming mediated by FOXA1 was shown during progression from a local to a metastatic tumor (Roe *et al.*, 2017). In breast cancer, enhancer reprogramming indicated by altered chromatin modifications has been reported in response to short-term trametinib treatment (Zawistowski *et al.*, 2017). In the presented thesis the modulation of enhancer activity by DNA methylation is postulated. Together with the clonal outgrowth (4.1) and phenotypic plasticity (4.2) observed for the MEK_i resistant cells, these data suggest a concept of the selection of cells with

epigenetic plasticity leading to adaptive DNA hypermethylation. Thus, MEK_i resistance relied on both a classical selection of a distinct cell clone and the acquiring of resistance by epigenetic and phenotypic plasticity. Thereby, these two concepts of resistance evolution are integrated in the same system as previously proposed by Kim *et al.* for chemoresistant breast cancer (Kim *et al.*, 2018). In contrast to a report by Shaffer *et al.* (Shaffer *et al.*, 2017), where a former transient resistant state became irreversibly locked, the resistant state remained reversible upon MEK_i withdrawal. However, their assumption was based on the observation that $BRAF_i$ resistant melanoma cell lines did not show a reverting transcriptional profile or resistant phenotype after longest 1 to 3 weeks of drug withdrawal (Shaffer *et al.*, 2017). Possibly, resistance reversibility requires a longer time frame. Even though in most resistant cell lines a partial MEK_i sensitivity was regained already after 12 passages, the complete resistance reversal required about 40 passages.

Amongst the TFBS in the reverting DMRs, motifs for components of the dimeric transcription factor AP-1 were most frequently affected by DNA hypermethylation in the resistant cells which prevents the protein binding (Xuan Lin *et al.*, 2019; Yin *et al.*, 2017). Additionally, potential new binding sites for JUN, an AP-1 building protein, were generated by DNA methylation in the reverting DMRs (Gustems *et al.*, 2014; Hong *et al.*, 2017; Tulchinsky *et al.*, 1996). The activity of AP-1 and its downstream effects depend on the dimer composition as well as the tumor type, its genetic background and differentiation state (Eferl and Wagner, 2003; Lopez-Bergami *et al.*, 2010). Together with the variety of AP-1 target genes, the effects of the methylated binding sites are difficult to assess (Eferl and Wagner, 2003; Lopez-Bergami *et al.*, 2010). As already mentioned above, the annotation of the closest gene is not sufficient to imply a functional association with the DMR. In addition, AP-1 proteins are subject to a complex and dynamic regulation consisting of post-translational modifications and regulatory feedback loops (Lopez-Bergami *et al.*, 2010). Neither for *JUN* nor for *FOS* mutations in tumors have been described so far, although both are frequently overexpressed in cancer (Lopez-Bergami *et al.*, 2010). A *JUN* amplification was only shown in sarcomas (Mariani *et al.*, 2007). However, its central role in MAPK signaling, renders AP-1 susceptible to deregulation of oncogenic signals (Lopez-Bergami *et al.*, 2010). For example, JUN was upregulated and stabilized by hyperactivated ERK1/2 in *BRAF* mutant melanoma (Lopez-Bergami *et al.*, 2007). Since ERK phosphorylation remained blocked in the MEK_i resistant cells, the observed upregulation of JUN had to rely on a different activator. Overexpression of JUN was shown to mediate an EMT-

like phenotypic switch and intrinsic resistance to $BRAF_i$ or MEK_i in *BRAF* p.V600 mutant melanoma (Ramsdale *et al.*, 2015). In the MEK_i resistance model evaluated in this thesis, not only a differential expression of JUN but also an epigenetic regulation of its binding sites' accessibility by DNA methylation is suggested. While the canonical signaling was potentially inhibited, an alternative signaling using newly generated binding sites might be enabled. Notably, in $BRAF_i$ resistant melanoma cells, AP-1 binding sites gained accessibility detected by ATAC-seq that indicates open chromatin (Shaffer *et al.*, 2017). Thus, deregulation of AP-1 binding sites seems to contribute to resistance against MEK pathway inhibition.

Within the reverting DMRs, a potential *Casp3* enhancer containing AP-1 binding sites could be identified whose methylation status correlated inversely with *Casp3* expression. When MEK_i was present in the culture medium, CASP3 activity was attenuated in the resistant cells, but could be re-activated by $DNMT_i$ treatment. A synergistic effect of MEK_i and $DNMT_i$ could not only be observed *in vitro* but also in a small PDX cohort underpinning a putative translational relevance of the reported findings. CASP3 deregulation has already been frequently observed in therapy resistance of several tumor entities (Bernard *et al.*, 2019; Devarajan *et al.*, 2002; Friedrich *et al.*, 2001; Yang *et al.*, 2007; Zhou *et al.*, 2018). Here, the methylation change at distal regions was identified as a possible regulator of CASP3 leading to modulation of treatment-induced apoptosis. However, it remains to be clarified, if DNA methylation changes, especially of regions located outside of CpG islands, are cause or consequence of differential transcription (Bestor *et al.*, 2015).

Due to the rational of their correlation with MEK_i sensitivity, this thesis focused on the reverting DMRs. However, it should be finally mentioned that the non-reverting DMRs may not only represent unfunctional passenger modifications of MEK_i resistance. Its stability putatively makes DNA methylation a suitable memory of the resistant state that could be passed on to the daughter cells and potentially provides them with the ability to faster evade MEK inhibition (Kim and Costello, 2017). It remains to be elucidated, how the resistant cells react on the re-treatment with increasing trametinib doses longer than 72 h, the time point assessed in the cell viability measurements. Such approaches will help to further characterize and define epigenetic plasticity as a MEK_i resistance-mediating cellular escape mechanism.

4.4 Conclusion and Outlook

Based on a comprehensive characterization of the MEK_i resistant PDAC model, known resistance phenomena as tumor subtype switching and cell death evasion could be embedded into the context of comprehensive (epi-)genomics. The generated results support a concept of MEK_i resistance as the selection of a distinct cell clone harboring the property for epigenetic plasticity reflected by DNA hypermethylation of regulatory regions which contained transcription factor binding sites. The resulting transcriptional reprogramming mediated phenotypic plasticity characterized by EMT and a PDAC subtype switch and led to aberrantly regulated CASP3 activation. Thus, modulation of apoptosis is a potential transient resistance mechanism in the presence of MEK_i that could be overcome by $DNMT_i$ treatment or potentially avoided by an intermittent treatment regimen.

Due to the *in vitro* cell line-based model used, it remains to be elucidated, whether and how the tumor microenvironment may contribute to the development of MEK_i resistance *in vivo*. In addition, it has to be assessed to which extent the conclusions drawn from the murine model system are applicable to the human disease and may improve the therapeutic options for PDAC patients. However, the synergistic effect of MEK_i and $DNMT_i$ was already confirmed in a small PDX cohort. Furthermore, it remains questionable whether the association of DNA methylation changes and CASP3 modulation shown represents a MEK_i-specific or a general resistance mechanism of PDAC cells. Therefore, the effect of other therapies would have to be evaluated. Further analyses in this particular model system are necessary to validate and concretize the effect of DNA methylation on canonical JUN binding sites and the generation of potential new ones. In addition, the consequences of altered AP-1 signaling remain to be elucidated. As this study focused on the reverting DMRs, it might be interesting to define, if the non-reverting DMRs represent bystanders or display a functional role for example as a cellular memory, that possibly enables faster adaptation to a MEK_i retreatment. Also the concept of epigenetic plasticity introduced based on the multidimensional results needs further specification. Putative regulators of adaptive DNA hypermethylation have to be identified. Even if no direct consequence of the coding mutations on resistance could be deduced, it may be possible that non-coding variants or variants not found due to the sample size mediate epigenetic plasticity. Furthermore, using deep sequencing or single cell-derived populations the question could be answered, whether the selected resistant clone was already present in the parental cell population or emerged as a result of MEK_i treatment.

REFERENCES

Amrutkar, M., and Gladhaug, I.P. (2017). Pancreatic cancer chemoresistance to gemcitabine. Cancers *9*, 157.

Arumugam, T., Ramachandran, V., Fournier, K.F., Wang, H., Marquis, L., Abbruzzese, J.L., Gallick, G.E., Logsdon, C.D., McConkey, D.J., and Choi, W. (2009). Epithelial to mesenchymal transition contributes to drug resistance in pancreatic cancer. Cancer Res. *69*, 5820-5828.

Assenov, Y., Brocks, D., and Gerhauser, C. (2018). Intratumor heterogeneity in epigenetic patterns. Semin. Cancer Biol. *51*, 12-21.

Bailey, P., Chang, D.K., Nones, K., Johns, A.L., Patch, A.M., Gingras, M.C., Miller, D.K., Christ, A.N., Bruxner, T.J., Quinn, M.C*., et al.* (2016). Genomic analyses identify molecular subtypes of pancreatic cancer. Nature *531*, 47-52.

Bardeesy, N., Aguirre, A.J., Chu, G.C., Cheng, K.-H., Lopez, L.V., Hezel, A.F., Feng, B., Brennan, C., Weissleder, R., Mahmood, U*., et al.* (2006). Both p16(Ink4a) and the p19(Arf)-p53 pathway constrain progression of pancreatic adenocarcinoma in the mouse. Proc. Natl. Acad. Sci. USA *103*, 5947-5952.

Barth, T.K., and Imhof, A. (2010). Fast signals and slow marks: the dynamics of histone modifications. Trends Biochem. Sci. *35*, 618-626.

Baylin, S.B., and Jones, P.A. (2016). Epigenetic determinants of cancer. Cold Spring Harb. Perspect. Biol. *8*.

Becker, A., Crombag, L., Heideman, D.A.M., Thunnissen, F.B., van Wijk, A.W., Postmus, P.E., and Smit, E.F. (2011). Retreatment with erlotinib: regain of TKI sensitivity following a drug holiday for patients with NSCLC who initially responded to EGFR-TKI treatment. Eur. J. Cancer *47*, 2603-2606.

Benjamini, Y., and Hochberg, Y. (1995). Controlling the false discovery rate: a practical and powerful approach to multiple testing. J. R. Stat. Soc. Ser. B Methodol. *57*, 289-300.

Bernard, A., Chevrier, S., Beltjens, F., Dosset, M., Viltard, E., Lagrange, A., Derangere, V., Oudot, A., Ghiringhelli, F., Collin, B*., et al.* (2019). Cleaved Caspase-3 transcriptionally regulates angiogenesis-promoting chemotherapy resistance. Cancer Res. *79*, 5958-5970.

Bernhart, S.H., Kretzmer, H., Holdt, L.M., Jühling, F., Ammerpohl, O., Bergmann, A.K., Northoff, B.H., Doose, G., Siebert, R., Stadler, P.F*., et al.* (2016). Changes of bivalent chromatin coincide with increased expression of developmental genes in cancer. Sci. Rep. *6*, 37393.

Bernstein, B.E., Mikkelsen, T.S., Xie, X., Kamal, M., Huebert, D.J., Cuff, J., Fry, B., Meissner, A., Wernig, M., Plath, K.*, et al.* (2006). A bivalent chromatin structure marks key developmental genes in embryonic stem cells. Cell *125*, 315-326.

Bestor, T.H., Edwards, J.R., and Boulard, M. (2015). Notes on the role of dynamic DNA methylation in mammalian development. Proc. Natl. Acad. Sci. U.S.A. *112*, 6796.

Bhattacharyya, S., Pradhan, K., Campbell, N., Mazdo, J., Vasantkumar, A., Maqbool, S., Bhagat, T.D., Gupta, S., Suzuki, M., Yu, Y.*, et al.* (2017). Altered hydroxymethylation is seen at regulatory regions in pancreatic cancer and regulates oncogenic pathways. Genome Res. *27*, 1830-1842.

Boj, S.F., Hwang, C.I., Baker, L.A., Chio, II, Engle, D.D., Corbo, V., Jager, M., Ponz-Sarvise, M., Tiriac, H., Spector, M.S.*, et al.* (2015). Organoid models of human and mouse ductal pancreatic cancer. Cell *160*, 324-338.

Botla, S.K., Savant, S., Jandaghi, P., Bauer, A.S., Mücke, O., Moskalev, E.A., Neoptolemos, J.P., Costello, E., Greenhalf, W., Scarpa, A.*, et al.* (2016). Early epigenetic downregulation of microRNA-192 expression promotes pancreatic cancer progression. Cancer Res. *76*, 4149.

Boumahdi, S., and de Sauvage, F.J. (2020). The great escape: tumour cell plasticity in resistance to targeted therapy. Nat. Rev. Drug Discov. *19*, 39-56.

Bryant, K.L., Stalnecker, C.A., Zeitouni, D., Klomp, J.E., Peng, S., Tikunov, A.P., Gunda, V., Pierobon, M., Waters, A.M., George, S.D.*, et al.* (2019). Combination of ERK and autophagy inhibition as a treatment approach for pancreatic cancer. Nat. Med. *25*, 628-640.

Cancer Genome Atlas Research Network (2017). Integrated genomic characterization of pancreatic ductal adenocarcinoma. Cancer Cell *32*, 185-203.

Cao, J., and Yan, Q. (2012). Histone ubiquitination and deubiquitination in transcription, DNA damage response, and cancer. Front. Oncol. *2*, 26-26.

Cao, R., Wang, L., Wang, H., Xia, L., Erdjument-Bromage, H., Tempst, P., Jones, R.S., and Zhang, Y. (2002). Role of histone H3 lysine 27 methylation in polycomb-group silencing. Science *298*, 1039.

Caunt, C.J., Sale, M.J., Smith, P.D., and Cook, S.J. (2015). MEK1 and MEK2 inhibitors and cancer therapy: the long and winding road. Nat. Rev. Cancer *15*, 577-592.

Celeste, A., Fernandez-Capetillo, O., Kruhlak, M.J., Pilch, D.R., Staudt, D.W., Lee, A., Bonner, R.F., Bonner, W.M., and Nussenzweig, A. (2003). Histone H2AX phosphorylation is dispensable for the initial recognition of DNA breaks. Nat. Cell Biol. *5*, 675-679.

Chan-Seng-Yue, M., Kim, J.C., Wilson, G.W., Ng, K., Figueroa, E.F., O'Kane, G.M., Connor, A.A., Denroche, R.E., Grant, R.C., McLeod, J.*, et al.* (2020). Transcription

phenotypes of pancreatic cancer are driven by genomic events during tumor evolution. Nat. Genet. *52*, 231-240.

Chapman, P.B., Hauschild, A., Robert, C., Haanen, J.B., Ascierto, P., Larkin, J., Dummer, R., Garbe, C., Testori, A., Maio, M.*, et al.* (2011). Improved survival with vemurafenib in melanoma with BRAF V600E mutation. N. Engl. J. Med. *364*, 2507-2516.

Chinwalla, A.T., Cook, L.L., Delehaunty, K.D., Fewell, G.A., Fulton, L.A., Fulton, R.S., Graves, T.A., Hillier, L.W., Mardis, E.R., McPherson, J.D.*, et al.* (2002). Initial sequencing and comparative analysis of the mouse genome. Nature *420*, 520-562.

Chodavarapu, R.K., Feng, S., Bernatavichute, Y.V., Chen, P.-Y., Stroud, H., Yu, Y., Hetzel, J.A., Kuo, F., Kim, J., Cokus, S.J.*, et al.* (2010). Relationship between nucleosome positioning and DNA methylation. Nature *466*, 388-392.

Chung, V., McDonough, S., Philip, P.A., Cardin, D., Wang-Gillam, A., Hui, L., Tejani, M.A., Seery, T.E., Dy, I.A., Al Baghdadi, T.*, et al.* (2017). Effect of selumetinib and MK-2206 vs axaliplatin and fluorouracil in patients with metastatic pancreatic cancer after prior therapy: SWOG S1115 study randomized clinical trial. JAMA Oncol. *3*, 516-522.

Ciliberto, D., Staropoli, N., Chiellino, S., Botta, C., Tassone, P., and Tagliaferri, P. (2016). Systematic review and meta-analysis on targeted therapy in advanced pancreatic cancer. Pancreatology *16*, 249-258.

Collins, M.A., Bednar, F., Zhang, Y., Brisset, J.C., Galban, S., Galban, C.J., Rakshit, S., Flannagan, K.S., Adsay, N.V., and Pasca di Magliano, M. (2012). Oncogenic Kras is required for both the initiation and maintenance of pancreatic cancer in mice. J. Clin. Invest. *122*, 639-653.

Collins, M.A., and Pasca di Magliano, M. (2013). Kras as a key oncogene and therapeutic target in pancreatic cancer. Front. Physiol. *4*, 407.

Collisson, E.A., Sadanandam, A., Olson, P., Gibb, W.J., Truitt, M., Gu, S., Cooc, J., Weinkle, J., Kim, G.E., Jakkula, L.*, et al.* (2011). Subtypes of pancreatic ductal adenocarcinoma and their differing responses to therapy. Nat. Med. *17*, 500-503.

Collisson, E.A., Trejo, C.L., Silva, J.M., Gu, S., Korkola, J.E., Heiser, L.M., Charles, R.P., Rabinovich, B.A., Hann, B., Dankort, D.*, et al.* (2012). A central role for RAF-->MEK-->ERK signaling in the genesis of pancreatic ductal adenocarcinoma. Cancer Discov. *2*, 685-693.

Corcoran, R.B., Dias-Santagata, D., Bergethon, K., Iafrate, A.J., Settleman, J., and Engelman, J.A. (2010). BRAF gene amplification can promote acquired resistance to MEK inhibitors in cancer cells harboring the BRAF V600E mutation. Sci. Signal. *3*, ra84.

Costantino, C.L., Witkiewicz, A.K., Kuwano, Y., Cozzitorto, J.A., Kennedy, E.P., Dasgupta, A., Keen, J.C., Yeo, C.J., Gorospe, M., and Brody, J.R. (2009). The role of

HuR in gemcitabine efficacy in pancreatic cancer: HuR Up-regulates the expression of the gemcitabine metabolizing enzyme deoxycytidine kinase. Cancer Res. *69*, 4567-4572.

Creyghton, M.P., Cheng, A.W., Welstead, G.G., Kooistra, T., Carey, B.W., Steine, E.J., Hanna, J., Lodato, M.A., Frampton, G.M., Sharp, P.A.*, et al.* (2010). Histone H3K27ac separates active from poised enhancers and predicts developmental state. Proc. Natl. Acad. Sci. USA *107*, 21931.

Dauer, P., Nomura, A., Saluja, A., and Banerjee, S. (2017). Microenvironment in determining chemo-resistance in pancreatic cancer: neighborhood matters. Pancreatology *17*, 7-12.

Dawson, M.A., Bannister, A.J., Göttgens, B., Foster, S.D., Bartke, T., Green, A.R., and Kouzarides, T. (2009). JAK2 phosphorylates histone H3Y41 and excludes HP1α from chromatin. Nature *461*, 819-822.

Dawson, M.A., Foster, S.D., Bannister, A.J., Robson, S.C., Hannah, R., Wang, X., Xhemalce, B., Wood, A.D., Green, A.R., Göttgens, B.*, et al.* (2012). Three distinct patterns of histone H3Y41 phosphorylation mark active genes. Cell Rep. *2*, 470-477.

Deer, E.L., Gonzalez-Hernandez, J., Coursen, J.D., Shea, J.E., Ngatia, J., Scaife, C.L., Firpo, M.A., and Mulvihill, S.J. (2010). Phenotype and genotype of pancreatic cancer cell lines. Pancreas *39*, 425-435.

Dekker, J. (2008). Gene regulation in the third dimension. Science *319*, 1793-1794.

Delitto, D., Black, B.S., Sorenson, H.L., Knowlton, A.E., Thomas, R.M., Sarosi, G.A., Moldawer, L.L., Behrns, K.E., Liu, C., George, T.J.*, et al.* (2015). The inflammatory milieu within the pancreatic cancer microenvironment correlates with clinicopathologic parameters, chemoresistance and survival. BMC Cancer *15*, 783-783.

Demetri, G.D., Von Mehren, M., Blanke, C.D., Van Den Abbeele, A.D., Eisenberg, B., Roberts, P.J., Heinrich, M.C., Tuveson, D.A., Singer, S., Janicek, M.*, et al.* (2002). Efficacy and safety of imatinib mesylate in advanced gastrointestinal stromal tumors. N. Engl. J. Med. *347*, 472-480.

Devarajan, E., Sahin, A.A., Chen, J.S., Krishnamurthy, R.R., Aggarwal, N., Brun, A.-M., Sapino, A., Zhang, F., Sharma, D., Yang, X.-H.*, et al.* (2002). Down-regulation of caspase 3 in breast cancer: a possible mechanism for chemoresistance. Oncogene *21*, 8843-8851.

Di Veroli, G.Y., Fornari, C., Wang, D., Mollard, S., Bramhall, J.L., Richards, F.M., and Jodrell, D.I. (2016). Combenefit: an interactive platform for the analysis and visualization of drug combinations. Bioinformatics *32*, 2866-2868.

Ding, L., Ley, T.J., Larson, D.E., Miller, C.A., Koboldt, D.C., Welch, J.S., Ritchey, J.K., Young, M.A., Lamprecht, T., McLellan, M.D.*, et al.* (2012). Clonal evolution in relapsed

acute myeloid leukaemia revealed by whole-genome sequencing. Nature *481*, 506-510.

Edlund, H. (2002). Pancreatic organogenesis--developmental mechanisms and implications for therapy. Nat. Rev. Genet. *3*, 524-532.

Eferl, R., and Wagner, E.F. (2003). AP-1: a double-edged sword in tumorigenesis. Nat. Rev. Cancer *3*, 859-868.

Emery, C.M., Vijayendran, K.G., Zipser, M.C., Sawyer, A.M., Niu, L., Kim, J.J., Hatton, C., Chopra, R., Oberholzer, P.A., Karpova, M.B.*, et al.* (2009). MEK1 mutations confer resistance to MEK and B-RAF inhibition. Proc. Natl. Acad. Sci. USA *106*, 20411.

Engelman, J.A., and Jänne, P.A. (2008). Mechanisms of acquired resistance to epidermal growth factor receptor tyrosine kinase inhibitors in non–small cell lung cancer. Clin. Cancer Res. *14*, 2895.

Erkan, M., Hausmann, S., Michalski, C.W., Fingerle, A.A., Dobritz, M., Kleeff, J., and Friess, H. (2012). The role of stroma in pancreatic cancer: diagnostic and therapeutic implications. Nat. Rev. Gastroenterol. Hepatol. *9*, 454-467.

Esteller, M. (2008). Epigenetics in cancer. N. Engl. J. Med. *358*, 1148-1159.

Fedele, C., Ran, H., Diskin, B., Wei, W., Jen, J., Geer, M.J., Araki, K., Ozerdem, U., Simeone, D.M., Miller, G.*, et al.* (2018). SHP2 inhibition prevents adaptive resistance to MEK inhibitors in multiple cancer models. Cancer Discov. *8*, 1237-1249.

Feng, J., Zhou, Y., Campbell, S.L., Le, T., Li, E., Sweatt, J.D., Silva, A.J., and Fan, G. (2010a). Dnmt1 and Dnmt3a maintain DNA methylation and regulate synaptic function in adult forebrain neurons. Nat. Neurosci. *13*, 423-430.

Feng, S., Jacobsen, S.E., and Reik, W. (2010b). Epigenetic reprogramming in plant and animal development. Science *330*, 622.

Fernandez-Zapico, M.E., Gonzalez-Paz, N.C., Weiss, E., Savoy, D.N., Molina, J.R., Fonseca, R., Smyrk, T.C., Chari, S.T., Urrutia, R., and Billadeau, D.D. (2005). Ectopic expression of VAV1 reveals an unexpected role in pancreatic cancer tumorigenesis. Cancer Cell *7*, 39-49.

Fischer, K.R., Durrans, A., Lee, S., Sheng, J., Li, F., Wong, S.T.C., Choi, H., El Rayes, T., Ryu, S., Troeger, J.*, et al.* (2015). Epithelial-to-mesenchymal transition is not required for lung metastasis but contributes to chemoresistance. Nature *527*, 472-476.

Flaherty, K.T., Infante, J.R., Daud, A., Gonzalez, R., Kefford, R.F., Sosman, J., Hamid, O., Schuchter, L., Cebon, J., Ibrahim, N.*, et al.* (2012a). Combined BRAF and MEK inhibition in melanoma with BRAF V600 mutations. N. Engl. J. Med. *367*, 1694-1703.

Flaherty, K.T., Robert, C., Hersey, P., Nathan, P., Garbe, C., Milhem, M., Demidov, L.V., Hassel, J.C., Rutkowski, P., Mohr, P.*, et al.* (2012b). Improved survival with MEK inhibition in BRAF-mutated melanoma. N. Engl. J. Med. *367*, 107-114.

Francescangeli, F., Contavalli, P., De Angelis, M.L., Careccia, S., Signore, M., Haas, T.L., Salaris, F., Baiocchi, M., Boe, A., Giuliani, A.*, et al.* (2020). A pre-existing population of ZEB2+ quiescent cells with stemness and mesenchymal features dictate chemoresistance in colorectal cancer. J. Exp. Clin. Cancer Res. *39*, 2.

Friedrich, K., Wieder, T., Von Haefen, C., Radetzki, S., Jänicke, R., Schulze-Osthoff, K., Dörken, B., and Daniel, P.T. (2001). Overexpression of caspase-3 restores sensitivity for drug-induced apoptosis in breast cancer cell lines with acquired drug resistance. Oncogene *20*, 2749-2760.

Fujisawa, T., and Filippakopoulos, P. (2017). Functions of bromodomain-containing proteins and their roles in homeostasis and cancer. Nat. Rev. Mol. Cell Biol. *18*, 246-262.

Galle, E., Thienpont, B., Cappuyns, S., Venken, T., Busschaert, P., Van Haele, M., Van Cutsem, E., Roskams, T., van Pelt, J., Verslype, C.*, et al.* (2020). DNA methylation-driven EMT is a common mechanism of resistance to various therapeutic agents in cancer. Clin. Epigenetics *12*, 27.

Garrido-Laguna, I., and Hidalgo, M. (2015). Pancreatic cancer: from state-of-the-art treatments to promising novel therapies. Nat. Rev. Clin. Oncol. *12*, 319-334.

Garrison, E., and Gabor, M. (2012). Haplotype-based variant detection from short-read sequencing. arXiv, https://arxiv.org/abs/1207.3907.

Gaspar, J.M. (2018). Improved peak-calling with MACS2. bioRxiv, https://doi.org/10.1101/496521.

Geller, L.T., Barzily-Rokni, M., Danino, T., Jonas, O.H., Shental, N., Nejman, D., Gavert, N., Zwang, Y., Cooper, Z.A., Shee, K.*, et al.* (2017). Potential role of intratumor bacteria in mediating tumor resistance to the chemotherapeutic drug gemcitabine. Science *357*, 1156-1160.

Goldberg, A.D., Allis, C.D., and Bernstein, E. (2007). Epigenetics: a landscape takes shape. Cell *128*, 635-638.

Goll, M.G., and Bestor, T.H. (2005). Eukaryotic cytosine methyltransferases. Annu. Rev. Biochem. *74*, 481-514.

Gopinathan, A., Morton, J.P., Jodrell, D.I., and Sansom, O.J. (2015). GEMMs as preclinical models for testing pancreatic cancer therapies. Dis. Models Mech. *8*, 1185-1200.

Gottesman, M.M. (2002). Mechanisms of cancer drug resistance. Annu. Rev. Med. *53*, 615-627.

Grant, C.E., Bailey, T.L., and Noble, W.S. (2011). FIMO: scanning for occurrences of a given motif. Bioinformatics *27*, 1017-1018.

Grapin-Botton, A. (2005). Ductal cells of the pancreas. Int. J. Biochem. Cell Biol. *37*, 504-510.

Grasso, C., Jansen, G., and Giovannetti, E. (2017). Drug resistance in pancreatic cancer: impact of altered energy metabolism. Crit. Rev. Oncol./Hematol. *114*, 139-152.

Greenberg, M.V.C., and Bourc'his, D. (2019). The diverse roles of DNA methylation in mammalian development and disease. Nat. Rev. Mol. Cell Biol. *20*, 590-607.

Greer, E.L., and Shi, Y. (2012). Histone methylation: a dynamic mark in health, disease and inheritance. Nat. Rev. Genet. *13*, 343-357.

Guler, G.D., Tindell, C.A., Pitti, R., Wilson, C., Nichols, K., KaiWai Cheung, T., Kim, H.-J., Wongchenko, M., Yan, Y., Haley, B.*, et al.* (2017). Repression of stress-induced LINE-1 expression protects cancer cell subpopulations from lethal drug exposure. Cancer Cell *32*, 221-237.e213.

Gustems, M., Woellmer, A., Rothbauer, U., Eck, S.H., Wieland, T., Lutter, D., and Hammerschmidt, W. (2014). c-Jun/c-Fos heterodimers regulate cellular genes via a newly identified class of methylated DNA sequence motifs. Nucleic Acids Res. *42*, 3059-3072.

Hanahan, D., and Coussens, L.M. (2012). Accessories to the crime: functions of cells recruited to the tumor microenvironment. Cancer Cell *21*, 309-322.

Hansen, K.D., Langmead, B., and Irizarry, R.A. (2012). BSmooth: from whole genome bisulfite sequencing reads to differentially methylated regions. Genome Biol. *13*, R83.

Hata, A.N., Niederst, M.J., Archibald, H.L., Gomez-Caraballo, M., Siddiqui, F.M., Mulvey, H.E., Maruvka, Y.E., Ji, F., Bhang, H.E., Krishnamurthy Radhakrishna, V.*, et al.* (2016). Tumor cells can follow distinct evolutionary paths to become resistant to epidermal growth factor receptor inhibition. Nat. Med. *22*, 262-269.

Hatzivassiliou, G., Liu, B., Brien, C., Spoerke, J.M., Hoeflich, K.P., Haverty, P.M., Soriano, R., Forrest, W.F., Heldens, S., Chen, H.*, et al.* (2012). ERK inhibition overcomes acquired resistance to MEK inhibitors. Mol. Cancer Ther. *11*, 1143.

Heid, I., Steiger, K., Trajkovic-Arsic, M., Settles, M., Eßwein, M.R., Erkan, M., Kleeff, J., Jäger, C., Friess, H., Haller, B.*, et al.* (2016). Co-clinical assessment of tumor cellularity in pancreatic cancer. Clin. Cancer Res. *23*, 1461-1470.

Heintzman, N.D., Stuart, R.K., Hon, G., Fu, Y., Ching, C.W., Hawkins, R.D., Barrera, L.O., Van Calcar, S., Qu, C., Ching, K.A.*, et al.* (2007). Distinct and predictive chromatin signatures of transcriptional promoters and enhancers in the human genome. Nat. Genet. *39*, 311-318.

Heinz, S., Benner, C., Spann, N., Bertolino, E., Lin, Y.C., Laslo, P., Cheng, J.X., Murre, C., Singh, H., and Glass, C.K. (2010). Simple combinations of lineage-determining transcription factors prime cis-regulatory elements required for macrophage and B cell identities. Mol. Cell *38*, 576-589.

Henriksen, S.D., Madsen, P.H., Larsen, A.C., Johansen, M.B., Pedersen, I.S., Krarup, H., and Thorlacius-Ussing, O. (2017). Promoter hypermethylation in plasma-derived cell-free DNA as a prognostic marker for pancreatic adenocarcinoma staging. Int. J. Cancer *141*, 2489-2497.

Hessmann, E., Johnsen, S.A., Siveke, J.T., and Ellenrieder, V. (2017). Epigenetic treatment of pancreatic cancer: is there a therapeutic perspective on the horizon? Gut *66*, 168-179.

Hezel, A.F., Kimmelman, A.C., Stanger, B.Z., Bardeesy, N., and Depinho, R.A. (2006). Genetics and biology of pancreatic ductal adenocarcinoma. Genes Dev. *20*, 1218-1249.

Hidalgo, M. (2010). Pancreatic cancer. N. Engl. J. Med. *362*, 1605-1617.

Hidalgo, M., Amant, F., Biankin, A.V., Budinská, E., Byrne, A.T., Caldas, C., Clarke, R.B., de Jong, S., Jonkers, J., Mælandsmo, G.M.*, et al.* (2014). Patient-derived xenograft models: an emerging platform for translational cancer research. Cancer Discov. *4*, 998-1013.

Hidalgo, M., Cascinu, S., Kleeff, J., Labianca, R., Löhr, J.M., Neoptolemos, J., Real, F.X., Van Laethem, J.-L., and Heinemann, V. (2015). Addressing the challenges of pancreatic cancer: future directions for improving outcomes. Pancreatology *15*, 8-18.

Hingorani, S.R., Petricoin, E.F., Maitra, A., Rajapakse, V., King, C., Jacobetz, M.A., Ross, S., Conrads, T.P., Veenstra, T.D., Hitt, B.A.*, et al.* (2003). Preinvasive and invasive ductal pancreatic cancer and its early detection in the mouse. Cancer Cell *4*, 437-450.

Hingorani, S.R., Wang, L., Multani, A.S., Combs, C., Deramaudt, T.B., Hruban, R.H., Rustgi, A.K., Chang, S., and Tuveson, D.A. (2005). Trp53R172H and KrasG12D cooperate to promote chromosomal instability and widely metastatic pancreatic ductal adenocarcinoma in mice. Cancer Cell *7*, 469-483.

Hong, S., Wang, D., Horton, J.R., Zhang, X., Speck, S.H., Blumenthal, R.M., and Cheng, X. (2017). Methyl-dependent and spatial-specific DNA recognition by the orthologous transcription factors human AP-1 and Epstein-Barr virus Zta. Nucleic Acids Res. *45*, 2503-2515.

Housman, G., Byler, S., Heerboth, S., Lapinska, K., Longacre, M., Snyder, N., and Sarkar, S. (2014). Drug resistance in cancer: an overview. Cancers *6*, 1769-1792.

Hwang, C.I., Boj, S.F., Clevers, H., and Tuveson, D.A. (2016). Preclinical models of pancreatic ductal adenocarcinoma. J. Pathol. *238*, 197-204.

Infante, J.R., Somer, B.G., Park, J.O., Li, C.-P., Scheulen, M.E., Kasubhai, S.M., Oh, D.-Y., Liu, Y., Redhu, S., Steplewski, K.*, et al.* (2014). A randomised, double-blind, placebo-controlled trial of trametinib, an oral MEK inhibitor, in combination with gemcitabine for patients with untreated metastatic adenocarcinoma of the pancreas. Eur. J. Cancer *50*, 2072-2081.

Irizarry, R.A., Ladd-Acosta, C., Wen, B., Wu, Z., Montano, C., Onyango, P., Cui, H., Gabo, K., Rongione, M., Webster, M.*, et al.* (2009). The human colon cancer methylome shows similar hypo- and hypermethylation at conserved tissue-specific CpG island shores. Nat. Genet. *41*, 178-186.

Jager, M., Wang, K., Bauer, S., Smedley, D., Krawitz, P., and Robinson, P.N. (2014). Jannovar: a java library for exome annotation. Hum. Mutat. *35*, 548-555.

Jiang, H., Lei, R., Ding, S.-W., and Zhu, S. (2014). Skewer: a fast and accurate adapter trimmer for next-generation sequencing paired-end reads. BMC bioinformatics *15*, 182-182.

Jing, J., Greshock, J., Holbrook, J.D., Gilmartin, A., Zhang, X., McNeil, E., Conway, T., Moy, C., Laquerre, S., Bachman, K.*, et al.* (2012). Comprehensive predictive biomarker analysis for MEK inhibitor GSK1120212. Mol. Cancer Ther. *11*, 720-729.

Jones, P.A. (2012). Functions of DNA methylation: islands, start sites, gene bodies and beyond. Nat. Rev. Genet. *13*, 484-492.

Jones, P.A., Issa, J.-P.J., and Baylin, S. (2016). Targeting the cancer epigenome for therapy. Nat. Rev. Genet. *17*, 630-641.

Katan-Khaykovich, Y., and Struhl, K. (2002). Dynamics of global histone acetylation and deacetylation *in vivo*: rapid restoration of normal histone acetylation status upon removal of activators and repressors. Genes Dev. *16*, 743-752.

Kent, W.J., Sugnet, C.W., Furey, T.S., Roskin, K.M., Pringle, T.H., Zahler, A.M., and Haussler, D. (2002). The human genome browser at UCSC. Genome Res. *12*, 996-1006.

Kim, C., Gao, R., Sei, E., Brandt, R., Hartman, J., Hatschek, T., Crosetto, N., Foukakis, T., and Navin, N.E. (2018). Chemoresistance evolution in triple-negative breast cancer delineated by single-cell sequencing. Cell *173*, 879-893 e813.

Kim, M., and Costello, J. (2017). DNA methylation: an epigenetic mark of cellular memory. Exp. Mol. Med. *49*, e322-e322.

Kinsey, C.G., Camolotto, S.A., Boespflug, A.M., Guillen, K.P., Foth, M., Truong, A., Schuman, S.S., Shea, J.E., Seipp, M.T., Yap, J.T.*, et al.* (2019). Protective autophagy elicited by RAF-->MEK-->ERK inhibition suggests a treatment strategy for RAS-driven cancers. Nat. Med. *25*, 620-627.

Kleeff, J., Korc, M., Apte, M., La Vecchia, C., Johnson, C.D., Biankin, A.V., Neale, R.E., Tempero, M., Tuveson, D.A., Hruban, R.H.*, et al.* (2016). Pancreatic cancer. Nat. Rev. Dis. Primers *2*, 16022.

Klemm, S.L., Shipony, Z., and Greenleaf, W.J. (2019). Chromatin accessibility and the regulatory epigenome. Nat. Rev. Genet. *20*, 207-220.

Knudsen, E.S., Balaji, U., Mannakee, B., Vail, P., Eslinger, C., Moxom, C., Mansour, J., and Witkiewicz, A.K. (2017). Pancreatic cancer cell lines as patient-derived avatars: genetic characterisation and functional utility. Gut.

Koizumi, F., Shimoyama, T., Taguchi, F., Saijo, N., and Nishio, K. (2005). Establishment of a human non-small cell lung cancer cell line resistant to gefitinib. Int. J. Cancer *116*, 36-44.

Konieczkowski, D.J., Johannessen, C.M., and Garraway, L.A. (2018). A convergence-based framework for cancer drug resistance. Cancer Cell *33*, 801-815.

Köster, J., Dijkstra, L.J., Marschall, T., and Schönhuth, A. (2019). Enhancing sensitivity and controlling false discovery rate in somatic indel discovery. bioRxiv, https://doi.org/10.1101/741256.

Kottakis, F., Nicolay, B.N., Roumane, A., Karnik, R., Gu, H., Nagle, J.M., Boukhali, M., Hayward, M.C., Li, Y.Y., Chen, T.*, et al.* (2016). LKB1 loss links serine metabolism to DNA methylation and tumorigenesis. Nature *539*, 390-395.

Kouzarides, T. (2007). Chromatin modifications and their function. Cell *128*, 693-705.

Kroep, J.R., Loves, W.J.P., van der Wilt, C.L., Alvarez, E., Talianidis, I., Boven, E., Braakhuis, B.J.M., van Groeningen, C.J., Pinedo, H.M., and Peters, G.J. (2002). Pretreatment deoxycytidine kinase levels predict *in vivo* gemcitabine sensitivity. Mol. Cancer Ther. *1*, 371.

Kuczynski, E.A., Sargent, D.J., Grothey, A., and Kerbel, R.S. (2013). Drug rechallenge and treatment beyond progression—implications for drug resistance. Nat. Rev. Clin. Oncol. *10*, 571-587.

Kundaje, A., Meuleman, W., Ernst, J., Bilenky, M., Yen, A., Heravi-Moussavi, A., Kheradpour, P., Zhang, Z., Wang, J., Ziller, M.J.*, et al.* (2015). Integrative analysis of 111 reference human epigenomes. Nature *518*, 317-330.

Kurtova, A.V., Xiao, J., Mo, Q., Pazhanisamy, S., Krasnow, R., Lerner, S.P., Chen, F., Roh, T.T., Lay, E., Ho, P.L.*, et al.* (2015). Blocking PGE2-induced tumour repopulation abrogates bladder cancer chemoresistance. Nature *517*, 209-213.

Lee, D.Y., Hayes, J.J., Pruss, D., and Wolffe, A.P. (1993). A positive role for histone acetylation in transcription factor access to nucleosomal DNA. Cell *72*, 73-84.

Leitao, E., Beygo, J., Zeschnigk, M., Klein-Hitpass, L., Bargull, M., Rahmann, S., and Horsthemke, B. (2018). Locus-specific DNA methylation analysis by targeted deep bisulfite sequencing. Methods Mol. Biol. *1767*, 351-366.

Leitlinienprogramm Onkologie (Deutsche Krebsgesellschaft. Deutsche Krebshilfe. AWMF) (2013). S3-Leitlinie Exokrines Pankreaskarzinom, Langversion 1.0, 2013.

Li, E. (2002). Chromatin modification and epigenetic reprogramming in mammalian development. Nat. Rev. Genet. *3*, 662-673.

Li, E., and Zhang, Y. (2014). DNA methylation in mammals. Cold Spring Harb. Perspect. Biol. *6*, a019133-a019133.

Li, H. (2011). A statistical framework for SNP calling, mutation discovery, association mapping and population genetical parameter estimation from sequencing data. Bioinformatics *27*, 2987-2993.

Li, H. (2013). Aligning sequence reads, clone sequences and assembly contigs with BWA-MEM. arXiv, https://arxiv.org/abs/1303.3997.

Li, L.-C., and Dahiya, R. (2002). MethPrimer: designing primers for methylation PCRs. Bioinformatics *18*, 1427–1431.

Ligorio, M., Sil, S., Malagon-Lopez, J., Nieman, L.T., Misale, S., Di Pilato, M., Ebright, R.Y., Karabacak, M.N., Kulkarni, A.S., Liu, A.*, et al.* (2019). Stromal microenvironment shapes the intratumoral architecture of pancreatic cancer. Cell *178*, 160-175 e127.

Lim, S.M., Westover, K.D., Ficarro, S.B., Harrison, R.A., Choi, H.G., Pacold, M.E., Carrasco, M., Hunter, J., Kim, N.D., Xie, T.*, et al.* (2014). Therapeutic targeting of oncogenic K-Ras by a covalent catalytic site inhibitor. Angew. Chem. Int. Ed. *53*, 199-204.

Lin, L., Sabnis, A.J., Chan, E., Olivas, V., Cade, L., Pazarentzos, E., Asthana, S., Neel, D., Yan, J.J., Lu, X.*, et al.* (2015). The Hippo effector YAP promotes resistance to RAF- and MEK-targeted cancer therapies. Nat. Genet. *47*, 250-256.

Lito, P., Saborowski, A., Yue, J., Solomon, M., Joseph, E., Gadal, S., Saborowski, M., Kastenhuber, E., Fellmann, C., Ohara, K.*, et al.* (2014). Disruption of CRAF-mediated MEK activation is required for effective MEK inhibition in KRAS mutant tumors. Cancer Cell *25*, 697-710.

Little, A.S., Balmanno, K., Sale, M.J., Newman, S., Dry, J.R., Hampson, M., Edwards, P.A.W., Smith, P.D., and Cook, S.J. (2011). Amplification of the driving oncogene, KRAS or BRAF, underpins acquired resistance to MEK1/2 inhibitors in colorectal cancer cells. Sci. Signal. *4*, ra17.

Livak, K.J., and Schmittgen, T.D. (2001). Analysis of relative gene expression data using real-time quantitative PCR and the 2(-Delta Delta C(T)) Method. Methods *25*, 402-408.

Loewe, S. (1953). The problem of synergism and antagonism of combined drugs. Arzneimittelforschung *3*, 285-290.

Lomberk, G., Blum, Y., Nicolle, R., Nair, A., Gaonkar, K.S., Marisa, L., Mathison, A., Sun, Z., Yan, H., Elarouci, N.*, et al.* (2018). Distinct epigenetic landscapes underlie the pathobiology of pancreatic cancer subtypes. Nat. Commun. *9*, 1978.

Lomberk, G., Dusetti, N., Iovanna, J., and Urrutia, R. (2019). Emerging epigenomic landscapes of pancreatic cancer in the era of precision medicine. Nat. Commun. *10*, 3875.

Long, J., Zhang, Y., Yu, X., Yang, J., LeBrun, D.G., Chen, C., Yao, Q., and Li, M. (2011). Overcoming drug resistance in pancreatic cancer. Expert Opin. Ther. Targets *15*, 817-828.

Lopez-Bergami, P., Huang, C., Goydos, J.S., Yip, D., Bar-Eli, M., Herlyn, M., Smalley, K.S.M., Mahale, A., Eroshkin, A., Aaronson, S.*, et al.* (2007). Rewired ERK-JNK signaling pathways in melanoma. Cancer Cell *11*, 447-460.

Lopez-Bergami, P., Lau, E., and Ronai, Z.e. (2010). Emerging roles of ATF2 and the dynamic AP1 network in cancer. Nat. Rev. Cancer *10*, 65-76.

Love, M.I., Huber, W., and Anders, S. (2014). Moderated estimation of fold change and dispersion for RNA-seq data with DESeq2. Genome Biol. *15*, 550.

Luger, K., Mäder, A.W., Richmond, R.K., Sargent, D.F., and Richmond, T.J. (1997). Crystal structure of the nucleosome core particle at 2.8 Å resolution. Nature *389*, 251-260.

Lynch, T.J., Bell, D.W., Sordella, R., Gurubhagavatula, S., Okimoto, R.A., Brannigan, B.W., Harris, P.L., Haserlat, S.M., Supko, J.G., Haluska, F.G.*, et al.* (2004). Activating mutations in the epidermal growth factor receptor underlying responsiveness of non-small-cell lung cancer to gefitinib. N. Engl. J. Med. *350*, 2129-2139.

Macdonald, J.S., McCoy, S., Whitehead, R.P., Iqbal, S., Wade, J.L., Giguere, J.K., and Abbruzzese, J.L. (2005). A phase II study of farnesyl transferase inhibitor R115777 in pancreatic cancer: A Southwest oncology group (SWOG 9924) study. Invest. New Drugs *23*, 485-487.

Mackey, J.R., Mani, R.S., Selner, M., Mowles, D., Young, J.D., Belt, J.A., Crawford, C.R., and Cass, C.E. (1998). Functional nucleoside transporters are required for gemcitabine influx and manifestation of toxicity in cancer cell lines. Cancer Res. *58*, 4349.

Maleszewska, M., and Kaminska, B. (2013). Is Glioblastoma an Epigenetic Malignancy? Cancers *5*, 1120-1139.

Mariani, O., Brennetot, C., Coindre, J.M., Gruel, N., Ganem, C., Delattre, O., Stern, M.H., and Aurias, A. (2007). JUN oncogene amplification and overexpression block adipocytic differentiation in highly aggressive sarcomas. Cancer Cell *11*, 361-374.

Maunakea, A.K., Chepelev, I., Cui, K., and Zhao, K. (2013). Intragenic DNA methylation modulates alternative splicing by recruiting MeCP2 to promote exon recognition. Cell Res. *23*, 1256-1269.

Mazur, P.K., Herner, A., Mello, S.S., Wirth, M., Hausmann, S., Sanchez-Rivera, F.J., Lofgren, S.M., Kuschma, T., Hahn, S.A., Vangala, D.*, et al.* (2015a). Combined inhibition of BET family proteins and histone deacetylases as a potential epigenetics-based therapy for pancreatic ductal adenocarcinoma. Nat. Med. *21*, 1163-1171.

Mazur, P.K., Herner, A., Neff, F., and Siveke, J.T. (2015b). Current methods in mouse models of pancreatic cancer. Methods Mol. Biol. *1267*, 185-215.

McDonald, O.G., Li, X., Saunders, T., Tryggvadottir, R., Mentch, S.J., Warmoes, M.O., Word, A.E., Carrer, A., Salz, T.H., Natsume, S.*, et al.* (2017). Epigenomic reprogramming during pancreatic cancer progression links anabolic glucose metabolism to distant metastasis. Nat. Genet. *49*, 367-376.

Mikkelsen, T.S., Ku, M., Jaffe, D.B., Issac, B., Lieberman, E., Giannoukos, G., Alvarez, P., Brockman, W., Kim, T.-K., Koche, R.P.*, et al.* (2007). Genome-wide maps of chromatin state in pluripotent and lineage-committed cells. Nature *448*, 553-560.

Moffitt, R.A., Marayati, R., Flate, E.L., Volmar, K.E., Loeza, S.G., Hoadley, K.A., Rashid, N.U., Williams, L.A., Eaton, S.C., Chung, A.H.*, et al.* (2015). Virtual microdissection identifies distinct tumor- and stroma-specific subtypes of pancreatic ductal adenocarcinoma. Nat. Genet. *47*, 1168-1178.

Moore, M.J., Goldstein, D., Hamm, J., Figer, A., Hecht, J.R., Gallinger, S., Au, H.J., Murawa, P., Walde, D., Wolff, R.A.*, et al.* (2007). Erlotinib plus gemcitabine compared with gemcitabine alone in patients with advanced pancreatic cancer: a phase III trial of the national cancer institute of canada clinical trials group. J. Clin. Oncol. *25*, 1960-1966.

Müerköster, S., Wegehenkel, K., Arlt, A., Witt, M., Sipos, B., Kruse, M.-L., Sebens, T., Klöppel, G., Kalthoff, H., Fölsch, U.R.*, et al.* (2004). Tumor stroma interactions induce chemoresistance in pancreatic ductal carcinoma cells involving increased secretion and paracrine effects of nitric oxide and interleukin-1β. Cancer Res. *64*, 1331-1337.

Nakano, Y., Tanno, S., Koizumi, K., Nishikawa, T., Nakamura, K., Minoguchi, M., Izawa, T., Mizukami, Y., Okumura, T., and Kohgo, Y. (2007). Gemcitabine chemoresistance and molecular markers associated with gemcitabine transport and metabolism in human pancreatic cancer cells. Br. J. Cancer *96*, 457-463.

Nardi, V., Azam, M., and Daley, G.Q. (2004). Mechanisms and implications of imatinib resistance mutations in BCR-ABL. Curr. Opin. Hematol. *11*.

Neesse, A., Algul, H., Tuveson, D.A., and Gress, T.M. (2015). Stromal biology and therapy in pancreatic cancer: a changing paradigm. Gut *64*, 1476-1484.

Neoptolemos, J.P., Kleeff, J., Michl, P., Costello, E., Greenhalf, W., and Palmer, D.H. (2018). Therapeutic developments in pancreatic cancer: current and future perspectives. Nat. Rev. Gastroenterol. Hepat. *15*, 333-348.

Ng, P.C., and Henikoff, S. (2003). SIFT: predicting amino acid changes that affect protein function. Nucleic Acids Res. *31*, 3812-3814.

Nicolle, R., Blum, Y., Marisa, L., Loncle, C., Gayet, O., Moutardier, V., Turrini, O., Giovannini, M., Bian, B., Bigonnet, M.*, et al.* (2017). Pancreatic adenocarcinoma therapeutic targets revealed by tumor-stroma cross-talk analyses in patient-derived xenografts. Cell Rep. *21*, 2458-2470.

Nishiyama, A., Yamaguchi, L., Sharif, J., Johmura, Y., Kawamura, T., Nakanishi, K., Shimamura, S., Arita, K., Kodama, T., Ishikawa, F.*, et al.* (2013). Uhrf1-dependent H3K23 ubiquitylation couples maintenance DNA methylation and replication. Nature *502*, 249-253.

Noguchi, G.M., and Huising, M.O. (2019). Integrating the inputs that shape pancreatic islet hormone release. Nat. Metab. *1*, 1189-1201.

Nones, K., Waddell, N., Song, S., Patch, A.M., Miller, D., Johns, A., Wu, J., Kassahn, K.S., Wood, D., Bailey, P.*, et al.* (2014). Genome-wide DNA methylation patterns in pancreatic ductal adenocarcinoma reveal epigenetic deregulation of SLIT-ROBO, ITGA2 and MET signaling. Int. J. Cancer *135*, 1110-1118.

Ohren, J.F., Chen, H., Pavlovsky, A., Whitehead, C., Zhang, E., Kuffa, P., Yan, C., McConnell, P., Spessard, C., Banotai, C.*, et al.* (2004). Structures of human MAP kinase kinase 1 (MEK1) and MEK2 describe novel noncompetitive kinase inhibition. Nat. Struct. Mol. Biol. *11*, 1192-1197.

Ostrem, J.M., Peters, U., Sos, M.L., Wells, J.A., and Shokat, K.M. (2013). K-Ras(G12C) inhibitors allosterically control GTP affinity and effector interactions. Nature *503*, 548-551.

Ottaiano, A., Capozzi, M., De Divitiis, C., De Stefano, A., Botti, G., Avallone, A., and Tafuto, S. (2017). Gemcitabine mono-therapy versus gemcitabine plus targeted therapy in advanced pancreatic cancer: a meta-analysis of randomized phase III trials. Acta Oncol. *56*, 377-383.

Patch, A.-M., Christie, E.L., Etemadmoghadam, D., Garsed, D.W., George, J., Fereday, S., Nones, K., Cowin, P., Alsop, K., Bailey, P.J.*, et al.* (2015). Whole–genome characterization of chemoresistant ovarian cancer. Nature *521*, 489-494.

Patro, R., Duggal, G., Love, M.I., Irizarry, R.A., and Kingsford, C. (2017). Salmon provides fast and bias-aware quantification of transcript expression. Nat. Methods *14*, 417-419.

Pedersen, B.S., Eyring, K., De, S., Yang, I.V., and Schwartz, D.A. (2014). Fast and accurate alignment of long bisulfite-seq reads. arXiv, https://arxiv.org/abs/1401.1129.

Peng, J.F., Zhuang, Y.Y., Huang, F.T., and Zhang, S.N. (2016). Noncoding RNAs and pancreatic cancer. World J. Gastroenterol. *22*, 801-814.

Plass, C., Pfister, S.M., Lindroth, A.M., Bogatyrova, O., Claus, R., and Lichter, P. (2013). Mutations in regulators of the epigenome and their connections to global chromatin patterns in cancer. Nat. Rev. Genet. *14*, 765-780.

Provenzano, P.P., Cuevas, C., Chang, A.E., Goel, V.K., Von Hoff, D.D., and Hingorani, S.R. (2012). Enzymatic targeting of the stroma ablates physical barriers to treatment of pancreatic ductal adenocarcinoma. Cancer Cell *21*, 418-429.

Quinlan, A.R., and Hall, I.M. (2010). BEDTools: a flexible suite of utilities for comparing genomic features. Bioinformatics *26*, 841-842.

Rahib, L., Smith, B.D., Aizenberg, R., Rosenzweig, A.B., Fleshman, J.M., and Matrisian, L.M. (2014). Projecting cancer incidence and deaths to 2030: the unexpected burden of thyroid, liver, and pancreas cancers in the United States. Cancer Res. *74*, 2913-2921.

Raimondi, S., Maisonneuve, P., and Lowenfels, A.B. (2009). Epidemiology of pancreatic cancer: an overview. Nat. Rev. Gastroenterol. Hepat. *6*, 699-708.

Ramsdale, R., Jorissen, R.N., Li, F.Z., Al-Obaidi, S., Ward, T., Sheppard, K.E., Bukczynska, P.E., Young, R.J., Boyle, S.E., Shackleton, M.*, et al.* (2015). The transcription cofactor c-JUN mediates phenotype switching and BRAF inhibitor resistance in melanoma. Sci. Signal. *8*.

Rea, S., Eisenhaber, F., O'Carroll, D., Strahl, B.D., Sun, Z.-W., Schmid, M., Opravil, S., Mechtler, K., Ponting, C.P., Allis, C.D.*, et al.* (2000). Regulation of chromatin structure by site-specific histone H3 methyltransferases. Nature *406*, 593-599.

Rhim, A.D., Oberstein, P.E., Thomas, D.H., Mirek, E.T., Palermo, C.F., Sastra, S.A., Dekleva, E.N., Saunders, T., Becerra, C.P., Tattersall, I.W.*, et al.* (2014). Stromal elements act to restrain, rather than support, pancreatic ductal adenocarcinoma. Cancer Cell *25*, 735-747.

Riva, G., Pea, A., Pilati, C., Fiadone, G., Lawlor, R.T., Scarpa, A., and Luchini, C. (2018). Histo-molecular oncogenesis of pancreatic cancer: From precancerous lesions to invasive ductal adenocarcinoma. World J. Gastrointest. Oncol. *10*, 317-327.

Roadmap Epigenomics Consortium (2015). Integrative analysis of 111 reference human epigenomes. Nature *518*, 317-330.

Robasky, K., Lewis, N.E., and Church, G.M. (2014). The role of replicates for error mitigation in next-generation sequencing. Nat. Rev. Genet. *15*, 56-62.

Roe, J.S., Hwang, C.I., Somerville, T.D.D., Milazzo, J.P., Lee, E.J., Da Silva, B., Maiorino, L., Tiriac, H., Young, C.M., Miyabayashi, K.*, et al.* (2017). Enhancer reprogramming promotes pancreatic cancer metastasis. Cell *170*, 875-888 e820.

Rubio-Viqueira, B., Jimeno, A., Cusatis, G., Zhang, X., Iacobuzio-Donahue, C., Karikari, C., Shi, C., Danenberg, K., Danenberg, P.V., Kuramochi, H.*, et al.* (2006). An *in vivo* platform for translational drug development in pancreatic cancer. Clin. Cancer Res. *12*, 4652.

Ruess, D.A., Heynen, G.J., Ciecielski, K.J., Ai, J., Berninger, A., Kabacaoglu, D., Görgülü, K., Dantes, Z., Wörmann, S.M., Diakopoulos, K.N.*, et al.* (2018). Mutant KRAS-driven cancers depend on PTPN11/SHP2 phosphatase. Nat. Med. *24*, 954-960.

Sato, N., Fukushima, N., Hruban, R.H., and Goggins, M. (2008). CpG island methylation profile of pancreatic intraepithelial neoplasia. Mod. Pathol. *21*, 238-244.

Sato, N., and Goggins, M. (2006). The role of epigenetic alterations in pancreatic cancer. J. Hepatobiliary Pancreat. Surg. *13*, 286-295.

Sato, N., Ueki, T., Fukushima, N., Iacobuzio–Donahue, C.A., Hruban, R.H., Goggins, M., Yeo, C.J., and Cameron, J.L. (2002). Aberrant methylation of CpG islands in intraductal papillary mucinous neoplasms of the pancreas. Gastroenterology *123*, 365-372.

Saxonov, S., Berg, P., and Brutlag, D.L. (2006). A genome-wide analysis of CpG dinucleotides in the human genome distinguishes two distinct classes of promoters. Proc. Natl. Acad. Sci. USA *103*, 1412.

Schubeler, D. (2015). Function and information content of DNA methylation. Nature *517*, 321-326.

Schutte, M., Hruban, R.H., Geradts, J., Maynard, R., Hilgers, W., Rabindran, S.K., Moskaluk, C.A., Hahn, S.A., Schwarte-Waldhoff, I., Schmiegel, W.*, et al.* (1997). Abrogation of the Rb/p16 tumor-suppressive pathway in virtually all pancreatic carcinomas. Cancer Res. *57*, 3126.

Sethi, T., Rintoul, R.C., Moore, S.M., MacKinnon, A.C., Salter, D., Choo, C., Chilvers, E.R., Dransfield, I., Donnelly, S.C., Strieter, R.*, et al.* (1999). Extracellular matrix proteins protect small cell lung cancer cells against apoptosis: a mechanism for small cell lung cancer growth and drug resistance *in vivo*. Nat. Med. *5*, 662-668.

Shaffer, S.M., Dunagin, M.C., Torborg, S.R., Torre, E.A., Emert, B., Krepler, C., Beqiri, M., Sproesser, K., Brafford, P.A., Xiao, M.*, et al.* (2017). Rare cell variability and drug-induced reprogramming as a mode of cancer drug resistance. Nature *546*, 431-435.

Shakya, R., Gonda, T., Quante, M., Salas, M., Kim, S., Brooks, J., Hirsch, S., Davies, J., Cullo, A., Olive, K.*, et al.* (2013). Hypomethylating therapy in an aggressive stroma-rich model of pancreatic carcinoma. Cancer Res. *73*, 885-896.

Sharma, S., Kelly, T.K., and Jones, P.A. (2010a). Epigenetics in cancer. Carcinogenesis *31*, 27-36.

Sharma, S.V., Lee, D.Y., Li, B., Quinlan, M.P., Takahashi, F., Maheswaran, S., McDermott, U., Azizian, N., Zou, L., Fischbach, M.A*., et al.* (2010b). A chromatin-mediated reversible drug-tolerant state in cancer cell subpopulations. Cell *141*, 69-80.

Shaul, Y.D., and Seger, R. (2007). The MEK/ERK cascade: from signaling specificity to diverse functions. Biochim. Biophys. Acta *1773*, 1213-1226.

Shen, H., and Laird, P.W. (2013). Interplay between the cancer genome and epigenome. Cell *153*, 38-55.

Shi, Y., Lan, F., Matson, C., Mulligan, P., Whetstine, J.R., Cole, P.A., Casero, R.A., and Shi, Y. (2004). Histone demethylation mediated by the nuclear amine oxidase homolog LSD1. Cell *119*, 941-953.

Shibue, T., and Weinberg, R.A. (2017). EMT, CSCs, and drug resistance: the mechanistic link and clinical implications. Nat. Rev. Clin. Oncol. *14*, 611-629.

Shih, H.P., Wang, A., and Sander, M. (2013). Pancreas organogenesis: from lineage determination to morphogenesis. Annu. Rev. Cell. Dev. Biol. *29*, 81-105.

Singh, A., Greninger, P., Rhodes, D., Koopman, L., Violette, S., Bardeesy, N., and Settleman, J. (2009). A gene expression signature associated with "K-Ras addiction" reveals regulators of EMT and tumor cell survival. Cancer Cell *15*, 489-500.

Skrypek, N., Goossens, S., De Smedt, E., Vandamme, N., and Berx, G. (2017). Epithelial-to-mesenchymal transition: epigenetic reprogramming driving cellular plasticity. Trends Genet. *33*, 943-959.

Soneson, C., Love, M.I., and Robinson, M.D. (2015). Differential analyses for RNA-seq: transcript-level estimates improve gene-level inferences. F1000Res. *4*, 1521.

Spandidos, A., Wang, X., Wang, H., and Seed, B. (2010). PrimerBank: a resource of human and mouse PCR primer pairs for gene expression detection and quantification. Nucleic Acids Res. *38*, D792-799.

Straussman, R., Morikawa, T., Shee, K., Barzily-Rokni, M., Qian, Z.R., Du, J., Davis, A., Mongare, M.M., Gould, J., Frederick, D.T*., et al.* (2012). Tumour micro-environment elicits innate resistance to RAF inhibitors through HGF secretion. Nature *487*, 500-504.

Subramanian, A., Tamayo, P., Mootha, V.K., Mukherjee, S., Ebert, B.L., Gillette, M.A., Paulovich, A., Pomeroy, S.L., Golub, T.R., Lander, E.S*., et al.* (2005). Gene set enrichment analysis: a knowledge-based approach for interpreting genome-wide expression profiles. Proc. Natl. Acad. Sci. USA *102*, 15545-15550.

Sun, Y., Campisi, J., Higano, C., Beer, T.M., Porter, P., Coleman, I., True, L., and Nelson, P.S. (2012). Treatment-induced damage to the tumor microenvironment promotes prostate cancer therapy resistance through WNT16B. Nat. Med. *18*, 1359-1368.

Sur, I., and Taipale, J. (2016). The role of enhancers in cancer. Nat. Rev. Cancer *16*, 483-493.

Swayden, M., Iovanna, J., and Soubeyran, P. (2018). Pancreatic cancer chemo-resistance is driven by tumor phenotype rather than tumor genotype. Heliyon *4*, e01055.

Tan, M., Luo, H., Lee, S., Jin, F., Yang, J.S., Montellier, E., Buchou, T., Cheng, Z., Rousseaux, S., Rajagopal, N.*, et al.* (2011). Identification of 67 histone marks and histone lysine crotonylation as a new type of histone modification. Cell *146*, 1016-1028.

Tarasov, A., Vilella, A.J., Cuppen, E., Nijman, I.J., and Prins, P. (2015). Sambamba: fast processing of NGS alignment formats. Bioinformatics *31*, 2032-2034.

Tse, C., Sera, T., Wolffe, A.P., and Hansen, J.C. (1998). Disruption of higher-order folding by core histone acetylation dramatically enhances transcription of nucleosomal arrays by RNA polymerase III. Mol. Cell. Biol. *18*, 4629.

Tulchinsky, E.M., Georgiev, G.P., and Lukanidin, E.M. (1996). Novel AP-1 binding site created by DNA-methylation. Oncogene *12*, 1737-1745.

U.S. Food and Drug Administration Center for Drug Evaluation and Research (2013). NDA 204114 MEKINIST® (trametinib) label (Reference ID: 3315791).

Van Cutsem, E., Hidalgo, M., Canon, J.L., Macarulla, T., Bazin, I., Poddubskaya, E., Manojlovic, N., Radenkovic, D., Verslype, C., Raymond, E.*, et al.* (2018). Phase I/II trial of pimasertib plus gemcitabine in patients with metastatic pancreatic cancer. Int. J. Cancer *143*, 2053-2064.

Van Laethem, J.L., Riess, H., Jassem, J., Haas, M., Martens, U.M., Weekes, C., Peeters, M., Ross, P., Bridgewater, J., Melichar, B.*, et al.* (2017). Phase I/II study of refametinib (BAY 86-9766) in combination with gemcitabine in advanced pancreatic cancer. Target. Oncol. *12*, 97-109.

Vasan, N., Baselga, J., and Hyman, D.M. (2019). A view on drug resistance in cancer. Nature *575*, 299-309.

Vena, F., Li Causi, E., Rodriguez-Justo, M., Goodstal, S., Hagemann, T., Hartley, J.A., and Hochhauser, D. (2015). The MEK1/2 inhibitor pimasertib enhances gemcitabine efficacy in pancreatic cancer models by altering ribonucleotide reductase subunit-1 (RRM1). Clin. Cancer Res. *21*, 5563-5577.

Viale, A., Pettazzoni, P., Lyssiotis, C.A., Ying, H., Sánchez, N., Marchesini, M., Carugo, A., Green, T., Seth, S., Giuliani, V.*, et al.* (2014). Oncogene ablation-resistant pancreatic cancer cells depend on mitochondrial function. Nature *514*, 628-632.

Villanueva, J., Infante, J.R., Krepler, C., Reyes-Uribe, P., Samanta, M., Chen, H.Y., Li, B., Swoboda, R.K., Wilson, M., Vultur, A.*, et al.* (2013). Concurrent MEK2 mutation and BRAF amplification confer resistance to BRAF and MEK inhibitors in melanoma. Cell Rep. *4*, 1090-1099.

Vincent, A., Herman, J., Schulick, R., Hruban, R.H., and Goggins, M. (2011). Pancreatic cancer. Lancet *378*, 607-620.

Waddell, N., Pajic, M., Patch, A.M., Chang, D.K., Kassahn, K.S., Bailey, P., Johns, A.L., Miller, D., Nones, K., Quek, K.*, et al.* (2015). Whole genomes redefine the mutational landscape of pancreatic cancer. Nature *518*, 495-501.

Waddington, C. (1942). The Epigenotype. Endeavour, 18-20.

Waddington, C. (1968). Towards a theoretical biology: prolegomena. International Union of Biological Sciences & Edinburgh University Press *1*, 1-32.

Wallner, S., Schroder, C., Leitao, E., Berulava, T., Haak, C., Beisser, D., Rahmann, S., Richter, A.S., Manke, T., Bonisch, U.*, et al.* (2016). Epigenetic dynamics of monocyte-to-macrophage differentiation. Epigenetics Chromatin *9*, 33.

Walters, D.M., Lindberg, J.M., Adair, S.J., Newhook, T.E., Cowan, C.R., Stokes, J.B., Borgman, C.A., Stelow, E.B., Lowrey, B.T., Chopivsky, M.E.*, et al.* (2013). Inhibition of the growth of patient-derived pancreatic cancer xenografts with the MEK inhibitor trametinib is augmented by combined treatment with the epidermal growth factor receptor/HER2 inhibitor lapatinib. Neoplasia *15*, 143-155.

Wang, H., Daouti, S., Li, W.-h., Wen, Y., Rizzo, C., Higgins, B., Packman, K., Rosen, N., Boylan, J.F., Heimbrook, D.*, et al.* (2011a). Identification of the MEK1(F129L) activating mutation as a potential mechanism of acquired resistance to MEK inhibition in human cancers carrying the B-RafV600E mutation. Cancer Res. *71*, 5535.

Wang, Z., Li, Y., Ahmad, A., Banerjee, S., Azmi, A.S., Kong, D., and Sarkar, F.H. (2011b). Pancreatic cancer: understanding and overcoming chemoresistance. Nat. Rev. Gastroenterol. Hepat. *8*, 27-33.

Waters, A.M., and Der, C.J. (2018). KRAS: the critical driver and therapeutic target for pancreatic cancer. Cold Spring Harb. Perspect. Med. *8*.

Wei, Y., Yu, L., Bowen, J., Gorovsky, M.A., and Allis, C.D. (1999). Phosphorylation of histone H3 is required for proper chromosome condensation and segregation. Cell *97*, 99-109.

Witkiewicz, A.K., McMillan, E.A., Balaji, U., Baek, G., Lin, W.-C., Mansour, J., Mollaee, M., Wagner, K.-U., Koduru, P., Yopp, A.*, et al.* (2015). Whole-exome sequencing of

pancreatic cancer defines genetic diversity and therapeutic targets. Nat. Commun. *6*, 6744-6744.

Xuan Lin, Q.X., Sian, S., An, O., Thieffry, D., Jha, S., and Benoukraf, T. (2019). MethMotif: an integrative cell specific database of transcription factor binding motifs coupled with DNA methylation profiles. Nucleic Acids Res. *47*, D145-D154.

Yachida, S., Jones, S., Bozic, I., Antal, T., Leary, R., Fu, B., Kamiyama, M., Hruban, R.H., Eshleman, J.R., Nowak, M.A.*, et al.* (2010). Distant metastasis occurs late during the genetic evolution of pancreatic cancer. Nature *467*, 1114-1117.

Yang, S., Zhou, Q., and Yang, X. (2007). Caspase-3 status is a determinant of the differential responses to genistein between MDA-MB-231 and MCF-7 breast cancer cells. Biochim. Biophys. Acta *1773*, 903-911.

Ye, J., Coulouris, G., Zaretskaya, I.C., Rozen, S., and Madden, T.L. (2012). Primer-BLAST: a tool to design target-specific primers for polymerase chain reaction. Bioinformatics *13*.

Yi, J.M., Guzzetta, A.A., Bailey, V.J., Downing, S.R., Van Neste, L., Chiappinelli, K.B., Keeley, B.P., Stark, A., Herrera, A., Wolfgang, C.*, et al.* (2013). Novel methylation biomarker panel for the early detection of pancreatic cancer. Clin. Cancer Res. *19*, 6544-6555.

Yin, Y., Morgunova, E., Jolma, A., Kaasinen, E., Sahu, B., Khund-Sayeed, S., Das, P.K., Kivioja, T., Dave, K., Zhong, F.*, et al.* (2017). Impact of cytosine methylation on DNA binding specificities of human transcription factors. Science *356*.

Ying, H., Dey, P., Yao, W., Kimmelman, A.C., Draetta, G.F., Maitra, A., and DePinho, R.A. (2016). Genetics and biology of pancreatic ductal adenocarcinoma. Genes Dev. *30*, 355-385.

Yue, F., Cheng, Y., Breschi, A., Vierstra, J., Wu, W., Ryba, T., Sandstrom, R., Ma, Z., Davis, C., Pope, B.D.*, et al.* (2014). A comparative encyclopedia of DNA elements in the mouse genome. Nature *515*, 355-364.

Zawistowski, J.S., Bevill, S.M., Goulet, D.R., Stuhlmiller, T.J., Beltran, A.S., Olivares-Quintero, J.F., Singh, D., Sciaky, N., Parker, J.S., Rashid, N.U.*, et al.* (2017). Enhancer Remodeling during Adaptive Bypass to MEK Inhibition Is Attenuated by Pharmacologic Targeting of the P-TEFb Complex. Cancer Discov. *7*, 302-321.

Zee, B.M., Levin, R.S., Xu, B., LeRoy, G., Wingreen, N.S., and Garcia, B.A. (2010). *In vivo* residue-specific histone methylation dynamics. J. Biol. Chem. *285*, 3341-3350.

Zerbino, D.R., Achuthan, P., Akanni, W., Amode, M.R., Barrell, D., Bhai, J., Billis, K., Cummins, C., Gall, A., Giron, C.G.*, et al.* (2018). Ensembl 2018. Nucleic Acids Res. *46*, D754-D761.

Zhang, Y., Liu, T., Meyer, C.A., Eeckhoute, J., Johnson, D.S., Bernstein, B.E., Nusbaum, C., Myers, R.M., Brown, M., Li, W.*, et al.* (2008). Model-based analysis of ChIP-Seq (MACS). Genome Biol. *9*, R137.

Zhao, Z., and Shilatifard, A. (2019). Epigenetic modifications of histones in cancer. Genome Biol. *20*, 245.

Zheng, X., Carstens, J.L., Kim, J., Scheible, M., Kaye, J., Sugimoto, H., Wu, C.-C., LeBleu, V.S., and Kalluri, R. (2015). Epithelial-to-mesenchymal transition is dispensable for metastasis but induces chemoresistance in pancreatic cancer. Nature *527*, 525-530.

Zhou, M., Liu, X., Li, Z., Huang, Q., Li, F., and Li, C.Y. (2018). Caspase-3 regulates the migration, invasion and metastasis of colon cancer cells. Int. J. Cancer *143*, 921-930.

APPENDIX

List of figures

List of tables

Supplementary figures

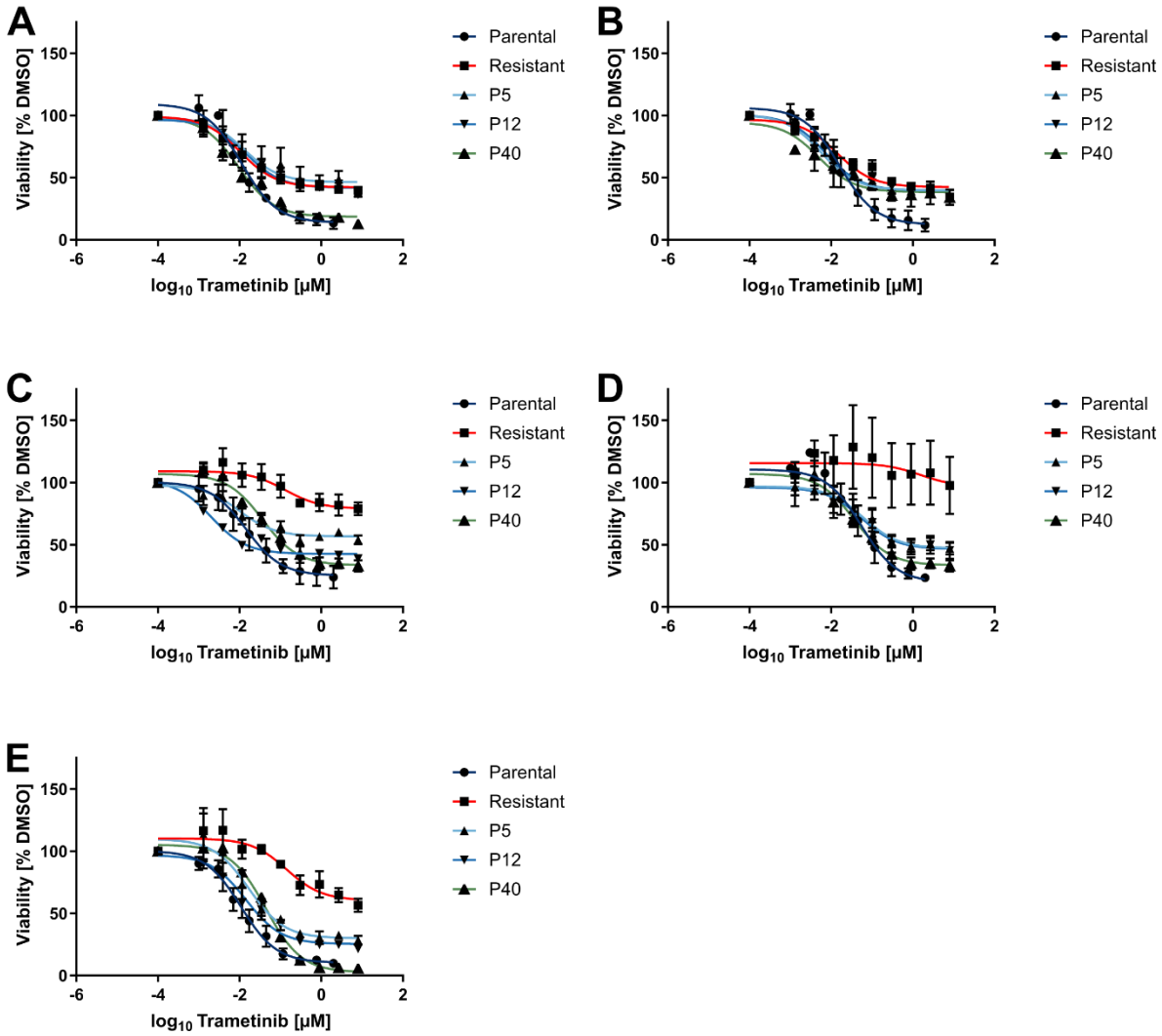

Supplementary Figure 1: Related to Figure 3-3

Reversibility of MEKi resistance after drug withdrawal in cell lines #4 **(A)**, #6 **(B)**, #7 **(C)**, #9 **(D)**, #10 **(E)**.The mean of three independent dose response curves after 72 h incubation ± SD is displayed.

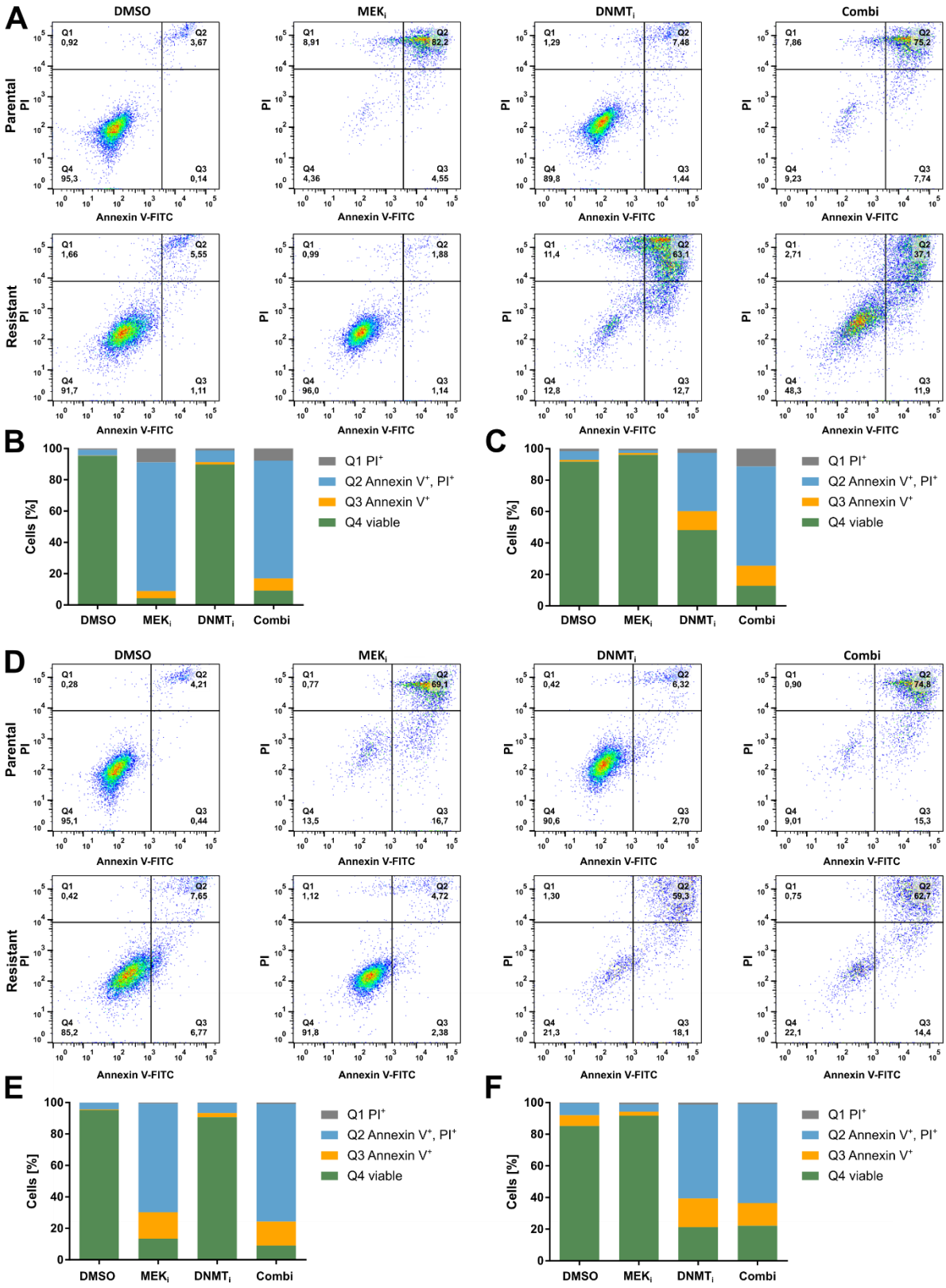

Supplementary Figure 2: Related to Figure 3-32

Annexin V-FITC/PI co-staining of parental and resistant cells of lines #3 **(A)** and #4 **(D)** after 84 h of the indicated treatment measured by FACS. Quantification of FACS results shown in (A) separated for parental **(B)** or resistant cells **(C)**. Quantification of FACS results shown in (D) separated for parental **(E)** or resistant cells **(F)**.

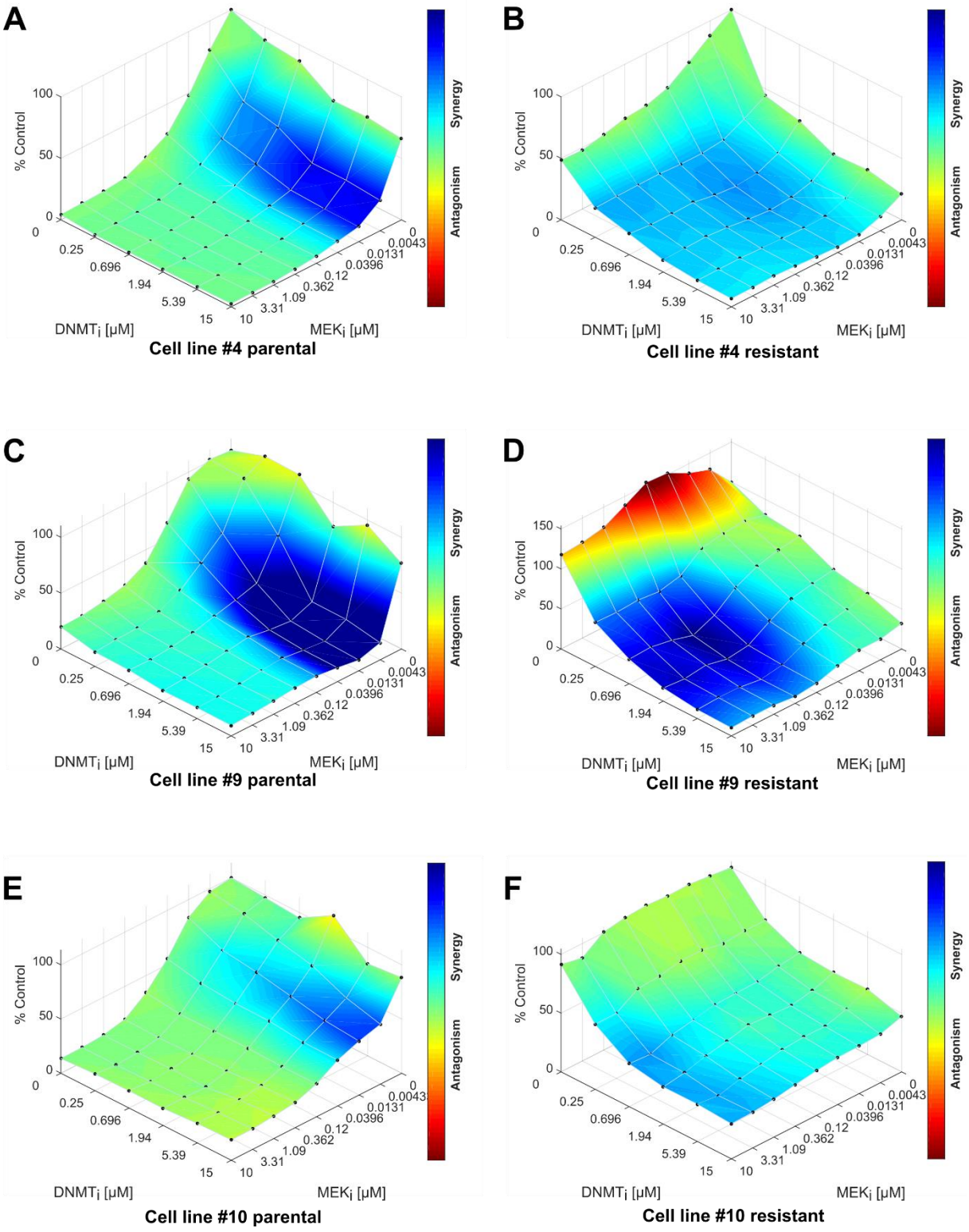

Supplementary Figure 3: Related to Figure 3-33

Synergism of MEK_i and $DNMT_i$ quantified by the Loewe method of the Combenefit software in cell lines #4 parental **(A)** and resistant **(B)**, #9 parental **(C)** and resistant **(D)** and #10 parental **(E)** and resistant **(F)**.

Supplementary tables

Supplementary Table 1: Variants exclusively detected in the resistant cells (VpRs) of cell line #3 that were predicted as deleterious by SIFT
(Ref, reference allele; Alt, alternative allele).

Chromosome	*Position [mm10]*	*Ref*	*Alt*	*Gene*	*Depth Parental*	*Alt_Frequency Parental*	*Depth Resistant*	*Alt_Frequency Resistant*	*Predicted_variant_influence Jannovar*
1	40471814	A	C	Il18r1	48	0	49	0.353469	MODERATE
10	127902156	G	A	Sdr9c7	45	0	43	0.256871	MODERATE
15	103242077	A	G	Hnrnpa1	41	0	65	0.215851	MODERATE
17	28217008	A	C	Def6	32	0	54	0.308642	MODERATE
17	37280261	T	C	Olfr99	50	0	50	0.442	MODERATE
3	55992459	G	A	Nbea	41	0	49	0.353469	MODERATE
3	158054805	T	A	Lrrc40	54	0	42	0.307823	MODERATE
4	45923498	A	C	Ccdc180	38	0	46	0.360586	MODERATE
4	156249094	T	G	Samd11	34	0	38	0.293629	MODERATE
6	55388291	C	G	Ghrhr	77	0	75	0.271228	MODERATE
7	86363944	T	A	Olfr305	29	0	20	0.235	MODERATE
8	93499492	A	C	Ces5a	41	0	43	0.276956	MODERATE
X	141629994	G	A	Col4a5	20	0	10	0.19	MODERATE
X	155586485	C	A	Ptchd1	20	0	10	0.19	MODERATE

Supplementary Table 2: Variants exclusively detected in the resistant cells (VpRs) of cell line #9 that were predicted as deleterious by SIFT

(Ref, reference allele; Alt, alternative allele).

Chromosome	*Position [mm10]*	*Ref*	*Alt*	*Gene*	*Depth Parental*	*Alt_Frequency Parental*	*Depth Resistant*	*Alt_Frequency Resistant*	*Predicted_variant_influence Jannovar*
1	17147094	G	T	Gdap1	59	0	31	0.237903	MODERATE
10	67035963	C	G	Reep3	43	0	43	0.317125	MODERATE
10	86850565	A	T	Stab2	31	0	47	0.236702	MODERATE
13	100160989	C	G	Naip2	37	0	38	0.246537	MODERATE
14	47290670	T	G	Socs4	38	0	42	0.244898	MODERATE
17	28297150	T	G	Ppard	46	0	39	0.282051	MODERATE
2	85429911	T	G	Olfr994	71	0	33	0.302139	MODERATE
4	138228705	A	G	Hp1bp3	26	0	26	0.319527	MODERATE
7	28085330	C	T	Fcgbp	23	0	29	0.252874	MODERATE
7	103358657	G	A	Olfr601	26	0	25	0.593846	MODERATE
9	56865200	G	T	Cspg4	44	0	27	0.333333	MODERATE

Supplementary Table 3: Variants exclusively detected in the parental cells (VpPs) of cell line #9 that were predicted as deleterious by SIFT

(Ref, reference allele; Alt, alternative allele).

Chromosome	*Position [mm10]*	*Ref*	*Alt*	*Gene*	*Depth Parental*	*Alt_Frequency Parental*	*Depth Resistant*	*Alt_Frequency Resistant*	*Predicted_variant_influence Jannovar*
13	22620221	A	G	Vmn1r206	48	0.216146	43	0	MODERATE
5	96714410	C	T	Fras1	36	0.358025	29	0	MODERATE

Supplementary Table 4: Top 25 hypermethylated reverting DMRs based on their reversion score and selected annotations

DMR	*DMR position [mm10 coordinates]*	*CpGs*	*CpG region*	*Genomic region*	*Distance Gene_A [bp]*	*Gene symbol Gene_A*	*Gene symbol Gene_B*	*Distance Gene_B [bp]*	*Reversion score*	*TFBS*
475	chr12:51866269-51866759	9	ocean	intergenic	-36733	Hectd1	Heatr5a	104563	1	na
829	chr16:24427123-24427493	5	ocean	intragenic	-33468	Lppos	Lpp	20598	1	na
2062	chr8:108755328-108755580	6	ocean	intragenic	-40685	Zfhx3	Mir3108	181280	1	na
1637	chr5:118410174-118410529	10	ocean	intergenic	-164948	2410131K14Rik	Med13l	150190	0.96	na
1094	chr19:37958986-37960367	21	ocean	intragenic	-261179	Cyp26a1	Myof	83211	0.96	na
796	chr15:101336815-101337068	7	ocean	intergenic	-43604	6030408B16Rik	Mir1941	32284	0.95	na
929	chr17:44717318-44718933	25	ocean	intragenic	-528747	Clic5	Runx2	17244	0.93	MYB:3
660	chr14:70332814-70333161	5	ocean	intragenic	-43317	Ppp3cc	Slc39a14	15273	0.92	na
78	chr1:127290230-127291199	19	ocean	intragenic	-85245	Mgat5	Tmem163	386823	0.92	na
1782	chr6:128296750-128297415	12	shelf	intragenic	-112947	9330102E08Rik	Tead4	3399	0.90	na
433	chr11:116615378-116616890	29	ocean	intragenic	-21692	Aanat	Rhbdf2	7363	0.89	CTCF:3 Esrrb:2 Tcfcp2l1:1
1785	chr6:129232196-129232413	4	ocean	intergenic	-51582	Clec2d	2310001H17Rik	5633	0.89	na
767	chr15:85574140-85575285	19	shore| shelf	intragenic	-70913	7530416G11Rik	Wnt7b	2786	0.89	na
1129	chr2:3659582-3660096	5	ocean	intergenic	-146518	Cdnf	Fam107b	53362	0.88	na

1589	chr5:90611828-90612487	7	ocean	intragenic	-50620	5830473C10Rik	Rassf6	28041	0.88	ETS1:1 ELF1:1 JUND:1 JUN:2
237	chr10:94047972-94048362	7	ocean	intragenic	-11972	Fgd6	Nr2c1	99569	0.87	GATA1:1
446	chr11:119855945-119857390	26	ocean	intragenic	-21580	Rptoros	Mir5098	24899	0.85	na
1211	chr2:102872350-102873792	12	ocean	intragenic	-165913	Slc1a2	Cd44	27874	0.85	na
1783	chr6:128298139-128299279	19	shore| shelf	intragenic	-114336	9330102E08Rik	Tead4	1535	0.83	na
640	chr14:47023430-47024302	16	ocean	intragenic	-22091	Samd4	Samd4	44675	0.82	na
639	chr14:47022407-47022945	5	ocean	intragenic	-21068	Samd4	Samd4	46032	0.82	na
1043	chr18:75455455-75455913	5	ocean	intragenic	-88091	Smad7	Gm10532	58732	0.82	Max:1
773	chr15:88854278-88855712	19	ocean	intergenic	-34633	Creld2	Pim3	6482	0.80	Esrrb:1
1506	chr4:137641026-137642234	15	ocean	intragenic	-46855	Usp48	Rap1gap	22492	0.79	na
1472	chr4:124703620-124704203	7	shelf	intragenic	-2922	Fhl3	Sf3a3	10658	0.78	Tcfcp2l1:1

Supplementary Table 5: All 8 hypomethylated reverting DMRs and selected annotations

DMR	*DMR position [mm10 coordinates]*	*CpGs*	*CpG region*	*Genomic region*	*Distance Gene_A [bp]*	*Gene symbol Gene_A*	*Gene symbol Gene_B*	*Distance Gene_B [bp]*	*Reversion score*	*TFBS*
104	chr1:156619232-156619512	7	ocean	intragenic	-60446	Abl2	Tor3a	54828	1	na
513	chr12:85859302-85859730	6	ocean	intragenic	-34353	Ttll5	Tgfb3	219312	0.58	na
1245	chr2:145682411-145682620	5	ocean	intergenic	-127429	Gm14092	BC039771	18575	0.58	na
1750	chr6:94594452-94595412	21	ocean	intragenic	-94139	Slc25a26	Mir7041	11004	0.55	na
862	chr16:89952302-89953265	11	ocean	intragenic	-133950	Tiam1	Tiam1	7563	0.53	na
522	chr12:101851491-101851718	10	ocean	intragenic	-32372	Fbln5	Trip11	61454	0.52	na
1463	chr4:119244557-119246311	39	ocean	intragenic	-10729	P3h1	Cldn19	9130	0.50	na
120	chr1:168472582-168472810	4	ocean	intergenic	-40413	Pbx1	Mir6348	17833	0.50	na

DANKSAGUNG

Diese Arbeit wäre ohne die Unterstützung von Betreuern, Kollegen und Kooperationspartnern nicht möglich gewesen.

Zuerst möchte ich Professor Jens Siveke für die Überlassung des spannenden Projekts und für seine Unterstützung auch in der Umsetzung eigener Ideen danken. Vielen Dank für die Übernahme des Erstgutachtens und die vielen Möglichkeiten zur persönlichen und fachlichen Weiterbildung.

Weiterhin danke ich Professor Bernhard Horsthemke für sein Interesse am Projekt und die freundliche Übernahme des Co-Referats. Vielen Dank für die richtige Frage zur richtigen Zeit und die konzeptionelle Unterstützung.

Besonders möchte ich mich bei Dr. Michael Zeschnigk für seine außergewöhnliche Unterstützung in der komplexen Welt der (Epi-)Genetik bedanken. Vielen Dank für die Möglichkeit, Hypothesen und Daten immer wieder zu diskutieren und daraus viele neue Denkanstöße mitzunehmen. Danke auch für die Mitwirkung in meinem Thesis Advisory Committee.

Ein riesiges Dankeschön gebührt Dr. Sven-Thorsten Liffers für sein stets offenes Ohr, die vielen methodischen Tricks und Kniffe und seine schonungslose Kritik an den richtigen Stellen. Vielen Dank auch für das gründliche Korrekturlesen dieser Arbeit.

Meiner gesamten Arbeitsgruppe möchte ich für eine spannende Promotionszeit danken. Vor allem danke ich Dr. Marija Trajkovic-Arsic für die Überlassung der Zelllinien als Grundlage dieser Arbeit. Besonders möchte ich meiner Kollegin Franziska Lang für die vielen fachlichen und manchmal auch „un-fachlichen“ Diskussionen über die gemeinsame Leidenschaft für Forschung und Natur danken.

Ich bedanke mich bei der Abteilung für Bioinformatik unter Leitung von Professor Sven Rahmann. Allen voran Jan Forster, der mich geduldig in den ersten Schritten mit R unterstützt und einen Großteil der NGS-Auswertungen übernommen hat. Weiterhin bedanke ich mich bei Dr. Christopher Schröder, Dr. Johannes Köster und Professor Sven Rahmann für ihre Mitwirkung am Projekt.

Mein herzlicher Dank gilt meiner ehemaligen Kommilitonin Leonie Henschel und Dr. Kerstin Ludwig für ihre kurzfristige und unkomplizierte Unterstützung bei der Auswertung der WGS Daten.

Vielen Dank an Dr. Kathrin Witzke, Kristin Fuchs und Professorin Barbara Sitek für die Massenspektrometrie der Zelllinien. Danke Kathrin für den spannend Tag im MS Labor, Deine ausführlichen Erklärungen und die Bereitstellung des zugehörigen Methodenteils.

Ich möchte mich bei Elke Jürgens und Regina Kubica für die Durchführung und Erklärung der Zytogenetik bedanken.

Für die zur Verfügung gestellten PDX Modelle danke ich Dr. Rita Lawlor und Professor Aldo Scarpa. Weiterhin bedanke ich mich bei Dr. Diana Behrens für die Durchführung der PDX Experimente und die Bereitstellung des zugehörigen Methodenteils.

Für die exzellente Durchführung von RNA-seq bzw. WGS und WGBS möchte ich mich bei der CeGaT GmbH und der Genomics & Proteomics Core Facility des DKFZ bedanken. PD Dr. Ludger Klein-Hitpass und seinem Team danke ich für das exzellente amplicon sequencing.

Als Mitglied im Thesis Advisory Committee danke ich Professorin Perihan Nalbant für ihre Zeit und die konstruktiven Diskussionen.

Vielen Dank an das gesamte Team des mentoring³ Programms der Research Academy Ruhr für die außerfachliche Unterstützung über zwei Jahre meiner Promotion. Besonders möchte ich mich bei meiner Mentoringgruppe und den Dozenten der Workshops für viele neue Sichtweisen bedanken. Mein herzlicher Dank gilt meiner Mentorin Professorin Konstanze Winklhofer für ihre Zeit und Unterstützung auch über das Mentoring Programm hinaus.

Mein größter Dank gilt meinen Eltern und meinem Mann. Danke, dass ihr immer für mich da seid und mir den Rücken freihaltet.

CURRICULUM VITAE

Der Lebenslauf ist in der Online-Version aus Gründen des Datenschutzes nicht enthalten.

Der Lebenslauf ist in der Online-Version aus Gründen des Datenschutzes nicht enthalten.

DECLARATIONS

Erklärung:

Hiermit erkläre ich, gem. § 6 Abs. (2) g) der Promotionsordnung der Fakultät für Biologie zur Erlangung des Dr. rer. nat., dass ich das Arbeitsgebiet, dem das Thema „Epigenetic and Phenotypic Plasticity as Mediators of Resistance to Oncogenic Pathway Targeting“ zuzuordnen ist, in Forschung und Lehre vertrete und den Antrag von Laura Godfrey befürworte und die Betreuung auch im Falle eines Weggangs, wenn nicht wichtige Gründe dem entgegenstehen, weiterführen werde.

Essen, den 08.06.2020 _____

Prof. Dr. Jens Siveke

Erklärung:

Hiermit erkläre ich, gem. § 7 Abs. (2) d) + f) der Promotionsordnung der Fakultät für Biologie zur Erlangung des Dr. rer. nat., dass ich die vorliegende Dissertation selbständig verfasst und mich keiner anderen als der angegebenen Hilfsmittel bedient, bei der Abfassung der Dissertation nur die angegebenen Hilfsmittel benutzt und alle wörtlich oder inhaltlich übernommenen Stellen als solche gekennzeichnet habe.

Essen, den 08.06.2020 _____

Laura Godfrey

Erklärung:

Hiermit erkläre ich, gem. § 7 Abs. (2) e) + g) der Promotionsordnung der Fakultät für Biologie zur Erlangung des Dr. rer. nat., dass ich keine anderen Promotionen bzw. Promotionsversuche in der Vergangenheit durchgeführt habe und dass diese Arbeit von keiner anderen Fakultät/Fachbereich abgelehnt worden ist.

Essen, den 08.06.2020 _____

Laura Godfrey